UNIVERSITY OF PUERTO RICO
Faculty of Natural Sciences
Department of Chemistry
Río Piedras Campus

Design of a Continuous Bio-Electrochemical Reactor System for Enhancement of Wastewater Treatment

by

Wilfredo Jabés Cardona Vélez

Doctoral Thesis Submitted in Partial Fulfillment

of the Requirements for the

Degree of Doctor of Philosophy

December 15, 2022

Accepted by the Faculty of the Department of Chemistry from the University of Puerto Rico in Partial Fulfillment of Requirements for the Degree of Doctor of Philosophy.

_____

Dr. Carlos R. Cabrera

_____

Dr. Jorge L. Colón

_____

Dr. Gary A. Toranzos

_____

Dr. Jorge Gardea-Toresdey

Acknowledgments

This work is the product obtained from the support that many people had given me through this academic journey. First, I want to thank my mother, who always supported my interest in science and the pursuit of knowledge and encouraged me to pursue my dream of being a scientist. Also, I want to thank both of my sisters, who always provided moral support and believed in me to achieve my goals. Also, I want to recognize the support of my friends Anais, and Rafael A., who supported me in my doctorate journey and constantly helped me to grow as a person and a professional.

I want to give a special acknowledgment to my thesis advisor, Dr. Carlos R. Cabrera, for taking the chance to welcome me into his laboratory, and from whom I have learned many things besides Analytical Chemistry; never giving up before trying, effective communication, and how to build strong interpersonal relations. I am truly grateful for his dedication as a mentor and his availability to guide me. Also, I would like to thank Dr. Jorge L. Colón, Dr. Gary A. Toranzos, Dr. Jorge Gardea-Torresday, and Santosh Vijapur and Timothy Hall from Faraday Technology, Inc. for their mentorship and for guiding me as a professional through the research and academic development.

I want to thank my friends at Cabrera's Lab who welcomed me into the lab and taught me different aspects of electrochemistry within their projects while allowing me to help with my engineering knowledge. I want to thank Dr. Arnulfo Rojas, and Dr. Ramonita Díaz for their mentorship in my project as part of Cabrera's Lab. Also, I want to thank Armando, Melissa, and Nadja, because they help me grow as a professional. I want to acknowledge my undergraduate students: Juan Suárez, Ángel Pagán, and Ivan Nieves; thank you for your work and all the late nights. This accomplishment is yours too! Especial thanks to Melanie Ortiz, the undergraduate student who

became a great friend and inspired me to always be the best version of myself. I also want to thank the friends I developed during my graduate studies and the good moment I will cherish forever.

Finally, I want to thank the following agencies that gave me their sponsorship. Puerto Rico NASA Space Grant Fellowship NNX15AI11H, NSF-CREST-CIRE2N Grant Number 1736093, and NASA STTR- NNX17CA30P and 80NSSC18C0222 with Faraday Technology, Inc.

Table of Content

List of Figures

Chapter 1

Chapter 3

Chapter 4

Chapter 5

List of Tables

Chapter 1

Chapter 4

Chapter 5

List of Abbreviations

% vol	Percent per volume
°C	Degree Celsius
A	ampere
AOC	Ammonia Oxidation Current
AOR	Ammonia oxidation reactor
BHI	Brain Heart Infusion
BSHU	Basal synthetic human urine
BSL	Biosafety level
C_1	Initial Bacteria concentration in CFU
C_2	Diluted Bacteria concentration in CFU
CE	counter electrode
CFBE	Carbon Fiber Brush electrode
CFU	colony forming units
cm	centimeter
cm^2	squared centimeters
CO	Carbon monoxide
CV	Cyclic voltammogram
E	potential
ECLSS	Environmental control and life support system
ECSA	Electrochemical surface area
EDS	Energy Dispersive Spectroscopy
Eq	Equation

GCE	glassy carbon electrode
H_2O	Water
H_2SO_4	Sulfuric Acid
HCl	Hydrochloric Acid
hr	hour/hours
I	current
ISE	Ion-selective Electrode
ISS	International Space Station
j	current density
M	molar concentration
mA	milliampers
min	minutes
mL	milliliter
NASA	National Aeronautics and Space Administration
NCs	Nano-cubes
NH_2 $(CO)NH_2$	Urea
NH_3	Ammonia
NPs	Nanoparticles
P. vulgaris	*Proteus vulgaris*
PBS	phosphate buffer solution
ppm	part per million
Pt	Platinum
RE	Reference electrode

RHE	reversible hydrogen electrode
s	seconds
SEM	Scanning Electron Microscopy
UPA	urine process assembly
UV	ultraviolet
UV-Vis	Ultraviolet-visible Spectroscopy
V_1	Volume for the Initial Bacteria Concentration
V_2	Volume for the final bacteria concentration
VCD	Vapor Compression Distillation
WE	working electrode
μA	microampere
V	volts

Chapter One

1. Introduction

Insufficient clean water is a significant problem in a world populated by over 8 billion people. Currently, slightly less than half of humanity worldwide, 4 billion people, or 50% of the population, live in areas that suffer water scarcity for at least one month each year.[1] Moreover, around 700 million people in 43 countries live without a safe and clean water supply.[2] Water is a critical natural resource upon which the ecosystem functions and all social and economic activities.[3] Although water demand management has been practiced in urban populations to improve consumption behavior and secure the water supply, there still is a need for other measures.[4]

Water reduction from extensive groundwater sinks greatly affects regional and local areas. Water extraction for irrigation is the primary driver of groundwater depletion worldwide. The increment of groundwater extractions by 2050 will be 1,100 kg per year, or 40%.[5] As for coastal civilization, these areas have unique problems. They are more intensely populated, exhibiting higher population growth rates and urbanization than their hinterland counterparts.[5] Water desalinization is an alternative method to increase water resources; however, the process requires considerable energy and is expensive. In countries with poor sanitary policies, water pollution threatens the availability of clean water.

Wastewater from domestic population is treated in facilities by biological, chemical, and physical methods.[6] Wastewater treatment and water recovery systems are limited to about 90% water reclamation.[7] In developing countries, untreated sewage is released into surface waters.[8] Pollution

from agriculture, industry and urban areas alters the global biodiversity and freshwater ecosystems.[8] Industrial and municipal wastewater are discharged untreated.

Additionally, urbanization expansion and the expense of wastewater treatment promote wastewater discharge to continue.[8] Fertilizers (nitrogen and phosphorus) used for agriculture can also impact water quality. Each treatment has advantages and constraints regarding cost, efficiency, feasibility, and environmental impact. However, most modern systems rely on a combination of methods to achieve the desired water quality cost-effectively.[9] These facilities on earth, although expensive and challenging, have easier access to earth resources, unlike environments in outer space, such as the closed-loop environment for space stations, Figure 1.1.

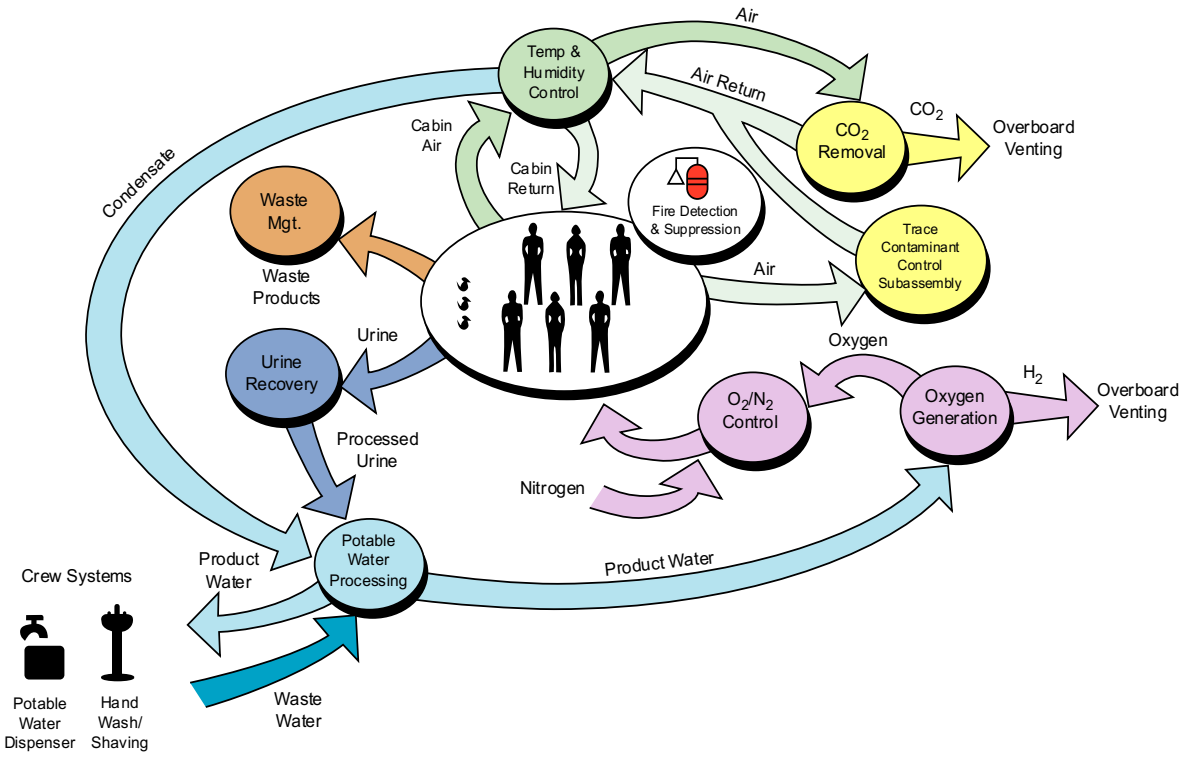

Figure 1.1. General flow diagram of a closed-loop environment in the Environmental Control and Life Support System (ECLSS) for the International Space Station (ISS).[10]

In Space, effective wastewater recycling systems are needed to satisfy the water demand in closed-loop environments for spacecraft and possible future colonies on the Moon and Mars. On average, humans drink approximately 2.5 L of water daily and release from 1 to 2 L of urine. However, they can utilize more on daily chores. While in space, they drink 2.2 L of water daily. Still, the total water consumption of water per person in space daily is 4 L.[11] The current Environmental Control Life and Support System (ECLSS) water recovery model in the International Space Station (ISS) is capable of recycling approximately 90% of total wastewater generated. This includes the 74%-85% that can be recovered from human urine.[12,13] Nonetheless, long-term space missions will not be able to waste any resources in the future. Hence, astronauts will be reliant on a more efficient recycling system. Among the various water recovery pathways included in the ECLSS, roughly 80% of the wastewater comes from human urine.[14]

This thesis studies an approach for self-sustainable technology that benefits the ECLSS by focusing on water reclamation pathways for urea removal from urine—using *Proteus vulgaris* (*P. vulgaris*) for a sustainable urine recycling system. The goal is to develop a prototype of a cost-effective process with potential application for a closed-loop environment. The first aim finds the parameters at which could be set a bioreactor system with *P. vulgaris* while working continuously, exploring bacterial dilution rate, pH influence on the culture, and electrochemical response of ammonia oxidation reaction current in a platinum (Pt) electrode. Moreover, designing and building a pH controller could help monitor and regulate the process pH. Secondly, develop and evaluate the tandem process of a bioreactor for urea consumption and an electrochemical cell reactor to remove ammonia. The final aim was to build an electrode using a carbon fiber brush modified with Pt (100) nanoparticles (NPs) and polycrystalline Ni NPs, to enhance the electrochemical oxidation of ammonia and urea from bioreactor-processed synthetic human urine.

1.1 Human Urine as an electrochemical system

Human urine (HU) consists of water (95%), inorganic compounds, a variable percentage of organic metabolites, and urea (approximately 2%).[15] Inorganic compounds and organic metabolites can be removed by reverse osmosis or membranes.[16] Generally, fresh urine has a pH between 4.8 and 7.5, which is associated with the concentration of ammonium ion.[17,18] The general human urine chemical composition from healthy adults is listed in Table 1. The list of components is retrieved from a NASA report, a chromatographic study publishing composition of amino acids in urine, and a recipe from the Cold Harbor Spring Protocol.

Table1. General human urine chemical composition from healthy adults, in concentrations of grams per liter. [19–21]

Components	g/L	Components	g/L
Sodium chloride	5.844	Aspartic Acid	0.0098
Sodium sulfate	2.414	Threonine	0.0194
Magnesium chloride · $6H_2O$	0.651	Serine	0.0423
Potassium chloride	2.832	Glutamic Acid	0.0072
Calcium chloride ·2 H_2O	0.444	Valine	0.0075
Creatinine	1.018	Methionine	0.0046
Sodium citrate ·2 H_2O	2.000	Leucine	0.0086
Potassium phosphate monobasic	2.177	Tyrosine	0.0419
Magnesium sulphate ·$7H_2O$	0.789	Phenylalanine	0.0140
Sodium oxalate	0.024	Histidine	0.1692
Uric acid	0.101	Lysine	0.0192
Sodium phosphate dibasic	0.923	Proline	0.0045
Urea	16.816	Glycine	0.1411
NH4Cl	1.070	Alanine	0.0429

Components	g/L
Sodium bicarbonate	1.134
D-glucose	2.000
Glyceraldehyde $C_3H_6O_3$	0.099
Iron (II) sulfate heptahydrate	0.001
Sodium phosphate monobasic · H_2O	0.562

Components	g/L
Isoleucine	0.0082
Taurine	0.1112
Cystine	0.0240

1.2 Urea and microbial urease

Urea is produced in the human body at 20-30 g per day.[22] Urea is a small uncharged molecule that is not easily removed from urine by size and charge exclusion. Other methods for urea removal include decomposition with strong oxidants, removal with adsorbents and hydrolysis, but these are not beneficial due to the process parameter requirements or matrix complexity incrementation.[23] Previous studies suggested using the enzyme urease to remove urea from the urine solution. The enzyme protein structure varies depending on the organism that produces it (*i.e.*, different plants, fungi, and bacteria).[24] Urease, shown in Figure 1.2, catalyzes the urea hydrolysis shown in the general chemical reaction (1.1). The most accepted reaction mechanism is explained in Figure 1.3.[24,25] Where the urea binds one of the amide sides of urea to one of the Ni sites. Then the urea hydrolysis produces one molecule of ammonia and a byproduct of carbamate. In the presence of water, the formed carbamate can go into a zwitterion configuration, which is unstable, promoting dissociation to ammonium ions and carbonic acid.[26] The carbonic acid forms an equilibrium with carbon dioxide gas in the solution.[27] These products increases the pH due to the ammonia formation in the system. Ureases are conservative enzymes that are stable in a pH close to 7 ±0.3.[14,28]

$$NH_2(CO)NH_2 + H_2O \rightarrow 2NH_3 + CO_2 \quad (1.1)$$

Urease is a nickel-containing enzyme, Figure 1.2, that requires the activity of a few additional proteins to acquire its hydrolytic properties.[29,30] This process involves coding structural enzyme polypeptides and coding accessory proteins in a joint cluster.[29]

Nevertheless, enzyme instability due to unfavorable microenvironment factors prevents efficient removal of urea.[31] This would require constant enzyme consumption for the process to compensate for the denatured enzymes. *P. vulgaris, shown in* Figure 1.4*,* has proven to be a potential alternative to provide urease within a stable environment. This gram-negative, facultative anaerobic bacterium can consume urea and metabolize it with urease.[32] In contrast to other urease-containing bacteria, *P. vulgaris* can be adapted to high urea concentration environments by increasing urea metabolization.[25] Using *P. vulgaris* for urea consumption provides urease stability since a variety of bacteria (*P. vulgaris* included) can survive and adapt to pH values between 5-8, without genetic modifications.[33]

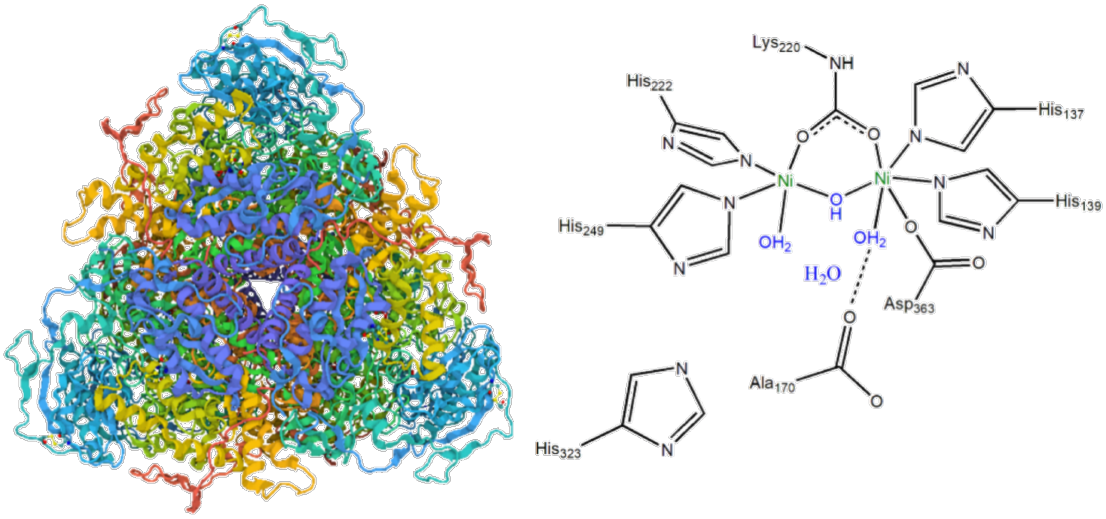

Figure 1.2. Urease Molecule diagrams. (right) Quaternary structure from protein structure base 3LA4.[30] (left) Urease's nickel binding site at the center of the urease, displaying the interaction with an ammonia molecule.[27] Urease illustration generated with app.biorender.com

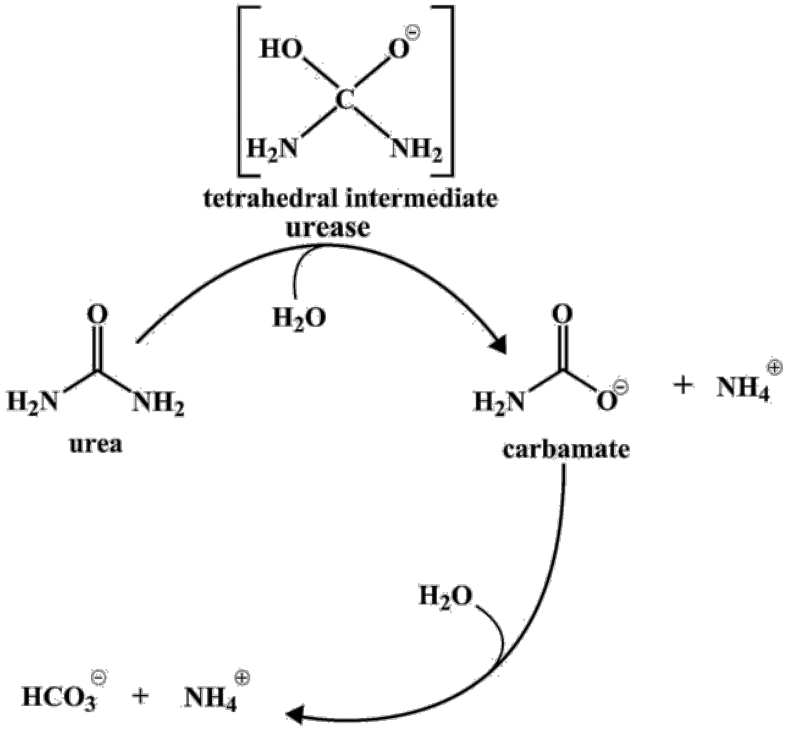

Figure 1.3. Urea hydrolysis mechanism catalyzed by urease. [24]

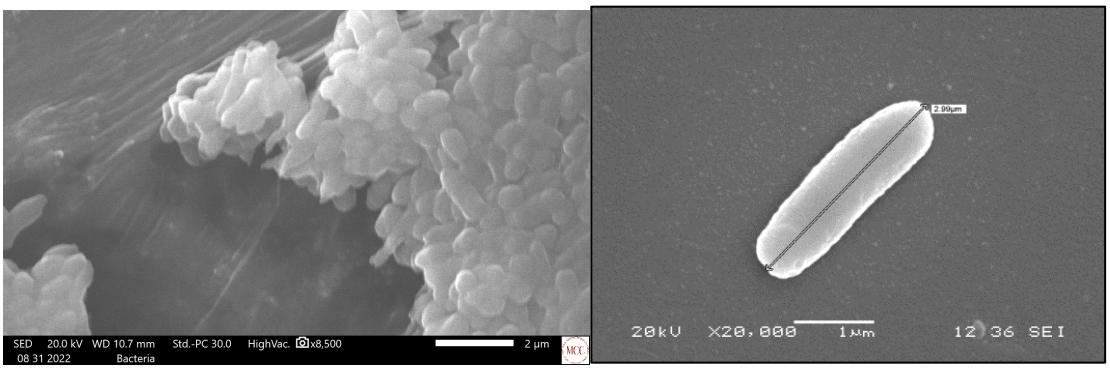

Figure 1.4. Scanning Electron Micrograph Image of *P. vulgaris* colony (left), and single *P. vulgaris* (right). Image is taken from M. Morales-Cruz et al., "Figure 1 of Proteus vulgaris-Pt electrode system for urea to nitrogen conversion in synthetic urine" with permission of Elsevier and Copyright Clearance Center.[16]

1.3 Continuous bioreactor

Bioreactors are essential industrial microbiology instruments that nourish microorganisms to their optimal physio-chemical and nutritional levels to produce various microbial products.[34] There are several types of bioreactors and they work as a batch, fed-batch, perfusion, and continuous process.[33] A batch process is a classic process whereas the bioreactor is filled with a predetermined number of media for a batch process. The inoculum is then added to the bioreactor. The cell culture grows until the nutrients are consumed, and the run is harvested. Nothing is added or removed from the bioreactor during a batch process. [35] The cells go through four main phases, observed in Figure 1.5.[33] These are known as lag, growth, stationary, and finally, death.

A continuous bioreactor is when the system reaches a steady state, where the cell growth rate equals the death rate.[34,35] A constant feed stream enters the bioreactor system, and an effluent stream exits as a product out of the bioreactor. Continuous bioprocessing is currently in the initial stages of development. A continuous process is beneficial as there is no downtime between

batches, no expensive and laborious cleaning, and no variability in the product from batch-to-batch production.[35]

The chemostat and perfusion systems are two of the most common types of continuous bioreactors.[33] Both systems control and maintain bacterial growth parameters while allowing a constant flow of fresh feeding media influx to the bioreactor.[33,36] The main difference between these systems is that the chemostat enables the outflow of the consumed media, by-products, and bacteria. In contrast, the perfusion system does not permit bacteria or tissue outflow.[33,37] However, in a perfusion system, the bacteria outflow hindrance ultimately results in a microbial clot which is not convenient in a continuous system as it interrupts the flow for closed-loop environments. *P. vulgaris* has been used in fed-batch and continuous-flow bioreactor systems.[38] The bioreactor process discussed in this thesis will be focused on using the approach for a chemostat bioreactor. Essentially, a chemostat bioreactor consists of a vessel that has controlled parameters such as temperature, feed flow, and effluent flow, pH, and aeration (i.e., O_2 and CO_2 control) controlled automatically, Figure 1.6.[33,39]

Urea is consumed by *P. vulgaris'* urease in a chemostat system, constantly producing ammonia and other byproduct metabolites. However, ammonia remains toxic for human consumption, so its removal is required. Air stripping and biological nitrification/denitrification are two of the most popular ammonia removal techniques. However, conventional natural degradation does not respond well to shock loads of ammonia, and air stripping provides acceptable results only at high pH conditions.[40] A less common technique but of most convenience is the electrochemical ammonia oxidation reaction (AOR) process, which removes ammonia through electrochemical oxidation yielding molecular N_2 and H_2.

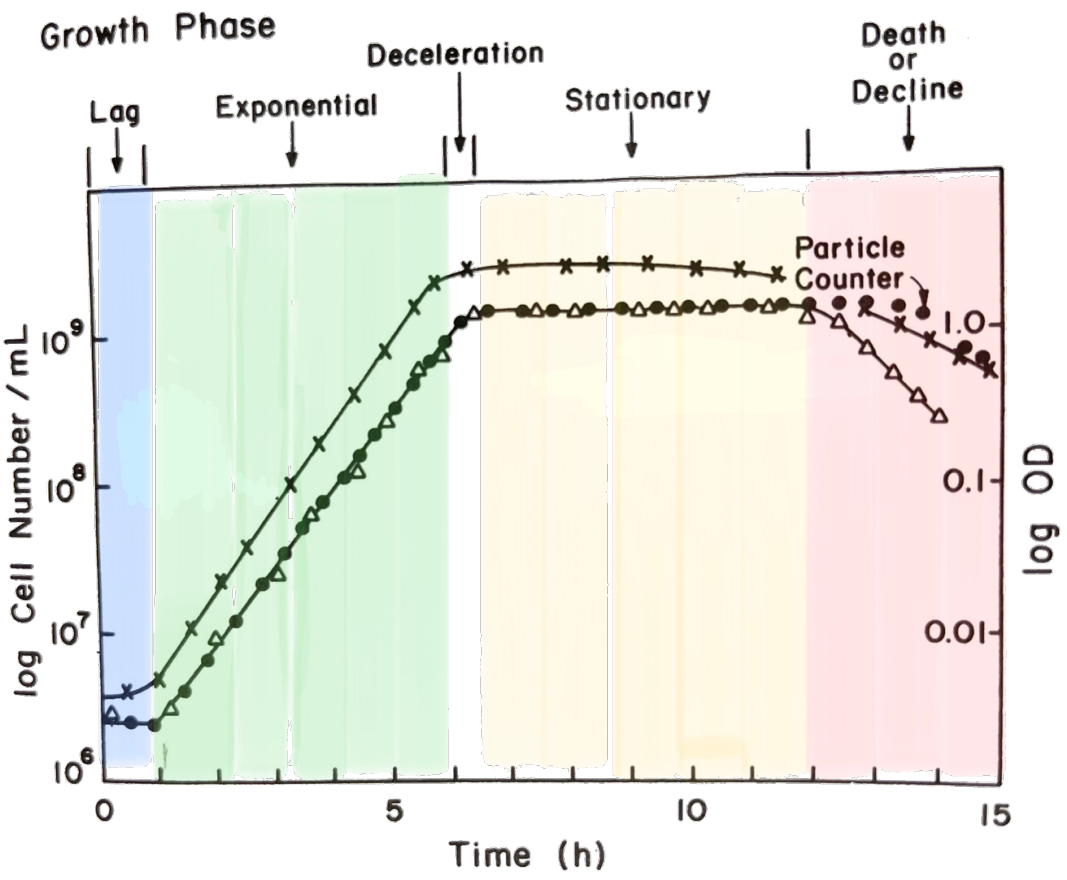

Figure 1.5. General description of the bacterial growth phase. In blue is the lag phase. Green the exponential growth of the bacteria. Yellow, stationary phase. Red, the death of decline phase. This image was modified from the original image, retrieved from Bioprocesses Engineering Basic concepts, by Michael L. Shuler.[33]

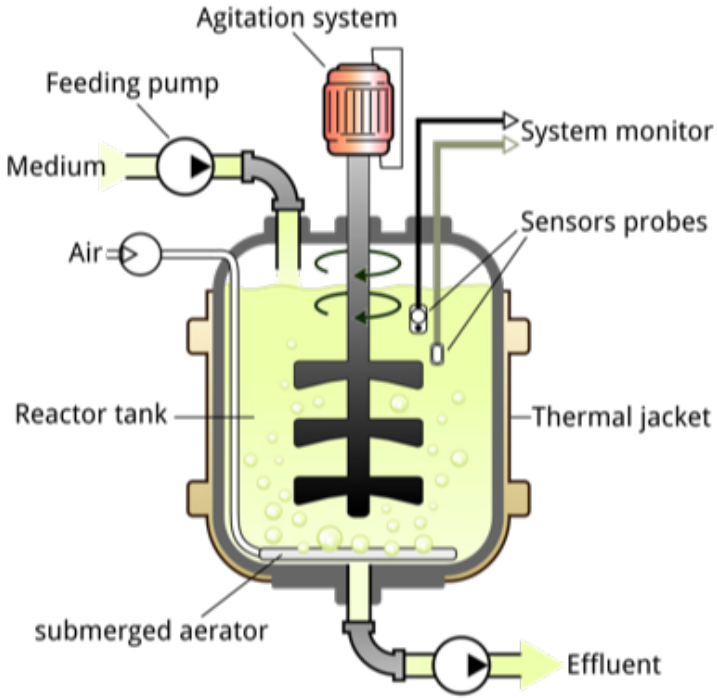

Figure 1.6. General schematic of a chemostat bioreactor and its controlled parameters. This system has controlled temperature, mixing, influent and effluent flow, and aeration. Also, illustrate the use of additional sensors; an example of such sensors is volume level, pH, and pO_2.

1.4 Platinum electrochemistry and electrochemical removal of ammonia

Platinum is a precious metal with excellent catalytic properties due to its high activity in fuel cell's reaction in oxidation and reduction processes.[41] Platinum's voltametric profile was based in 1970 on a consensus between electrochemists.[42] The Pt profile obtained from a cyclic voltammogram (CV), between the onset potential of hydrogen and oxygen evolution in diluted sulfuric acid, H_2SO_4 0.5 M. The charge transfer observed in the range of 0.05 V to 0.4 V vs. reversible hydrogen electrode (RHE) is assigned to hydrogen desorption and desorption due to the underpotential deposition of a hydrogen monolayer and the release of protons, Figure 1.7.[42] Due to energetic

considerations, the peaks at 0.27 V vs. RHE, were due to strongly adsorbed hydrogen atoms on Pt surface. The peak at 0.12 V vs. RHE corresponds to weakly adsorbed hydrogen. The charge of hydrogen peaks was determined to be 210 $\mu C/cm^2$, which determines the platinum's electrochemically active surface area.[42] The double-layer charging region characterized by the lack of peak is located between the potential of 0.4 and 0.9 V vs. RHE. After 0.9 V vs. RHE, this last part is attributed to the formation and dissolution of a monolayer of adsorbed oxygen and the oxygen evolution on Pt surface.

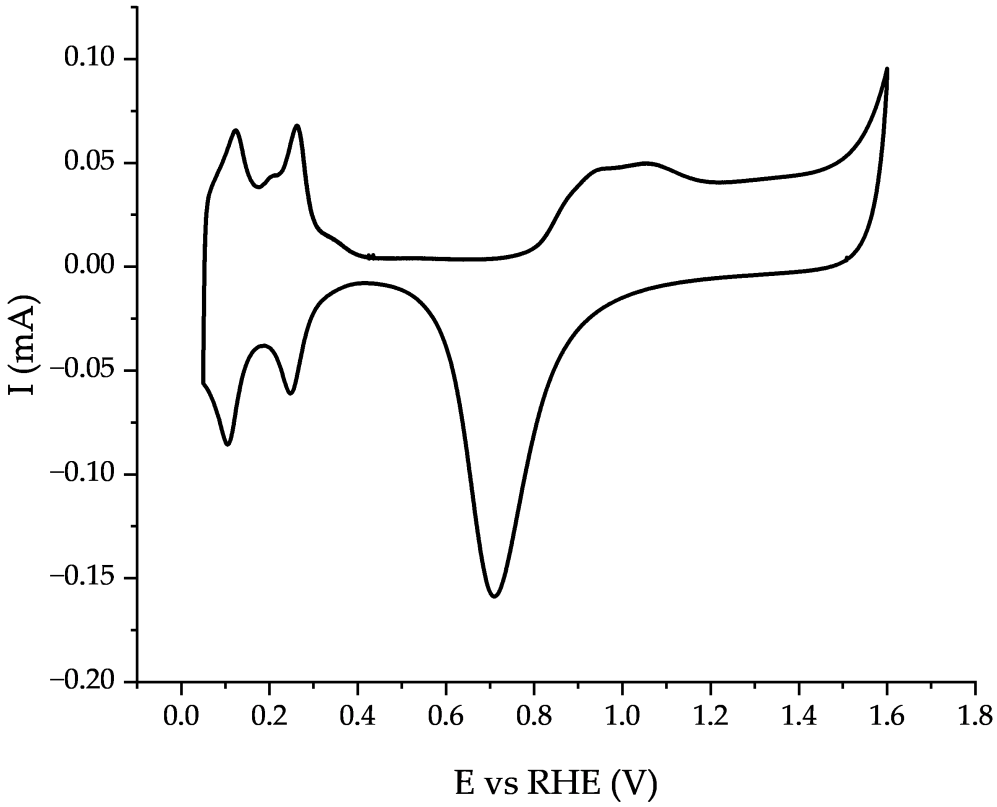

Figure. 1.7. Cyclic voltammogram of a Pt electrode in a 0.5 M H_2SO_4 solution at 50mV/s scan rate vs. RHE. The peaks shown at the potential range vs. RHE are the adsorption and desorption of hydrogen on the Pt electrode surface.

Since different geometries enhance specific reactions, scientists have explored synthesis processes to obtain platinum with certain defined facets. The control of platinum geometric characteristics (i.e., size, shape, morphology) is performed to fit the electrocatalytic properties better. Platinum with a Miller index of (100) is known for its function in ammonia oxidation reaction (AOR) (1.2). The oxidation of ammonia, which is a structurally sensitive reaction, takes place almost exclusively on Pt (100) sites.[41,43] The AOR is known to be catalyzed by Pt in an alkaline solution.

$$2\ NH_3 + 6\ OH^- \rightarrow N_2 + H_2O + 6\ e^- \quad (1.2)$$

In addition, Pt nanocubes (PtNCs) have proven to be very effective in this type of reaction under similar conditions.[16] PtNCs-modified anodes ensure highly efficient ammonia removal for the bioreactor efflux. It is anticipated that ammonia will be used for fuel cells because of its electrical charge density, low standard potential, and transportation safety.[44,45] Provided that N_2 is formed as a product, no contamination is generated when ammonia is used in fuel cells.[44] The reaction mechanism for the ammonia oxidations complex is still under discussion.[46] However, a general mechanism can be observed in equations 1.3 to 1.6.[46]

$$NH_3 + HO^- \rightarrow NH_{2(ads)} + H_2O + e^- \quad (1.3)$$

$$NH_{2(ads)} + HO^- \rightarrow NH_{(ads)} + H_2O + e^- \quad (1.4)$$

$$NH_{(ads)} + HO^- \rightarrow N_{(ads)} + H_2O + e^- \quad (1.5)$$

$$2N_{(ads)} \rightarrow N_2 \quad (1.6)$$

1.5 Nickel electrochemistry and electrochemical removal of urea

Nickel's mechanical strength, relatively low toxicity, and low cost are among the most important metals.[47] Furthermore, nickel and some of its alloys are among the more active electrode materials.[48] The Ni electrochemical profile can be characterized through different approaches (i.e., the alpha method,[48] the betta method,[49] the oxalate method,[50] and the capacitance method).[51] For this work, the Betta Method is used for characterization. The Beta Method consists of integrating the β-NiOOH reduction peak. This method studies the $Ni^{2+/}Ni^{3+}$ region at a potential range of 1.4 to 1.55 V vs. RHE, Figure 1.8. It can be explored by cycling potentials for enough cycles to reach a steady reduction of the β-NiOOH species in the anodic region of the CV. Although, the peak associated with the oxidation of β-$Ni(OH)_2$ will continue to increase.[52] The theoretical surface charge while using the betta method is 420 μC/cm^2.[53]

It is known that nickel is present in the biological catalysis of urea hydrolysis.[27] Nickel can also electro-catalyze the urea and ammonia oxidation reaction at alkaline pH.[54,55] The products of urea's oxidation are CO_2, H_2O, and N_2, as observed from the net chemical reaction.

Half Oxidation Reaction:

$$Ni(OH)_{2(s)} + OH^- \rightarrow NiOOH_{(s)} + H_2O_{(l)} + e^- \quad (1.7)$$

$$CO(NH_2)_{2(aq)} + 6\ OH^- \rightarrow N_{2(g)} + 5\ H_2O_{(l)} + CO_{2(g)} + 6\ e^- \quad (1.8)$$

Half Reduction Reaction:

$$6\ H_2O_{(l)} + 6\ e^- \rightarrow 3\ H_{2(g)} + 6\ OH^- \quad (1.9)$$

Net chemical:

$$CO(NH_2)_{2(aq)} + H_2O_{(l)} \rightarrow N_{2(g)} + 3\ H_{2(g)} + CO_{2(g)} \quad (1.10)$$

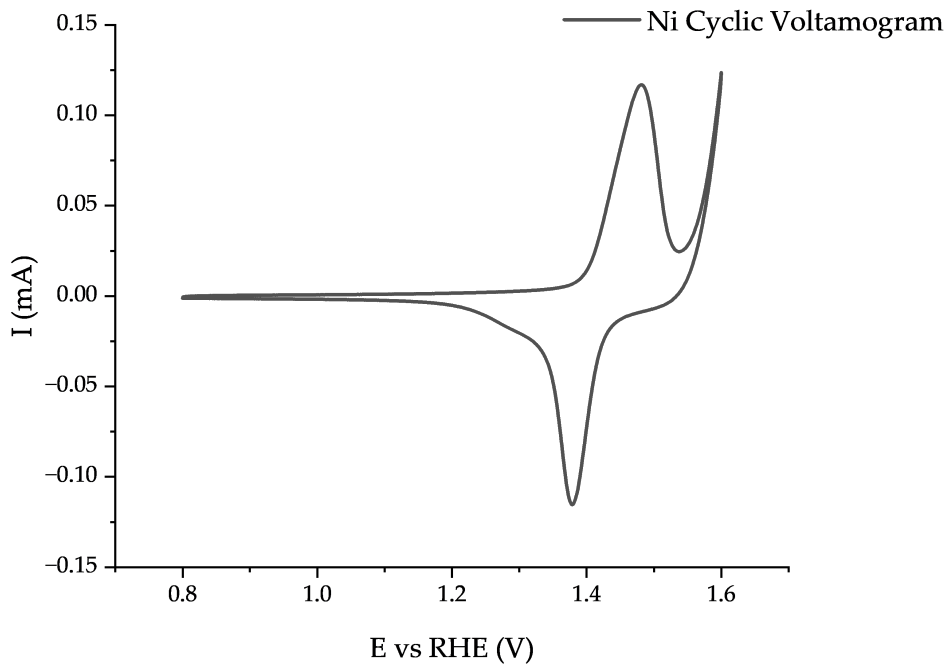

Figure 1.8. Cyclic voltammogram of a polycrystalline Ni electrode in a 0.1 KOH solution at 50mV/s scan rate vs. RHE.

1.6 Carbon brush electrode for ammonia and urea removal.

The design of the anode for the removal of ammonia and urea from the bioreactor's effluent is an important factor. The use of a carbon brush electrode has been reported for microbial fuel cell's anode.[56,57] It has been used in many types of research because of its economical material, good electrical conductivity, and large surface area suitable for modification with nanoparticles or bacteria. The carbon brushes can be made from carbon fibers and stainless-steel or titanium cores, Figure 1.9.

Modifying a carbon brush has been reported for microbial fuel cells to enhance the cells' power.[58] Many modifications can be performed on a carbon brush to enhance its electrochemical capacity to oxidize ammonia and urea. Additionally, platinum nanoparticle deposition on carbon fibers has

been previously achieved for fuel cell purposes. For this reason, adding a Nickel and platinum catalyst is of interest to improve the ammonia and urea oxidation reaction.

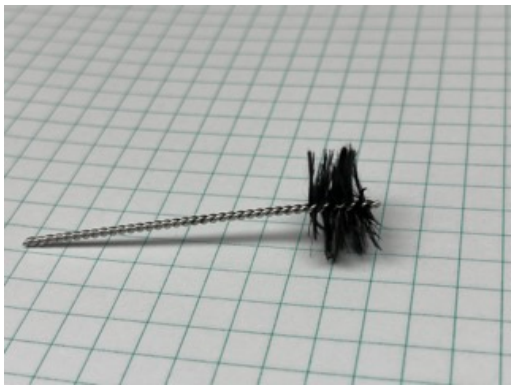

Figure 1.9. Carbon Fiber Brush Electrode, made from carbon fibers and stainless-steel wires.

Chapter Two

2. Significance and Problem Statement

The wastewater treatment and water recovery system within the ECLSS has durability limitations, with an approximately 90% of water recovery overall. The existing recovery system decrease with time due to contaminant received through wastewater. There are many approaches studied to treat wastewater in a closed loop environment, but the energy and resource demand is expensive. The integration of a *Proteus vulgaris* bioreactor into a wastewater system will provide a controlled environment to remove urea from wastewater produced in space. Since *Proteus vulgaris* is a robust microorganism capable of surviving in different conditions and producing stable urease. The urease catalyzes the hydrolysis of urea to ammonia. After the urea has reacted with the urease, producing ammonia that can be oxidized. This oxidation catalyzed by platinum can further produce hydrogen and nitrogen. Hence, controlling the urea breakdown into ammonia and removing in gross the urea and ammonia present in the urine through a tandem biological and electrochemical process was our goal.

Different urine flow rates to build a bioreactor system for the Proteus vulgaris in synthetic human urine were explored. After selecting an optimum flow rate, an automated bioreactor system was designed and built. The ammonia-rich effluent from the bioreactor was coupled to an ammonia oxidation cell. Furthermore, the behavior of the ammonia oxidation cell was explored in a microgravity environment. Then the automated bioreactor system was explored with real human urine as an electrolyte. In addition, an anode was built to enhance the oxidation selectivity of ammonia and urea present in the effluent using synthetic human urine.

2.1 Hypothesis

The research goal of this thesis is to remove urea and ammonia from urine using a bacterium, *Proteus vulgaris*, and an alkaline electrolyzer cell. In deep, the project has three main hypotheses set in motion in different experiments to prove the project's feasibility. The first hypothesis is that if we can sustain high concentrations of *Proteus vulgaris* in a urine media with a bioreactor, we can continuously remove urea from the media in an automated process. The second hypothesis of the project is that if we use the effluent obtained from the media in an alkaline cell with polycrystalline platinum foils, we can remove the gross ammonia produced and some of the initial ammonia content. Our third hypothesis is that if we successfully modify the surface of a carbon fiber brush electrode with nickel nanoparticles and platinum nano-cubes, then the efficiency of the platinum nano-cubes to oxidize ammonia in our system will be sustained when compared to a carbon fiber brush electrode's surface modified with only platinum nano-cubes.

2.2 Research goals and specific aims

This thesis aims to design and build a continuous flow bioreactor prototype coupled with an alkaline cell to remove urea and ammonia from synthetic and real human urine. Furthermore, it is desired to mitigate the passivation of the platinum electrode in the alkaline cell by using a modified carbon brush electrode with platinum nano-cubes and nickel nanoparticles as a working electrode.

2.2.1 Specific aims

- Design, build, and evaluate an automated continuous *Proteus vulgaris* Bioreactor prototype using synthetic human urine.

- Evaluate the joint bioreactor and electrochemical process to reduce urea and ammonia concentration from synthetic human urine.
- Evaluate the joint bioreactor and electrochemical process to reduce urea and ammonia concentration in human urine.
- Design a working electrode to enhance the selectivity of urea and ammonia oxidation from the effluent wastewater of the coupled bioreactor with the electrochemical system.

2.2.2 Techniques

The techniques used in this thesis project to design and characterize the materials developed and synthesized or modified were Scanning Electron Microscopy (SEM), Energy Dispersive Spectroscopy (EDS), and electrochemical technique such as Cyclic Voltammetry (CV) and Chronoamperometry. The approaches used to speciate and quantify urea and ammonia from the synthetic human urine, and real human urine were a colorimetric technique using ultraviolet-visible (UV-vis) spectroscopy and Ammonia Ion Specific Electrode (ISE), and electrochemical analysis such as Cyclic Voltammetry (CV) and Chronoamperometry.

Chapter Three

3. Materials, analytical and aseptic practices

This chapter describes the protocols used to execute the synthesis of nanoparticles, electrochemical analysis, and *P. vulgaris* culture experiments. Many activities of this project focus on the use of bacteria, and as such, an aseptic protocol is needed. Also, since the use of electrochemical techniques is sensitive requires precaution to avoid contamination of any kind. These precautions and protocols will be described next.

3.1 Materials and Reagents

To ensure clean and pure solutions nano pure water with a resistance of 18.2 ΩM – cm was used ensuring that metals, biological materials, and electroactive components would not contaminate the solutions prepared for the experiments. All glassware was cleaned with Alconox® detergent solution and tap water, followed by nano pure water triple rinse. The sulfuric acid solution was prepared from DI water (GEMINI-Ultra high purity water system) and Optima grade sulphuric acid reagent (Fisher). Materials for biological experimentation were bought sterile, while the glassware was autoclaved for 15 minutes at 121 °C before use.

The glassware used for electrochemical experiments was thoroughly cleaned with aqua regia solution overnight, then rinsed with nano pure water. For solution preparation, the purity of the reagents was considered to correct the weight, obtaining the correct concentration.

3.2 Safety Handling Bacteria

When culturing the bacteria, it was treated as a pathogen. All the equipment used to grow the bacteria was sterilized. The equipment sterilization process (i.e., glassware, solutions, tubing,

pipette tips) was exposed to autoclaving protocol at 121 °C for 15 minutes. Microorganisms are managed at a specific biosafety level (BSL). For the case of *P. vulgaris*, the biosafety level is 2. Thus, a biosafety cabinet BSL 2 was used. Before and after working in the biosafety cabinet, it was cleaned with the following protocol. The working surfaces and the equipment used for culturing were wiped with ethanol 70% vol. Then it was exposed to UV light for 15 minutes. The same protocol was repeated once the biosafety cabinet was cleared.

To the bacteria waste in liquid media, bleach 10%, was added for at least 30 minutes prior to disposal. The disposable consumables, in contact with the biowaste, were autoclaved and safely disposed of. The reusable equipment used for the experiments was cleaned by rinsing with 5% vol acetic acid solution for 15 minutes; then further washed with Alconox detergent. The pipes used in the process were flushed with 50 mL ethanol 70% vol and exposed to a recycled rinse of hydrogen peroxide 2% vol.

3.2.1 Biological Assays

A plate containing MacConkey-agar (without salt, Sigma-Aldrich) was inoculated with *P. vulgaris* (ATCC 8424, VWR) from a glycerol stock vial. The dish was incubated overnight at 37°C (Thelco Laboratory Incubator Precision). A bacterial colony was used to inoculate 50 mL of BactoTM Brain Heart Infusion (BHI) and incubated at 37°C while shaking at 180 rpm overnight using a New Brunswick Scientific I 24 Incubator Shaker. A 0.1 mL sample from the overnight bacterial culture was used to complete 250.0mL BHI scale-up process under the same incubation conditions for 3 hours to obtain metabolically active bacteria. The bacterial concentration was determined through a bacterial growth assay. From the 250 mL, BHI scale-up was harvested with *P. vulgaris* for inoculating 250.0 mL of basal synthetic human urine (BSHU). Harvesting includes initial

concentration selection and rinse, separated from the media, rinsed three times using 0.85 % NaCl solution, and centrifuged at 3,900rpm for 10 minutes.

3.3 Electrode Cleaning and Maintenance

The electrode potential was controlled using a BioLogic VMP3 multichannel potentiostat with a SAS low-current option attachment. Electrochemical cell arrangement consisted of a three-electrode system unless otherwise specified. The working electrodes (WE) were a polycrystalline Pt wire with a spherical ending and a BASI© Ni electrode. The counter electrode was coiled polycrystalline Pt wires. Potentials were measured against a Hydroflex® reversible hydrogen electrode (RHE). The Pt electrodes were cleaned using a butane torch for flame annealing and rinsing in nano-pure water, removing impurities from the working and counter. A BASI© Ni electrode was polished with alumina down to 0.05 micron. The working electrodes also were electrochemically cleaned by cycling in 0.5 M H_2SO_4 solution at a potential window between 0.05 V and 0.8 V and different scan rates, depending on each system characteristic, until a reproducible clean Ni and Pt voltammograms appeared. The RHE was stored in nano pure water when not in use, and the hydrogen cartridge from the RHE was changed periodically to provide reproducible results.

3.4 Electrochemical Surface Area (ECSA)

The electrochemical surface area or ECSA is an electrochemical measure of the extent to of the electrode surface undergoes electrochemical contribution. ECSA is calculated with the following equation (3.1):

$$ECSA\left(cm^2\right) = \frac{Q_E}{Q_R \times scan\ rate} \qquad \text{Eq. 3.1}$$

Here the Q_E (V A) refers to the experimental charge obtained from the integration of the peak signals associated with the hydrogen adsorption for the characterized metal, Q_R ($\mu C/cm^2$) is the theoretical charge density of the material, and the scan rate with units of V/s is the utilized velocity of sweeping the voltage in the cyclic voltammogram. The Pt electrode has a Q_R of 210 $\mu C/cm^2$. The Pt's Q_E is obtained from the hydrogen adhesion peaks observable in the cyclic voltammogram in Figure 3.1. The Ni electrode QR is 420 $\mu C/cm^2$ when using the β-method for characterization. The Ni's QE is obtained from the reduction peak observed in Figure 3.2.

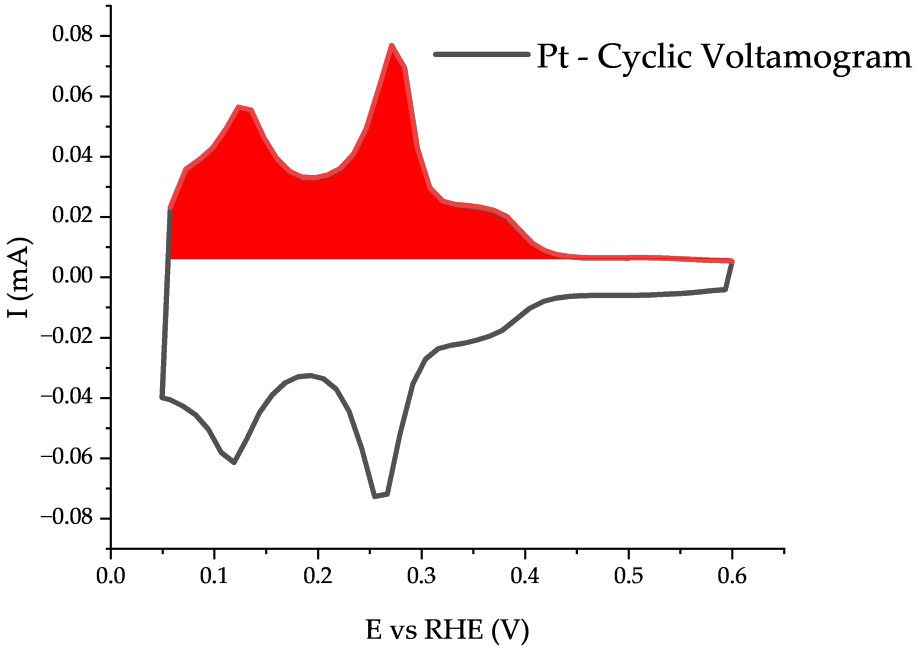

Figure 3.1. Cyclic voltammetry of a polycrystalline Pt wire with a rounded tip in a 0.5 M H_2SO_4 solution, highlighting in red the area used for normalization in the hydrogen desorption peaks.

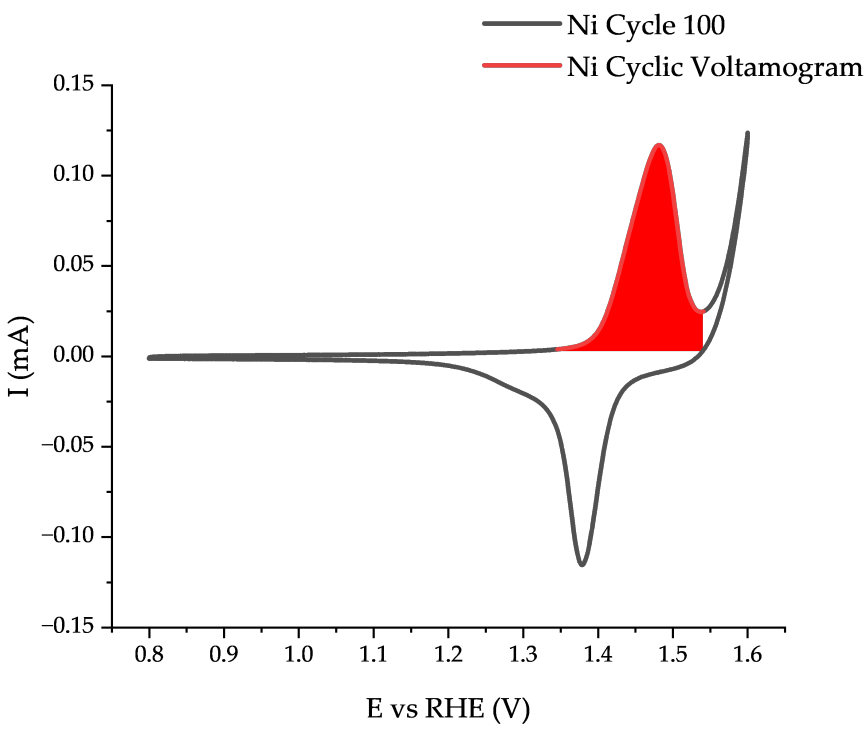

Figure 3.2 Cyclic voltammetry of a BASI© Ni electrode in a 0.1 M KOH solution, highlighting the area used for normalization in the reduction peak.

Chapter Four

4. Design and build an automated continuous *Proteus vulgaris* Bioreactor prototype using synthetic human urine.

This chapter studied the parameters required to design a bioreactor. Our design study started by evaluating the impact of a bacterial culture growth rate at different flow rates and with a pH control study. Alongside flow rate and pH control studies, we studied the effect of these factors on ammonia production from the batch cultures. Furthermore, we designed a pH controller that could control the culture's pH. Our results led to choosing a flow rate of 30% of the total volume of our culture every three hours (10% total vol per hour). Also, it indicates that pH control is highly beneficial in sustaining the *P. vulgaris* growth rate and ammonia production, which produce an ammonia oxidation current density higher than 17 $\mu A/cm^2$ for 24 hours of batch incubation.

4.1 Introduction

Worldwide water demand is foreseen to increase by 2050 from 20 to 30% of the current water requirement.[5] In recent times, 2 billion people have needed access to water services, and over 4 billion people need reliable sanitation reserves.[59] Consequently, a more efficient wastewater recycling system is needed to satisfy the water demand worldwide.[60] A possible solution to relieve the water scarcity relies on recycling human urine.

Another aspect that is under the scope of this investigation is that human urine is recycled during NASA manned Space missions. NASA relies on closed-loop spacecraft that have Environmental Control and Life Support Systems (ECLSS).[61] The current ECLSS water recovery system in the International Space Station (ISS) is capable of recycling approximately 90% of total wastewater generated, this includes the 74%-85% that can be recovered from human urine. [12,13] Nonetheless,

long-term space missions in the future will not be able to waste any resources. Hence, astronauts will be reliant on a more efficient recycling system. On the other hand, wastewater treatment and water recovery systems on earth are limited to about 87% water reclamation.[7] Each treatment has its advantages and constraints in terms of cost, efficiency, feasibility, and environmental impact. However, most modern systems rely on a combination of methods to achieve the desired water quality in a cost-effective manner.[9] As a consequence, our interest in providing a self-sustainable technology that benefits the ECLSS by focusing on water reclamation pathways is enabled. Among the various water recovery pathways included in the ECLSS, roughly 80% of the wastewater comes from human urine.

Human urine consists of water (95%), inorganic compounds, a variable percentage of organic metabolites, and urea (approximately 2%).[15] Inorganic compounds and organic metabolites can be removed by reverse osmosis or membranes.[16] Nonetheless, urea is a small uncharged molecule that is not easily removed from urine by means of size and charge exclusion. Other methods for urea removal include decomposition with strong oxidants, removal with adsorbents, and hydrolysis but these are not beneficial due to the process parameters requirements or matrix complexity incrementation.[23] Previous studies suggested the use of the enzyme urease to remove urea from the urine solution, which catalyses the urea hydrolysis, shown in reaction (4.1).[25] Nevertheless, enzyme instability due to unfavourable microenvironment factors prevents efficient removal of urea.[31]

$$NH_2(CO)NH_2 + H_2O \rightarrow 2NH_3 + CO_2 \qquad \text{Eq. 4.1}$$

Proteus vulgaris has proven to be a potential alternative to provide urease within a stable environment. This gram-negative, facultative anaerobic bacterium has the capacity to consume urea and metabolize it with urease. In contrast to other urease-containing bacteria, *P. vulgaris* can

be adapted to high urea concentration environments by increasing urea metabolization.[25] Using *P. vulgaris* for urea consumption ensures a constant and stable urease source for urea removal even at high pH.

P. vulgaris has been used in fed-batch and continuous flow bioreactor systems.[38] Two of the most common types of the bioreactor are the chemostat and perfusion systems. Both systems control and maintain bacterial growth parameters while allowing a continuous flow of fresh feeding media influx to the bioreactor.[33,36] The main difference between these systems is that the chemostat allows the outflow of the consumed media, by-products, and bacteria, while the perfusion does not permit bacterial outflow.[33] The bacteria outflow hindrance ultimately results in a microbial clot which is not the dilution of the system, approached with a general mass balance equation, Eq. 4.2. [33,62] Where $\dot{Q}$ is the flow rate of the influent and effluent, and δm/ δt stands for the accumulation of mass through time.

$$\sum \dot{Q}_{in} = \sum \dot{Q}_{out} + \frac{\delta m}{\delta t} \qquad \text{Eq. 4.2}$$

As urea is consumed in a chemostat system, ammonia is generated as the main product of the process. Nevertheless, ammonia remains toxic for human consumption, so its removal is required. Air stripping and biological nitrification/denitrification are two of the most popular ammonia removal techniques. However, conventional biological degradation does not have a good response to shock loads of ammonia, and air stripping provides acceptable results only at high pH conditions.[40]

A less common technique but of most convenient is the electrochemical ammonia oxidation reaction (AOR) process, which removes ammonia through electrochemical oxidation yielding elemental N_2 and H_2. Platinum (Pt) catalyzes the electrochemical oxidation of ammonia, shown in reaction (Eq. 4.3), at a potential of – 0.77 V vs. SHE and increases reaction efficiency.[63] Hence,

detecting ammonia with platinum would be beneficial for the end goal of electrochemically oxidize ammonia from the effluent.

$$NH_3 \rightarrow N_2 + 3H_2 \qquad \text{Eq. 4.3}$$

In the following work, we exposed different operating parameters for a shake-flask system which simulates a *P. vulgaris* chemostat bioreactor system. We provide base knowledge of the influence of flowrate in the *P. vulgaris* growth rate in the bioreactor system and the urea consumption. To study the urea consumption from the bioreactor system, we evaluated the ammonia oxidation peak current density at a polycrystalline Pt electrode in an electrochemical cell.

4.2 Experimental setup

This section explains the different experimental approaches performed to achieve this aim. It is divided into three sub-sections, 1) Determination of flow rate and pH control, 2) Evaluation of ammonia content in the effluent, and 3) Build a pH controller.

4.2.1 Experimental setup: Determination of flow rate and pH control

This section involves two types of methodologies, the bacterial growth assays and the chemical and experimental designs to study flow rate and pH control of the microbiological study.

4.2.1.1 Bacterial Growth

These sections explain the work regarding the bacteria preparation for flow rate experiments and pH control.

4.2.1.1.1 Bacterial Subculture

The process for bacterial subculture is the same as explained in Chapter 3.2.1. A summary of the process can be observed in Figure 4.1. Where the solid media is MacConkey, the liquid media is

BHI, the centrifugation separation after the bacterial growth assay is performed in saline solution. The bacteria inoculation ranges in the selection of $1x10^7$ cfu/mL and $1x10^8$ cfu/mL.

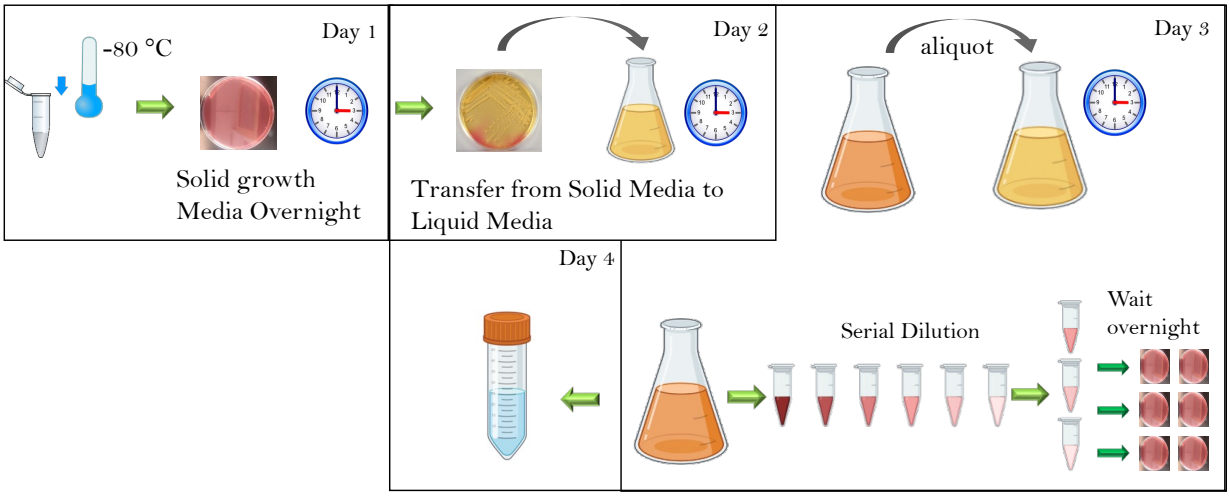

Figure 4.1. Flow chart of bacterial subculture process.

4.2.1.1.2 Bacterial Growth Assay

One mL was collected from 250mL of BHI culture to perform 1/10 serial dilutions with total volumes of 1mL. These dilutions were labeled as 10^{-1}, 10^{-2}, 10^{-3}, 10^{-4}, 10^{-5}, and 10^{-6}. Triplicates of 0.1mL from specific dilutions were spread into MacConkey agar plates. Control solutions without bacteria were also plated.

Plates were incubated at 37°C overnight. Using Eq. 4, the bacterial colonies were counted, and the concentration was calculated using the Colony-forming units per mL equation.

$$\frac{\text{CFU}}{\text{mL}} = \frac{\text{Number of Colonies x Total Dilution Factor}}{\text{Volume plated}} \qquad \text{Eq. 4.4}$$

The bacterial concentration obtained from the serial dilutions was used to calculate the desired initial bacterial concentration for the Bacterial Growth Curve Assay in synthetic human urine, using Eq 4.5.

$$C_1V_1 = C_2V_2 \qquad \text{Eq. 4.5}$$

Where:

C_1: Initial bacterial concentration obtained from the serial dilutions in BHI.

V_1: is the volume of the 250mL BHI culture that will be added to 250mL of synthetic urine culture

C_2: Diluted conetration, is the desired initial bacterial concentration of 1.0 x 107 cfu/mL

V_2: is 250mL of synthetic urine culture

4.2.1.1.3 Preparation media for bacteria: basal synthetic human urine (BSHU)

The BSHU was selected after a previous study of different synthetic human urines.[64] The BSHU media of the bioreactor is prepared by mixing the components in a 2000 mL volumetric in Table 4, followed by adjusting the pH to 6.20 while filling till the mark. The solution is then filtered using Corning® bottle-top vacuum filter system (polyether sulfone membrane, pore size 0.1 μm, filter capacity 1000 mL).

Table 4. Reagents used for the BSHU

Reagent	Amount per 1L ±0.001 (g)
Sodium chloride	5.844
Sodium sulfate	2.414
Magnesium chloride · $6H_2O$	0.651
Potassium chloride	2.832
Calcium chloride ·2 H_2O	0.444
Creatinine	1.018
Sodium citrate ·2 H_2O	2.000
Potassium phosphate monobasic	2.177
Magnesium sulphate ·$7H_2O$	0.789
Sodium oxalate	0.024
Uric acid	0.101
Sodium phosphate dibasic	0.923
Urea	16.816
NH4Cl	1.070
Sodium bicarbonate	1.134
D-glucose	2.000
Glyceraldehyde $C_3H_6O_3$	0.099
Iron (II) sulfate heptahydrate	0.001
Sodium phosphate monobasic · H_2O	0.562

Reagent	Amount per 1L ±0.0001 (g)
Aspartic Acid	0.0098
Threonine	0.0194
Serine	0.0423
Glutamic Acid	0.0072
Valine	0.0075
Methionine	0.0046
Leucine	0.0086
Tyrosine	0.0419
Phenylalanine	0.0140
Histidine	0.1692
Lysine	0.0192
Proline	0.0045
Glycine	0.1411
Alanine	0.0429
Isoleucine	0.0082
Taurine	0.1112
Cystine	0.0240

The shadowed components cannot be autoclaved.

4.2.2 Experimental design to study flow rate and pH control

4.2.2.1 Flow Rate

This process was performed in duplicate for each dilution rate. An initial bacterial concentration was inoculated in 250 mL of BSHU. The culture was incubated by shaking at 180 rpm, 37°C for 3 hrs. Then aliquots were collected every three hours from time 0 hours through time 12 hours and a final aliquot at time 24 hours to measure the bacterial concentration. One mL aliquot was collected from 250mL of BHI culture to perform 1/10 serial dilutions with total volumes of 1mL. These dilutions were labeled as 10^{-1}, 10^{-2}, 10^{-3}, 10^{-4}, 10^{-5}, 10^{-6}, and 10^{--7}. Triplicates of 0.1mL from specific dilutions were spread into MacConkey agar plates. Control solutions without bacteria were also plated. Plates were incubated at 37°C overnight. Bacterial colonies were counted, and the concentration was calculated using the Colony-forming units per mL equation.

After the aliquot was extracted, five different volume percentages were removed from independent cultures with a total culture volume of 250 mL. The volume percentages removed every three hours were as follow (A) 0%, (B) 10%, (C) 30%, (D) 50%, and (E) 80%. The volume removed from the 250 mL culture is equivalent to feed and effluent flow rate of 0.00 mL/min, 0.13 mL/min, 0.42 mL/min, 0.69 mL/min, and 1.11 mL/min, respectively. After removing the effluent, fresh BSHU was added to replenish the volume extracted and placed back in the incubator shaker until the next measurement.

4.2.2.2 pH control

This process was done in triplicate. An initial bacterial concentration of 1.0 x 10^7 CFU/mL were inoculated in 250 mL of BSHU. The culture was incubated shaking at 180 rpm, 37°C for 3 hrs. After three hours of incubation, aliquots were collected from h 0 through 12 within three hours. The aliquot served to measure the bacteria concentration and to measure and adjust the pH to 6.20

by adding HCl Solution. Then a proportional amount of HCl solution was added to the synthetic urine culture, and a new aliquot was taken to measure the new pH in the culture.

4.2.3. Experimental setup: Evaluation of ammonia content in the effluent

To evaluate ammonia content in the effluent first determined, the ECSA, as was discussed in Chapter 3.4 for Pt.

Then the obtained ECSAs were used for the proper normalization determination of ammonia oxidation current densities (AOC) from each electrochemical experiment. Culture samples were extracted at fixed times as described in section 4.3.2, then bubbled with inert N_2 gas for 10 min, and measured the AOC at 0.77 V vs. reversible hydrogen electrode (RHE) from CVs done at a scan rate of 10 mV/s in a potential window between 0.4 and 0.85 V vs. RHE, as seen in Figure 4.2. Blank measurements were taken from synthetic urine without bacteria and subtracted from the culture currents. The same protocol was followed to determine the storage time effect over samples stored in semi-closed 15 mL Falcon tubes. The discussed s protocol was used to assess different bioreactor variables that influence the electrochemically available ammonia in the effluent from the bioreactor experiments system.

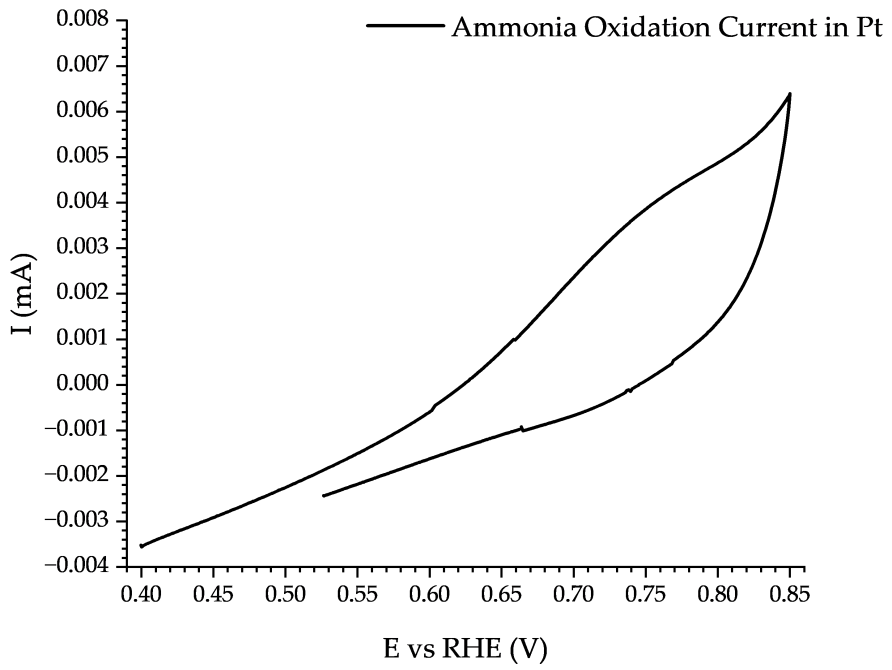

Figure 4.2. Cyclic voltammogram for ammonia oxidation current using Pt electrode in BSHU at a scan rate of 10 mV/s

4.2.4. Experimental setup: Build pH controller

To build the pH meter, uses of an Elegoo Uno, an analog processor for Arduino ®.[65] The circuitry design comprises the controller that monitors the changes in pH; whenever there is a change in pH higher than 6.5, the controller sends an electric signal to the relay, which activates the peristaltic pump (Gikfun 12V DC Dosing Pump Peristaltic from Amazon.com), which was adds a small volume of 4.0 M hydrochloric acid (HCl) solution, prepared from concentrated 12M HCl. The pH controller experiment consisted of stirring a solution with methylene red which was used to prove

the system worked as a visual indicator of pH changes. [66] The pumped solution would change the pH of the solution, hence the color of the solution would change.

4.3 Results and Discussion

This section will describe the analysis and explain the different experimental results achieved for this aim.

4.3.1 Result and Discussion: Determination of flow rate and pH control

The first guess for the flow rate was calculated by calculating the growth rate of *P. vulgaris* from hours 0 to 6 in batch culture. This estimation led to an initial flow rate of 80% of the total culture every 3 hours. In Figure 4.3, can be observed the contrast in the growth patterns of *P. vulgaris* after a culture volume of 250 mL for a single batch process, and a single trial of chemostat simulation, controlling the parameter of dilution rate through the removal of 80% of the culture volume and replenish it with new media. It can be observed that the Batch culture at the 24th hour did not have any viable bacteria. The culture, which was diluted and replenished with 80% of the total volume, had a bacteria concentration like the inoculation concentration. Performing this experiment in triplicate corroborates the behavior of *P. vulgaris* at a dilution rate of 80% of the total volume, as shown in Figure 4.4.

Even though we sustained the concentration of bacteria through time, the culture ammonia production is relatively low. An indicator of the low ammonia content is the low changes in pH values (see Figure 4.5). The culture did not increase the pH higher than 6.65, whereas, the BSHU stayed at approximately pH 6.4. Thus, the ammonia production is not high enough to increase the pH of the ammonia and ammonium equilibrium pH, 9.2.[16] This led to the exploration of new alternatives to flow rates. The flow rates studied in triplicate were batch cultures with 0%, 10%, 30%, and 50% of the total volume of the culture, 250mL. In Figure 4.6, bacterial cultures are

observed that the initial bacterial concentration (CFU/mL) was slightly higher for the 80% volume dilution than for the rest of the experiments with a dilution rate of 0%, 10%, 30%, and 50% total volume. We observed that diluting every 3 hours by 50%, 30%, and 10% of the total volume did not favor the life span of the bacteria at the 24th hour, as it did at 80%. Also, there is an inverse proportion between bacteria concentration and the dilution rate, observed in Figure 4.7, and associated with the increased extraction of bacteria and effluent, slowing the ammonia production process.

Exploring the influence of pH control through batch experiments for the bioreactor, we observed that the pH was the variable influencing the bacterial viability in the culture, because we observe, as seen in Figure 4.8, that the culture has viable bacteria concentration (2,000 CFU/mL) when it comes to the 24th hour. Hence, providing the bacteria with a more suitable environment between pH 5 and pH 8.[33]

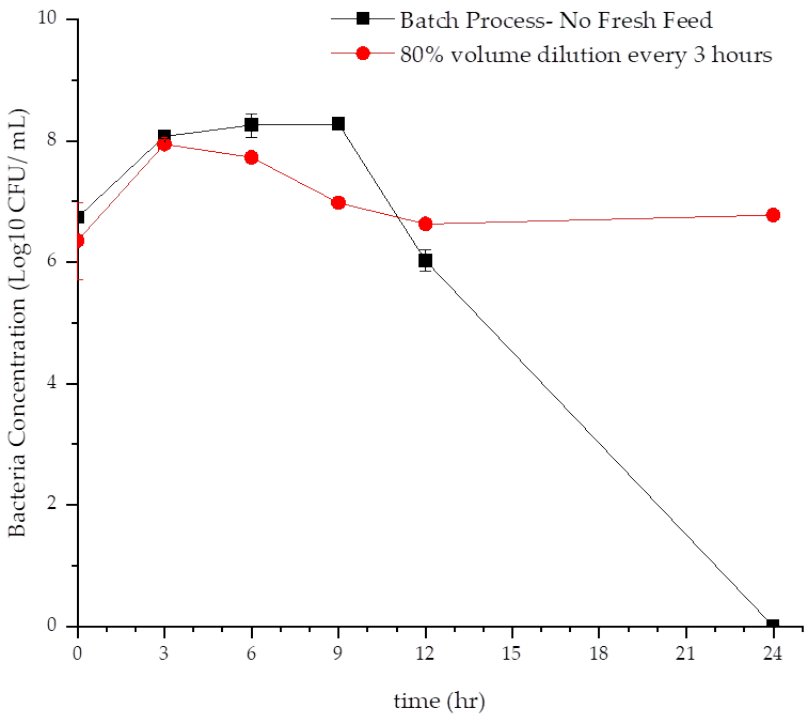

Figure 4.3. Bioreactor Dilution Rate Simulation Culture of *P. vulgaris* contrasted with Batch Culture of *P. vulgaris* in BSHU at a volume of 250 mL. The data shown is the single trial of 80% dilution rate (**red**) and batch process without adding fresh media (**black**). The initial bacterial concentration was adjusted to 10^5 CFU/mL. The samples present were taken before discarding and adding new media.

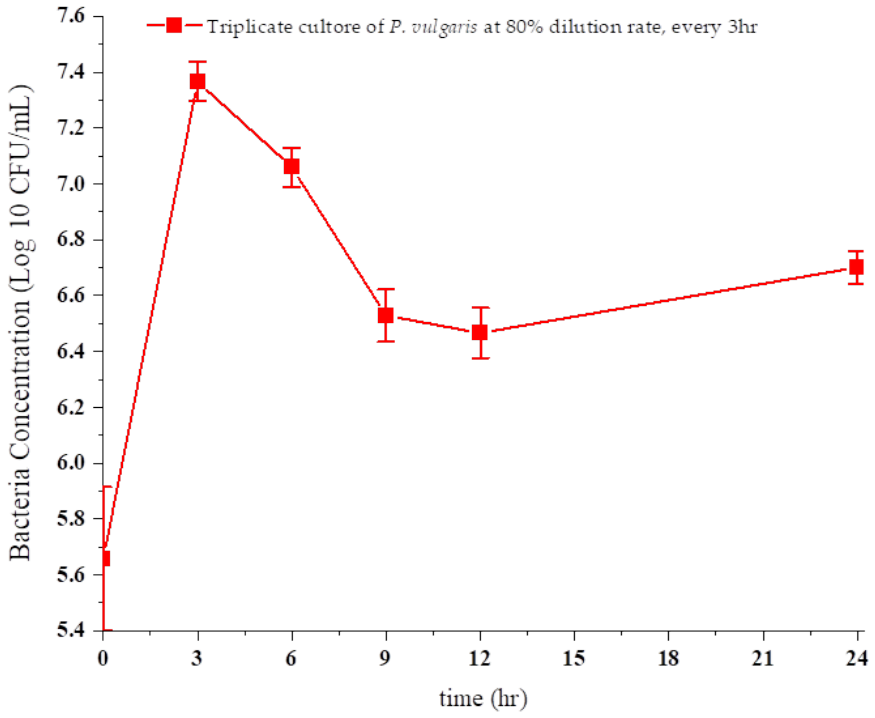

Figure 4.4. Triplicate of 80% Dilution Rate Simulation Culture of *P. vulgaris* in BSHU.

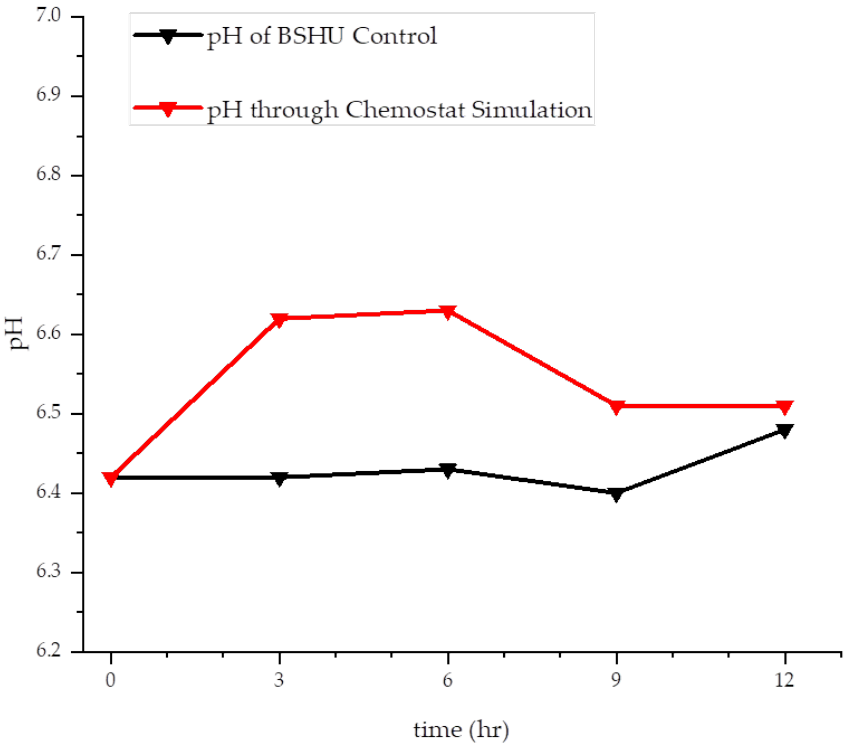

Figure 4.5. Measurements of pH through time for Bioreactor Dilution Rate Simulation Culture of *P. vulgaris* (**red**). The pH of BSHU Control through time (**black**).

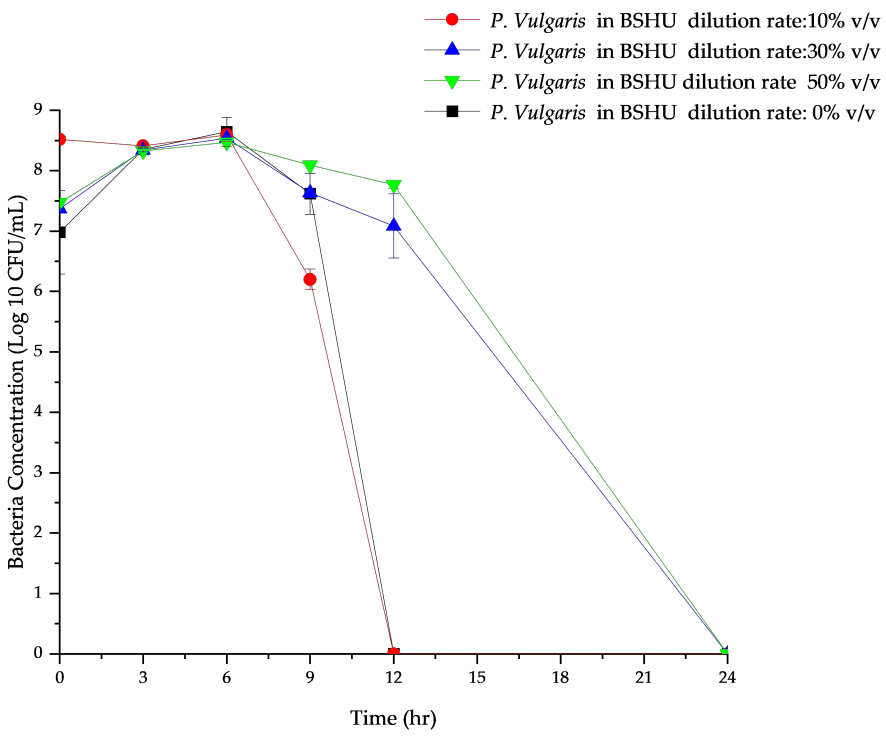

Figure 4.6. Bacterial growth rate from Chemostat simulation with *P. vulgaris* in BSHU at different dilution rates. Every 3 hours up to 12 hours were removed and replenished at 0%, 10%, 30%, and 50% of the culture volume.

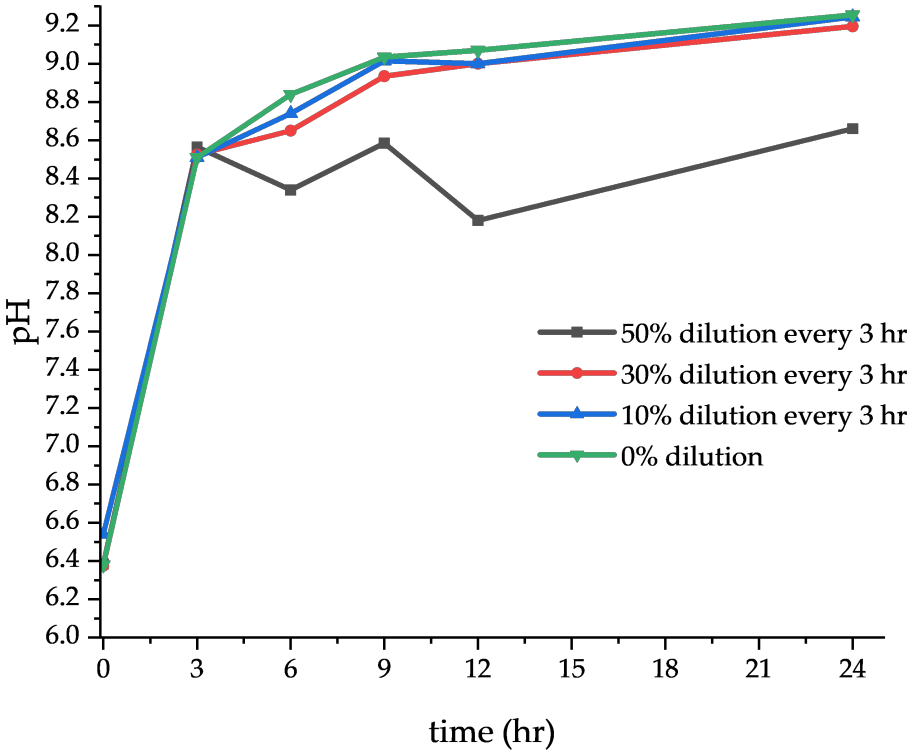

Figure 4.7. Measurements of pH during the dilution experiments. The experiment was performed twice. First trial: pH was measured every 3 hours, until 12 hr, and 24th hr. The second trial pH was measured at hours 0, 3, 9, and 24. On average, the initial pH was 6.42.

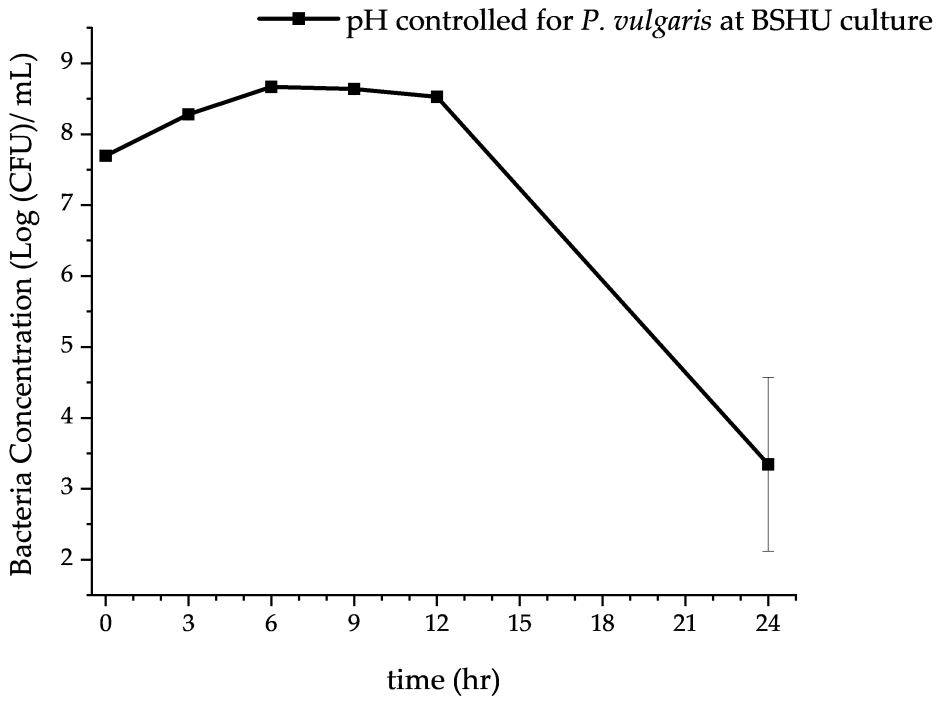

Figure 4.8. The growth rate of *P. vulgaris* during pH control experiment for batch BSHU culture.

4.3.2 Result and Discussion: Evaluation of ammonia content in the effluent

The evaluation of ammonia detection through the electrochemical method allowed us to observe the viable amount of ammonia produced by the bacteria.

The ammonia oxidation current obtained for the flowrates of 10%, 30%, and 50% of the total volume every three hours, as shown in Figure 4.9, observed that ammonia production did not follow a direct correlation to the increase of dilution rate. However, since the system is open, it allows the ammonia in the system to escape from the flask as time passes. Hence, in the short term, the lower amount of dilution would lead to the largest amount of ammonia, and a high dilution rate would cause lower ammonia production. The ammonia concentration at the 24th hour is higher for

a 50% volume dilution because it was left with the largest quantity of fresh media without extracting or interfering with the ammonia production from the bacteria.

The ammonia oxidation current was highest with a current density of approximately 25 μA/cm^2 during the batch experiment for the pH control, as shown in Figure 4.10, while for the dilution experiments was approximately 16 μA/cm^2. This was because there was no significant extraction of media while sustaining the bacteria alive for the longest period. Hence, a large amount of ammonia is produced.

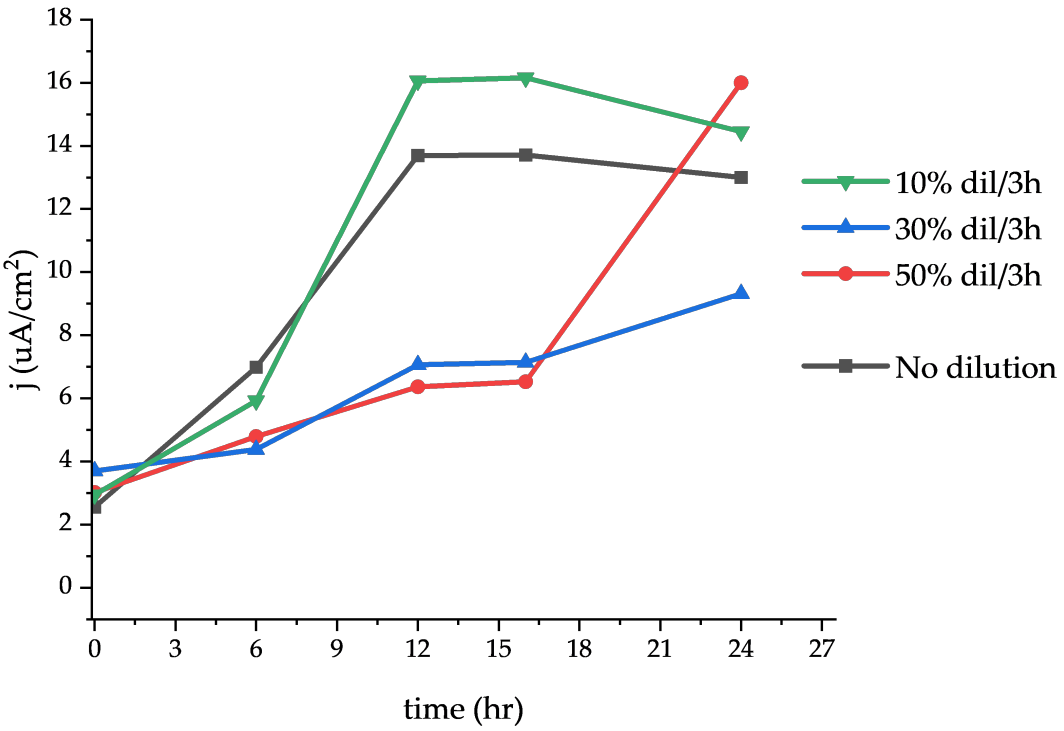

Figure 4.9. AOC density as a function of time for different dilution ratios. Data extracted from CV recorded from 0.4-0.85 V vs RHE. Peak current densities was taken at 0.77 V vs. RHE, at a scan rate of 10 mV/s.

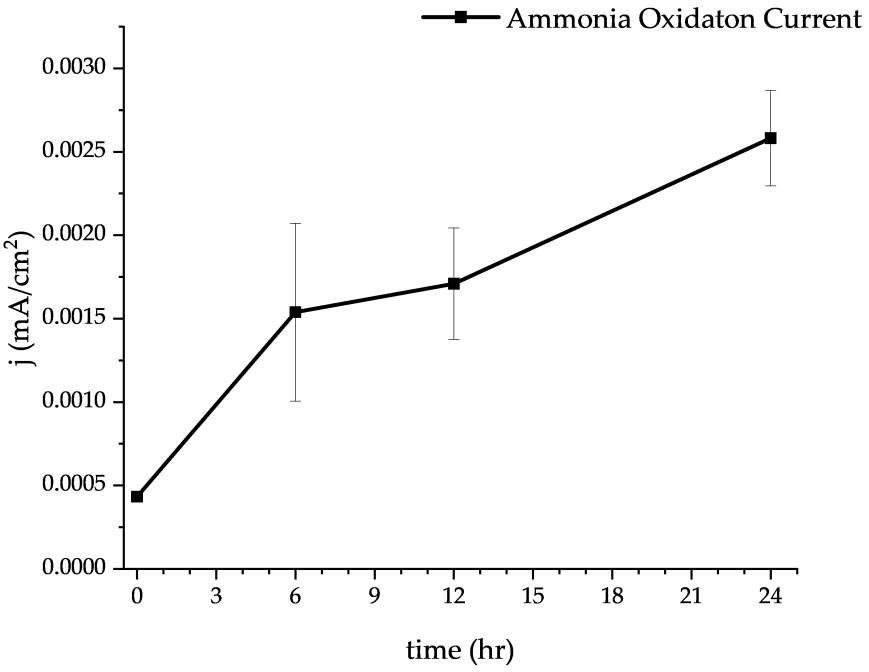

Figure 4.10. Ammonia oxidation from batch culture controlling pH. AOC measurements were taken before adjusting pH.

4.3.3. Result and Discussion: Build pH controller

The creation of a pH controller was possible after several programming iterations and using a base guide for coding Arduino ® for a pH meter. [65] The resulting circuit was able to measure the pH, which was shown in a PC that was required to power the controller and the circuit. The pump connected to a solution of 4 M HCl and accurately turned on to pour the acidic solution into the basified solution. Whenever the solution reached a pH higher than 6.5, the visual indicator, methyl red, turned yellow, and the pump added acid, turning the solution red/fuchsia, see Figure 4.11.

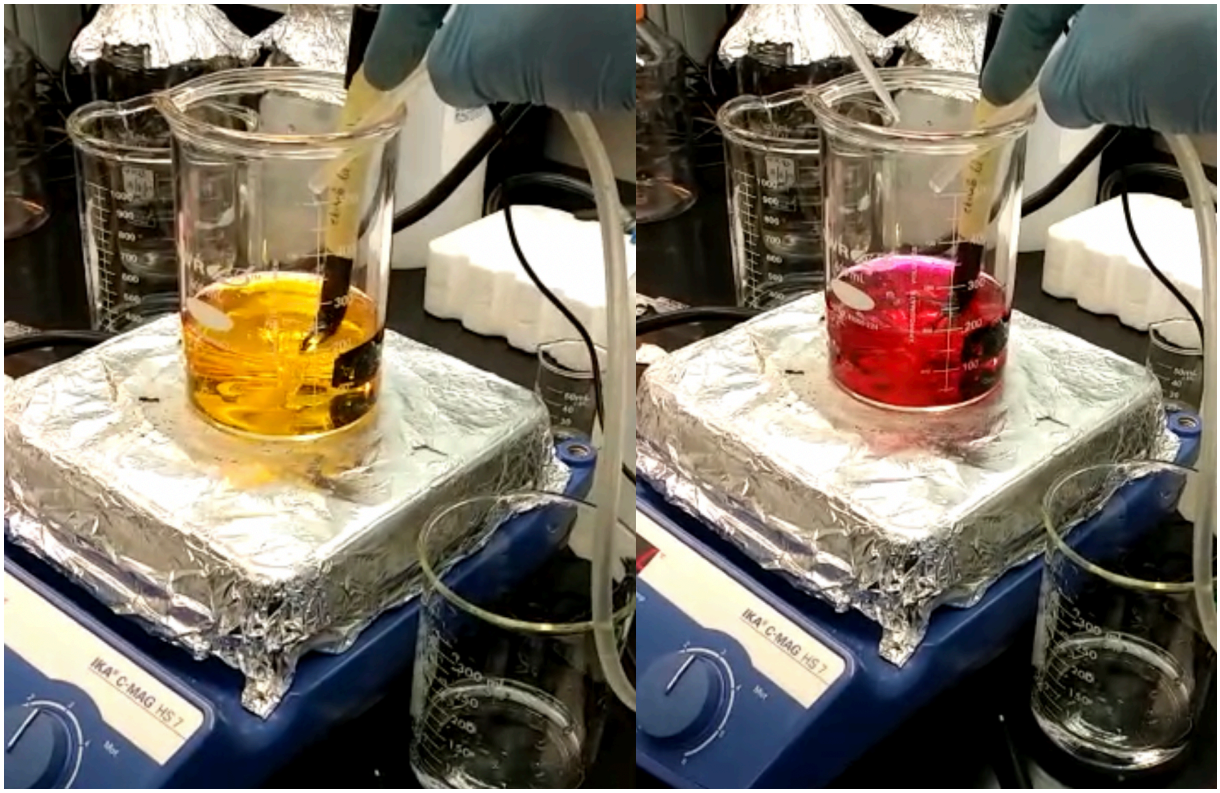

Figure 4.11. The pH controller changes the solution from basic (yellow) to acidic (Fuchsia).

4.4. Chapter Four: Conclusions

The results obtained through this chapter prove that it is feasible to design a continuous bioreactor that follows the chemostat design. It was shown different flow rates at which a bioreactor could operate and evaluated the possible outcome of each flow rate. Obtaining that the optimal flow rate would be slow, we decided to proceed using a flow rate equal to the 10% volume of the bioreactor total culture volume. Furthermore, we proved that controlling the pH for this system is beneficial since we will obtain higher ammonia production if the pH is controlled.

Since we plan to eliminate the produced ammonia from the effluent stream, the ammonia oxidation current was measured for the effluent of the different case studies. Obtaining an ammonia oxidation current of 16 $\mu A/cm^2$ and 25 $\mu A/cm^2$ for the dilution and pH studies, respectively.

Chapter Five

5. Proving that a *Proteus vulgaris* bioreactor, in combination with an ammonia oxidation reactor, can consistently treat real human urine and that the process can withstand microgravity operation.

This chapter demonstrates the resulting effluent from the bio-electrochemical system has significantly reduced ammonia and urea concentration when testing synthetic urine feed streams using basal synthetic human urine (BSHU).[67] Furthermore, a zero-gravity parabolic loop flight test with bioreactor-treated synthetic urine has validated the bio-electrochemical system. In addition, the bio-electrochemical system was used with real human urine, and results were reported in ICES 2022.[67] Overall, this chapter presents the potential of a continuous flow through a bio-electrochemical system that can improve the lifetime and durability of the water recovery system used in closed-loop living environments.

5.1. Introduction

Terrestrial water recovery and wastewater treatment systems are limited to about 87% efficiency.[7] The consistent loss of water during recovery is not sustainable for far-field missions. Subsequently, our interest is to reduce this water loss by combining biological and electrochemical technologies such that a self-sustainable system that benefits the ECLSS is enabled.

Urine is conventionally stabilized by adding pre-treatment chemicals (chromium trioxide and sulfuric acid) to the waste collection system. Water is then retrieved from the pre-treated urine by the Vapor Compression Distillation (VCD) subsystem within the Urine Processor Assembly (UPA) onboard the ISS.68,69 The solid by-products left in the VCD are a direct result of the presence of urea in the urine; these solids represent a large fraction of the water lost during the

operation of the current system. Other methods to eliminate urea from wastewater include decomposition with solid oxidants, reduction with adsorbents, and hydrolysis. Still, these are not beneficial due to the complex process parameters requirements. Incorporating a microbial urease to consume the urea from the urine electrolyte via reaction (5.1) can greatly reduce the amount of water loss during VCD.

$$NH_2(CO)NH_2 + H_2O \rightarrow 2NH_3 + CO_2 \quad (5.1)$$

Enabled by *Proteus vulgaris*, a gram-negative, facultatively anaerobic bacterium, it can efficiently consume and metabolize urea. This bacterium adapts to high urea concentration environments by increasing urea metabolization.[25] Using *P. vulgaris* in a bioreactor system provides a stable source of urease for urea removal. As urea is consumed in a bioreactor, ammonia is generated as the main product of the process. Once ammonia is produced, techniques such as air stripping and biological nitrification/denitrification can be used to remove it from the bioreactor effluent. This chapter focuses on investigating an electrochemical ammonia oxidation (AO) reaction process to remove the decomposing ammonia to N_2 and H_2.

Platinum (Pt) is used to catalyze the electrochemical oxidation of ammonia (at the anode), shown in reaction (5.2), at a potential of – 0.77 V vs. SHE, and increases reaction efficiency. [44,55] At the same time, water is simultaneously reduced at the cathode according to reaction (5.3), at a standard potential of -0.82 V vs. SHE.[69]

$$2NH_3 + 6OH^- \rightarrow N2 + 6\,H_2O + 6e^- \quad (5.2)$$

$$6\,H_2O + 6\,e^- \rightarrow 3\,H_2 + 6\,OH^- \quad (5.3)$$

The interactions among these reactions on any given electrode are intricate functions of the local conditions (*i.e.,* pH, temperature, catalytic surface area, etc.). Substantial research has been done

in this area, so the fundamental behavior of AO for highly efficient power sources and electro-reactors is well understood.[70,71]

The following work describes the automation of an ammonia shake flask system as chemostat bioreactor. Also, coupling the electrochemical ammonia oxidation to the bioreactor chemostat system consolidates the process of water recovery from human urine. The following study is built in collaboration with Faraday Technology Inc.[67,72] by demonstrating the feasibility of the combined system to withstand microgravity operation and perform consistently through simulating and real urine operations.

5.2. Experimental setup

This section explains the different experimental approaches performed to complete this aim. It is divided into three sub-sections, 1) Automated Bioreactor with BSHU, 2) Evaluate the compound system of bioreactor effluent and ammonia oxidation cell for microgravity environment, and 3) Automated Bioreactor with real human urine (RHU).

5.2.1. Experimental setup: Evaluate the automated shake-flask bioreactor with basal synthetic human urine (BSHU).

The BSHU media of the bioreactor is prepared by mixing in a 2000 mL volumetric flask, simultaneously adjusting to pH 6.20 until filling the mark. The solution is then filtered using Corning® bottle-top vacuum filter system (polyether sulfone membrane, pore size 0.1 μm, filter capacity 1000 mL). The experimental setup is based on a general chemostat flow system (Figure 1a). Then a 500 mL Erlenmeyer flask was filled with 250 mL of BSHU coupled with a pH electrode (Orion 8157BNUMD ROSS Ultra pH Triode) and three plastic tubes (Tyson-EE3603), Figure 1b. The samples were taken to monitor the bacterial concentration within the Bioreactor at the beginning of the experiment, denominated as hour zero. To monitor the bacteria concentration

through time, this process was repeated in selected 3 hours intervals for twenty-four-hour periods in triplicate to assure repeatability through the core process. The culture flask was placed inside an incubator shaker, Figure 5.1 at 37°C and 180 rpm. There were pumps connected to the culture flask (Gilson Peristaltic Pump) that were set to turn on two hours after inoculation. The inlet flow and outlet flow were set to flow at 10% of the total culture volume, which was equivalent to 0.42mL/min. The flows were calibrated by measuring the time it took to fill a graduated cylinder to a certain water volume. To explore the system behavior for a larger time interval, this process was modified from 30 hours to 77 hours. The modification reduced the time samples were collected and halted the effluent flow for a period of 3 hours.

To explore the optimization process of the design, samples of the bioreactor's effluent were stored for a period of 24 hours and 72 hours contrast. The parameters of the batch reactor were at 20°C, 37°C in an incubator shaker, and 37°C in a static incubator.

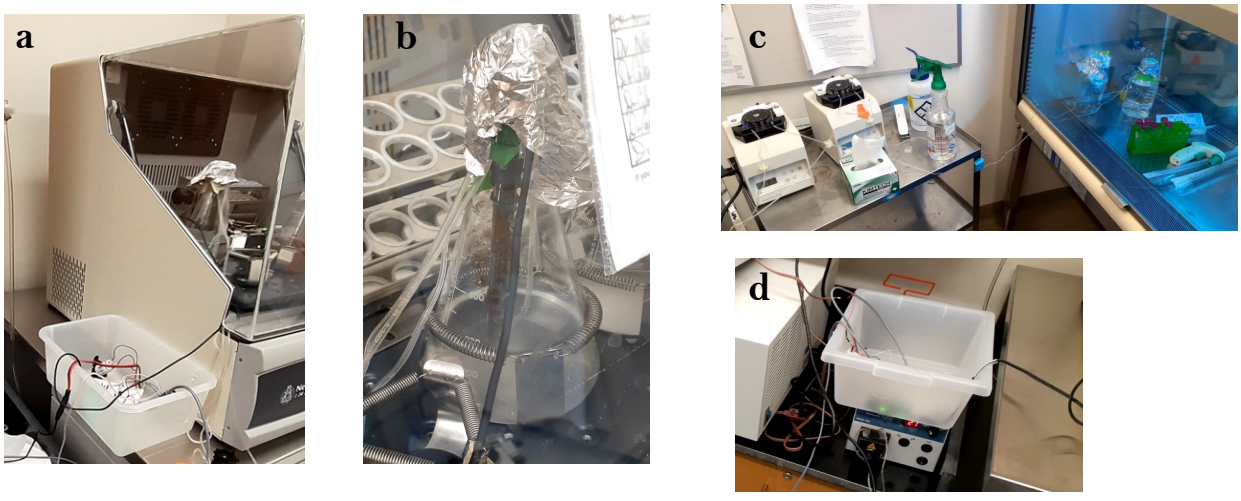

Figure 5.1. Assembly for Automated Bioreactor Simulation: (a) System interaction with incubator shaker, (b) Culture-flask with pH electrode and connected to pipes, (c) Feed and effluent Pump, and feed effluent bottles in a safety cabinet, (d) pH control with dispensing pump.

5.2.1.1 pH controller

The system was upgraded from the one mentioned in chapter 4. The pump was switched from Gikfun 12V DC Dosing Pump Peristaltic to a Welch Peristaltic Pump which provides a higher head force. The system was modified to enable the pump to turn on without the need for additional switches besides the relay. The peristaltic pump provided the inlet of a hydrochloric acid (HCl) solution to maintain a system pH under 6.50 with minimum volume. This was done through the usage of an ELEGOO UNO R3 board controller circuit and programmed using the Arduino® platform, the pH was monitored, and whenever the pH electrode detected a pH ≥6.50, the HCl solution was pumped into the flask lowering the media's pH. Furthermore, the program was upgraded to record each reading of pH and the time after the experiment started. Also, to validate the measurements of the controller at given times, the pH data were compared between the controller and an external bench pH meter.

5.2.1.2 Electrochemical Analysis of Automated Experiment with BSHU

A three-electrode electrochemical cell was used for all experiments. The electrode potential was controlled using a Biologic VMP3 multichannel potentiostat with a SAS low-current option attachment. The working and counter electrodes were Pt wires (WE with a spherical ending). Potentials were measured against a Hydroflex® reversible hydrogen electrode (RHE). The sulfuric acid solution was prepared from DI water (GEMINI-Ultra high purity water system) and Optima grade sulphuric acid reagent (Fisher).

Cyclic voltammetry (CV) was performed in 0.5 M H_2SO_4 to calculate the charge involved in the so-called hydrogen-under potential deposition region to determine the Pt electrode active surface area (EASA). The obtained EASAs were used for the proper normalization determination of ammonia oxidation current densities (AOC) from each electrochemical experiment. Culture

samples were extracted at fixed times, bubbled with inert N_2 gas for 10 min, and measured the AOC at 0.77 V vs. reversible hydrogen electrode (RHE) from CVs done at a scan rate of 10 mV/s in a potential window between 0.4 and 0.85 V vs. RHE. Blank measurements were taken from synthetic urine without bacteria and subtracted from the culture currents. The same protocol was followed to determine the storage time effect over samples stored in semi-closed 15 mL Falcon tubes.

5.2.2. Experimental setup: Explore ammonia oxidation cell in a microgravity environment.

The microgravity experiments were performed through parabolic flights in an aircraft owned by Zero-G. The Zero-G flight consisted of six (6) sets of five (5) parabolic loops, each set consisting of 30 s of zero gravity followed by 30 s of two times earth gravity. There is a 5 min earth gravity break between the 6 sets. When the parabolic loop reached zero gravity, a timer was manually triggered to collect the samples during the zero gravity moments. The samples were analyzed on the ground by ISE before and after the zero-gravity flight test.

The zero-gravity electrochemical flight test system designed by UPR and modified by Faraday was fixed in the Zero-G aircraft.[73] The box made of Makrolon®, shown in Figure 5.2a, is a triple containment system designed for a closed loop, dividing and containing the (1) supply of two synthetic urine folly bags and a waste collection folly bag, (2) the electrolytic cell, and (3) electrolytic cell effluent samples bag storage. The whole set-up was kept sealed in a polyvinyl chamber that immobilized the equipment. All parts of the system were tested to ensure functionality before starting the parabolas. The samples used for the microgravity experiment were two types of synthetic human urine. First, the BSHU samples, as discussed in an earlier section (5.2.1), and the second was not exposed to the bioreactor. The second synthetic urine assumes 90%

of urea conversion denominated as synthetic human urine (SHU), and the pH was adjusted to pH 9 but. [67, 72]

As a security measure, to ensure the removal of bacteria from BSHU prior to the microgravity flight test, it was filtered in triplicate with a 0.22 μm pore syringe filter (MilliporeSigma Millex-GP Sterile Syringe Filters with PES Membrane) and then was stored in folly bags. The SHU was filtered with a Buchner-Funnel and 100 μm pore size filters to remove any existent precipitate.

During the flight test, the folly bags were connected to a solenoid valve, which enabled ammonia reactor electrolyte flow from either the BSHU or SHU solutions, as represented in Figure 5.2b. During operation, the solutions flowed through a single-pass ammonia oxidation chamber (as described above) at fixed voltages of 6 V, 8 V, and 10 V. After either BSHU or SHU was passed through the ammonia reactor, it was stored in an empty waste bag, while samples were captured in 50 mL bags.

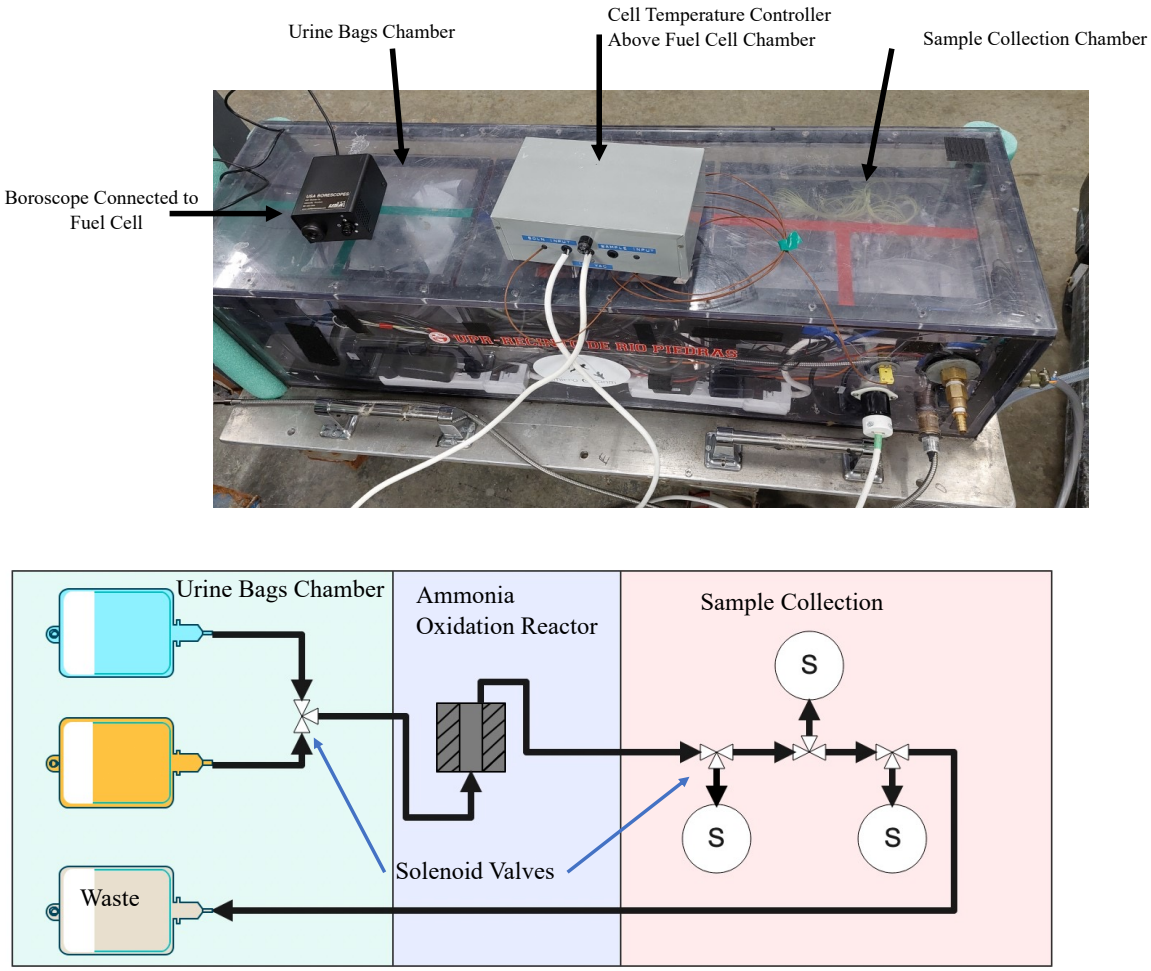

Figure 5.2. Equipment used in Microgravity flight: (Top) The Makrolon® box contains three smaller boxes with the bioreactor effluent and ammonia oxidation reactor (bottom) diagram of the equipment arrangement. From left to right, (1) BSHU and SHU folly bag, (2) ammonia oxidation reactor, (3) sample collection chamber.

5.2.3 Experimental setup: Evaluate the automated shake-flask bioreactor with real human urine joint with the ammonia oxidation reactor.

This section will explain the process used to develop the automated shake-flask bioreactor with real human urine, and the experimental process for the analysis of the electrochemical ammonia oxidation reactor.

5.2.3.1 P. vulgaris Growth Rate

The real human urine (RHU) was collected in 1L glass bottles and pre-treated before the Bioreactor was used. The human urine pre-treatment process involves centrifugation in batches of 50 mL at approximately 4,500 rpm for 10 min. The supernatant from the centrifuge tubes was collected in a sterile glass bottle which was later used to feed the bioreactor with fresh RHU. The experimental setup is based on a general chemostat flow system, as shown in Figure 5.3. This process is described in detail in Chapter 4.[67] In summary, a flask with 250 mL of RHU coupled with a pH electrode is placed in an incubator shaker at 37°C and 180 rpm. To evaluate bacteria growth, samples were taken from the effluent every 3 hours for 12 hours, 24 hours, and, finally, for 48 hours. The flask had connected three plastic tubes to provide a buffer solution, feed the solution to the flask, and remove the effluent, as shown in Figure 5.3a. For the experiments, two different pH controller solutions were used. First is the 4 M HCl solution, this contrasts with previous experiments with BSHU, section 5.2.1.[67] Aiming to explore alternatives to HCl that are easier to handle and transport, a 2M phosphate buffer (PB) at pH 1.86 was also evaluated. In all trials, the effluent was collected in a 1 L bottle, Figure 5.3b. To remove the precipitate and gross content of bacteria, the effluent is centrifuged three times which obtained the solutions shown in Figure 5.4c. Once the precipitate was removed through centrifugation from the processed RHU effluent, the first aliquot was used to measure the ammonia concentration using an ammonia Ion-Selective

Electrode (ISE) (Thermo Scientific™ Orion™ High-Performance Ammonia Electrode; and Thermo Scientific™ Orion™ Dual Star™ pH, ISE, mV, ORP and Temperature Dual Channel Benchtop Meter). We calibrated the ammonia ISE using standard ammonia solutions with the following ammonia concentration: 1 ppm, 10 ppm, 100 ppm, 1000 ppm, and 10000 ppm. Since we have concentrations above 1000 ppm, we modified the user's manual instruction and added 2 mL of 10 M NaOH for every 1 mL of Ammonia Standard ISA solution. Also, the pH was measured before and after measuring the ammonia concentration.

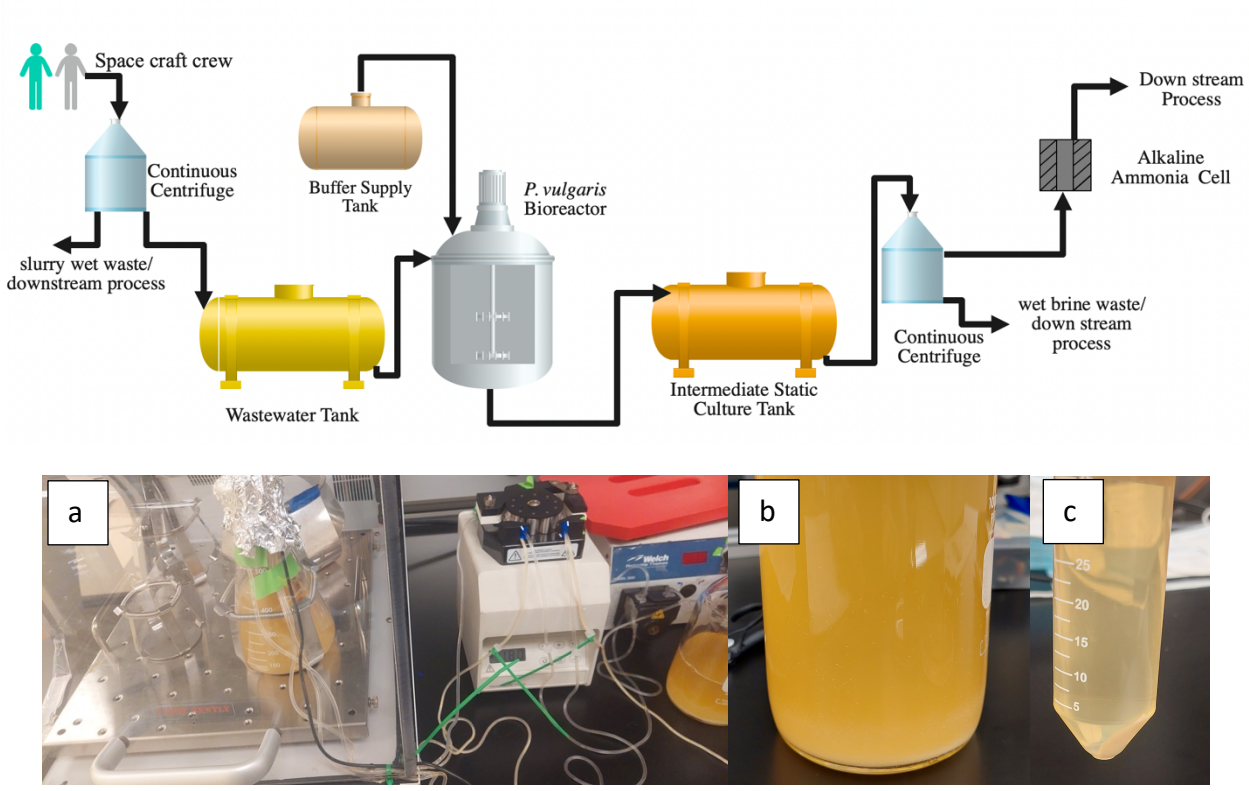

Figure 5.3. Continuous chemostat bioreactor and alkaline ammonia schematic: a) Shake-flask system used to simulate bioreactor, b) effluent collected, and c) centrifuged effluent with precipitate and bacteria at the bottom.

5.2.3.2 Electrochemical Analysis

The ammonia oxidation reactor was the same as Santosh *et al.,*[72] consisting of two graphite blocks that serve as the anode and cathode, two platinum foils with 5cm^2 in contact with the graphite block and exposed to the chamber separator, as shown in Figure 5.4a. During operation, Figure 5.4b has the system heated to 40°C, and the 50 mL of urine flowed in a closed loop which serves as a multi-pass flow (continuous recirculation). Before application of the voltage, we added 2 mL of NaOH 10 M to the RHU to bring the pH above 10. To measure ammonia removal efficiency from the bioreactor-treated RHU samples, we evaluated the current response through chronoamperometry at four different voltages: 4 V, 6 V, 8 V, and 10 V with a maximum current of 1 A. The time subjected to the samples was in the range of 2 hr to 12 hr. At the end of the process, the pH and ammonia concentrations were measured using an ammonia ion selective electrode (ISE).

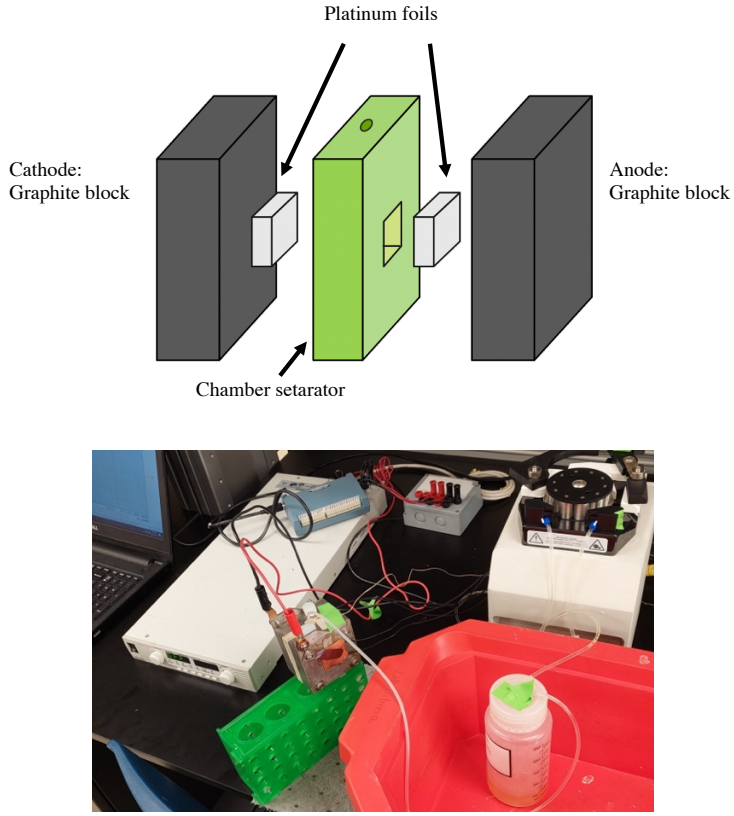

Figure 5.4. Ammonia Oxidation Reactor: (a) model of the ammonia oxidation cell and (b) multi-pass setup of the ammonia oxidation process.

5.3 Results and Discussion

5.3.1 Experimental setup: Evaluate the automated shake-flask bioreactor with basal synthetic human urine (BSHU).

This section discusses the results of developing the automated shake-flask bioreactor with BSHU regarding the growth rate behavior and the pH control results.

5.3.1.1 P. vulgaris Growth Rate

These experiments aim to understand the pattern of the *P. vulgaris* growth rate, which we associate proportionally with urea consumption when exposed to a continuous flow environment. In

Figure 5.5, the first successful attempt at running the automated process, we can observe that after allowing the two hours of inoculation to overcome the lag phase and enters the exponential phase of the bacterial growth, we started the flow rate. Resulting in a relatively small increase in the bacteria concentration due to the dilution and outflow from the culture flask. The presence of large error bars in Figure 5.6 is attributed to the first trial from the set of triplicates, which was inoculated with higher bacteria concentration than the other two trials. We observed that the two initial bacteria concentration used for the continuous flow system behaves alike but with a different maximum in bacteria concentration. This is true for the bacteria growth rate before the fifteen (15) hours, which means that at the early stages, the bacteria are overgrowing the flow rate at which it has been exposed. However, we observed a decrease in the growth rate pattern of *P. vulgaris* under these conditions, we attributed this to the fact that the flow rate could not be evenly controlled between the feed and exit.

The estimated flow rate difference between the pump and the pump effluent was estimated to be 0.05mL/min. This was assessed from the initial volume (250mL) and the volume difference in the 24^{th} hour. The flow difference was not resolved. Since it is attributed to the height differences (0.61 m) between the culture flask located in the incubator shaker to the fresh BSHU bottle and effluent container located in the Biosafety cabinet at a lower height. Since the effluent pump requires slightly less work to flow down toward the effluent container.

To explore the robustness of the process, the experiment period was extended from thirty (30) hours (Figure 5.6) to seventy-seven (77) hours (Figure 5.7). The required modification for the process allowed the bacteria to grow back and simultaneously supply time to fill up the flask. This step provided enough time to sustain the system CFU but was not enough time to completely fill the tank. The difference in flow rate between the feed and the effluent causes the shake-flask to

empty faster rate. However, this proves that the use of *P. vulgaris* in the continuous system is robust enough to withstand changes that cannot be controlled.

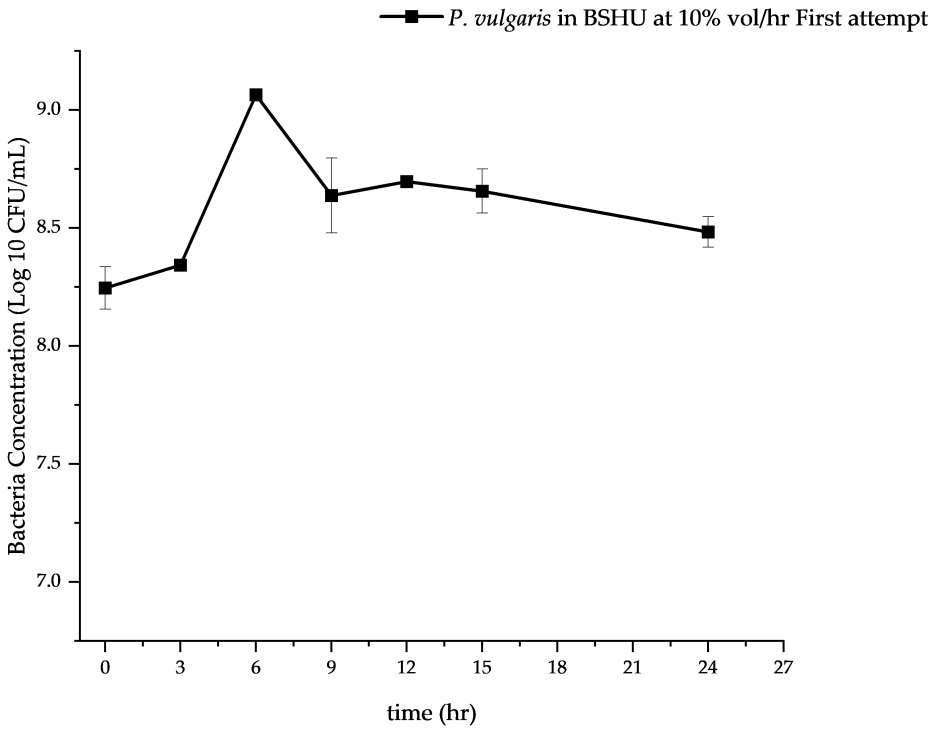

Figure 5.5. *P. vulgaris* growth rate in the shake-flask bioreactor. The first attempt of the automated shake-flask bioreactor system in BSHU media.

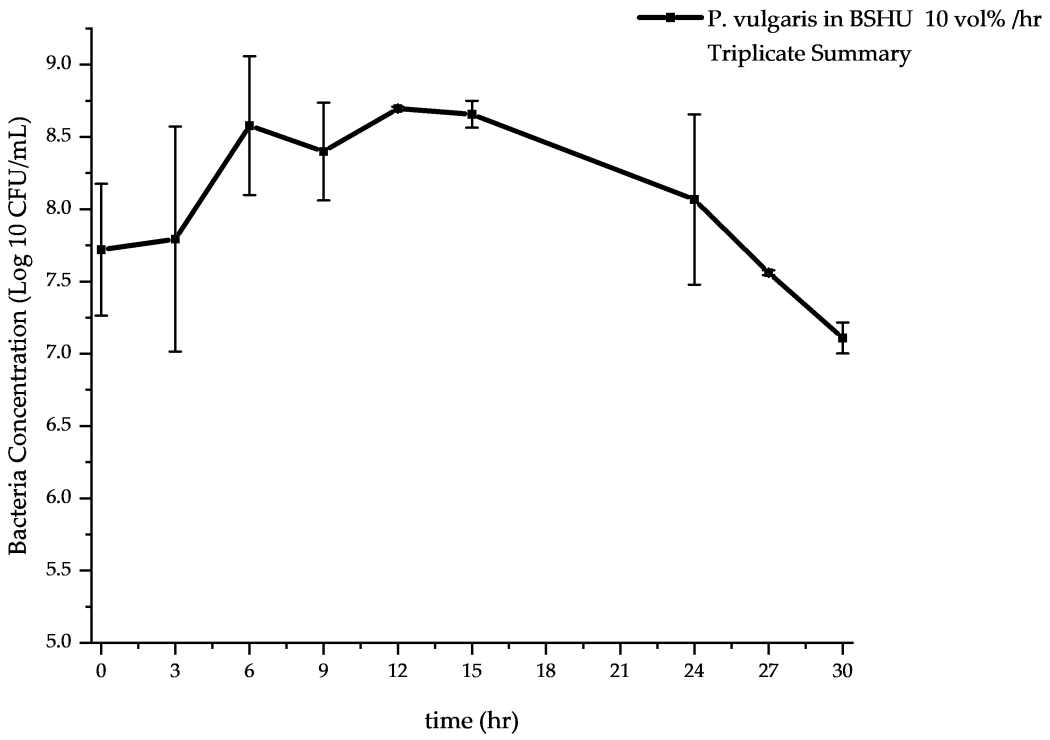

Figure 5.6. *P. vulgaris* growth rate in shake-flask bioreactor. Triplicate of the automated shake-flask bioreactor system in BSHU media.

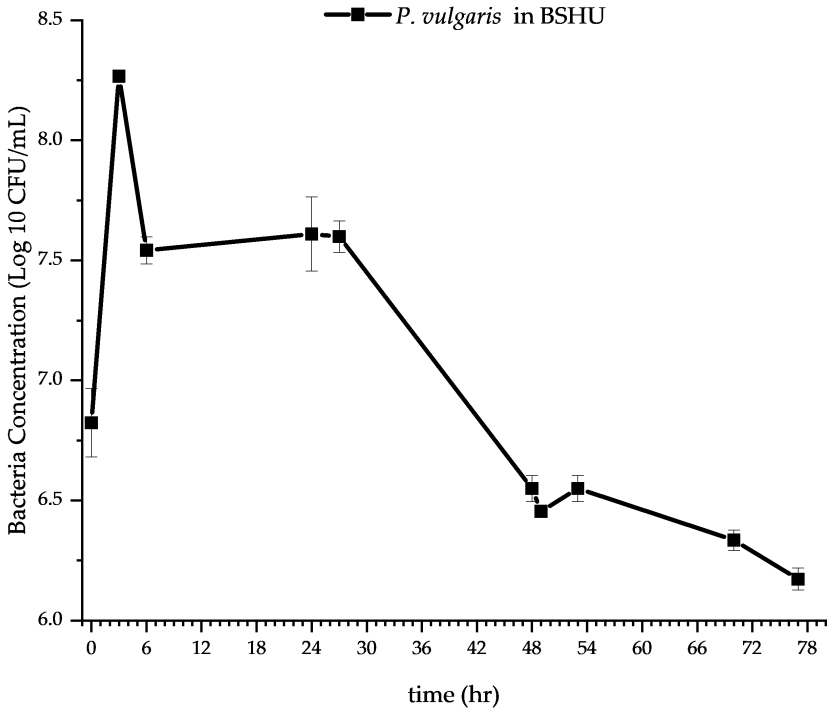

Figure 5.7. Bacterial growth rate from Chemostat simulation with *P. vulgaris* in BSHU for Continuous 77 hours. The synthetic urine flow rate is equivalent to 10% volume/hour of the culture's total volume (is equivalent to a 0.42mL/min flow of synthetic urine).

5.3.1.2 pH control

The pH controller provides us with an alternative way to evaluate and monitor the bacteria's metabolic profile throughout the extent of the experiment, Figure 5.8. If we contrast the bacteria concentration at given times from the triplicate study and the pH response, this provides a similar pattern in both monitoring approaches. Since on both, we can observe that during the inoculation phase and after the 20^{th} hour, the pH response corresponds to a bacteria concentration on the CFU order of 10^7, equivalent to Log CFU = 7. Furthermore, during the period of high bacteria concentration (3rd to 15th hour), we observe that the need for pH adjustments is high. In

Figure 5.8, we observe that there are undifferentiated measurements of pH, which indicates, a high ammonia production interacting with the pH controller. Since ammonia's pKa =9.2, the increase in ammonia concentration promotes an increase in the pH in the system that is originally at pH 6.2. The large ammonia production rate can be linked to the large concentration of bacteria in the media consuming urea. We also observe that there is a small signal in the range of pH 5.4, which comes from electrical interference from the controller. As a result, every time the pH meter detects pH≥ 6.50, the controller circuit uses power from the electrode grid to activate a relay, which in turn provides a false pH value. Nevertheless, values obtained from samples of the culture were taken at different times to measure in an external bench pH meter, Table 5. The measurements from the pH electrode in the circuit hand an accuracy of pH ±0.05.

Table 5.1. The contrast of pH values from the sensor of the pH controller vs. a benchtop pH meter

Time	pH Controller	Bench top pH meter
3	*6.34*	*6.34*
6	*6.54*	*6.46*
9	*6.53*	*6.47*
22	*6.64*	*6.37*
27	*6.29*	*6.43*

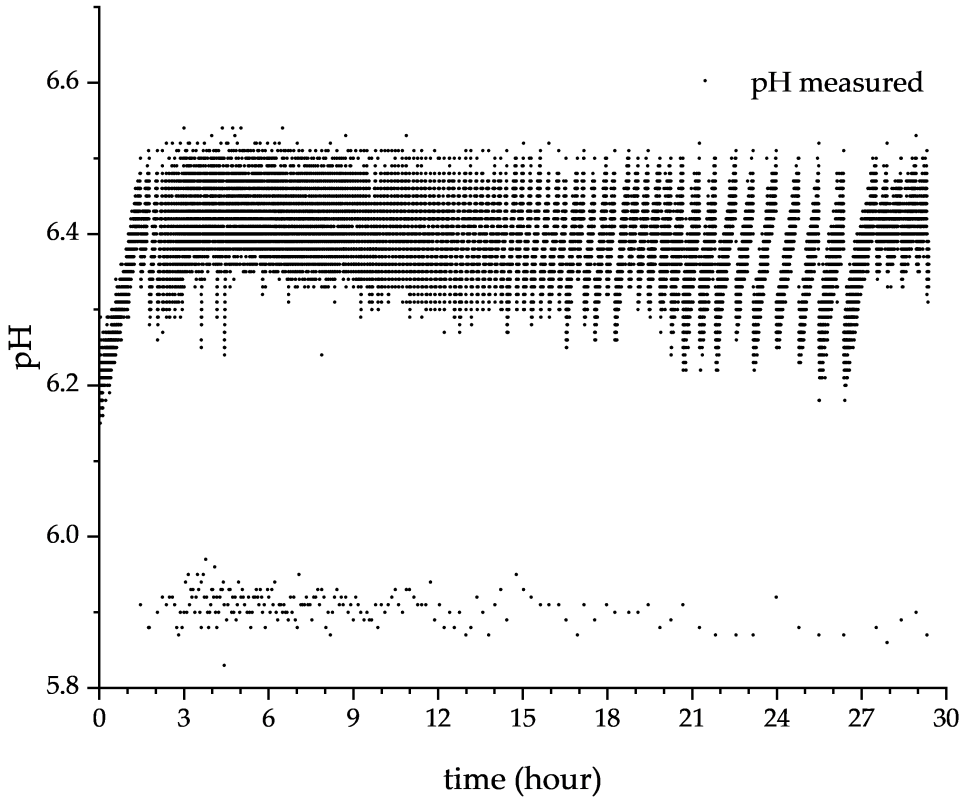

Figure 5.8. The pH vs. time measurement in a single automated *P. vulgaris* culture trial from the triplicates. The measurement of pH was recorded until the 30th hour of the experiment. Each data point was taken in an interval of approximately 3 seconds. This measurement was connected to the pH controller, which added BSHU at a flow rate of 0.42 mL/minute.

5.3.1.3 Electrochemical Analysis

Cyclic voltammetry was performed on extracted culture samples, and the values at 0.77 V vs. RHE were taken as ammonia oxidation signals. Even though the automated system proved the use of *P. vulgaris* robust enough to withstand the changes that could not be controlled in the shake-flask setup. It was found by electrochemical measurements that the amount of urea hydrolyzed by the bacteria at this dilution ratio was not enough to reach the approximately 16 μA/cm^2 ammonia

oxidation current achieved in batch experiments, as presented in Figure 5.9. This fast urea replenishment makes it difficult to obtain a suitable AOC since it is known the passivating effect of urea on Pt catalysts, especially when higher concentrations than 0.28 mM are present.[16]

To boost ammonia production and favors a noticeable feature for ammonia oxidation, we increased the *P. vulgaris* exposition time with the matrix in semi-closed falcon tubes at 37 °C and measured the AOC after the 72nd hour of storage. The approach of a serial reactor led to higher yield this can be observed in the ammonia oxidation current densities for each bioreactor extracted sample, Figure 5.10. After the 6th hour of incubating in the automated bioreactor, the ammonia produced from the effluent further incubated reaches a plateau.

Further experiments showed that even more ammonia could be oxidized by improving the storage conditions. For instance, at room temperature (20 °C) conditions and without shaking (static), the tubes resulted in a 150% increase in the current density, Figure 5.11, in contrast to incubation for the same period at 37 °C. Providing a better alternative to incubate at lower temperature conditions since it would preserve energy by lowering the energy input required for the in-sequence bioreactor for the period of 72 hrs of incubation. Thus, creating a two-step incubation system that has the potential to be a continuous stop-flow process.

As for the incubation conditions at 37ºC, the maximum current of approximately 16 μA/cm^2 is reached at 24h, and after that time, if the period of incubation is increased to 72 hrs, the current density increases by 2 μA/cm^2, which is not that no significant additional amount of ammonia is produced for total energy invested, as observed in Figure 5.12.

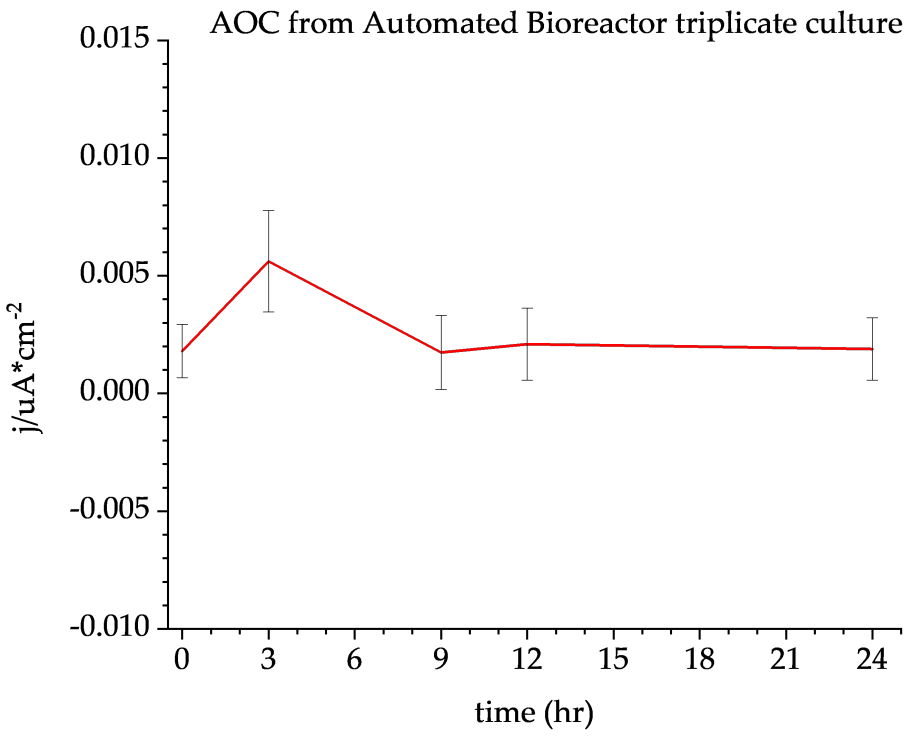

Figure 5.9. AOC as a function of time in a chemostat simulation. At a flow rate of 0.42 mL/min. Data extracted from CV was recorded from 0.4-0.85 V vs. RHE. Peak current densities were taken at 0.77 V vs. RHE. Scan rate 10 mV/s. Ammonia oxidation in stored cultures.

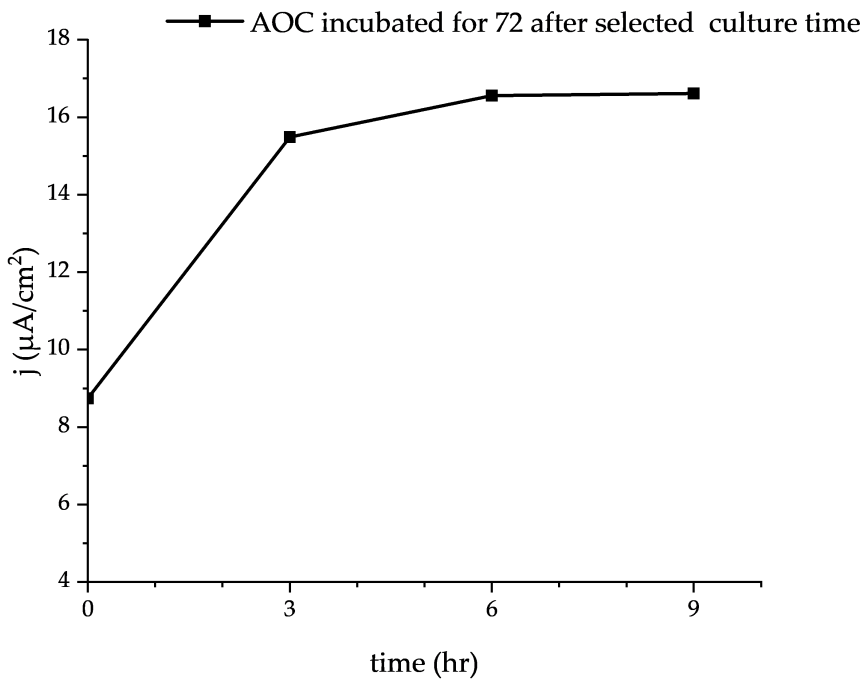

Figure 5.10. AOC after 72 h of storage time. Measurements correspond to samples extracted at 0, 3, 6, and 9 h of culture *P. vulgaris* bioreactor time.

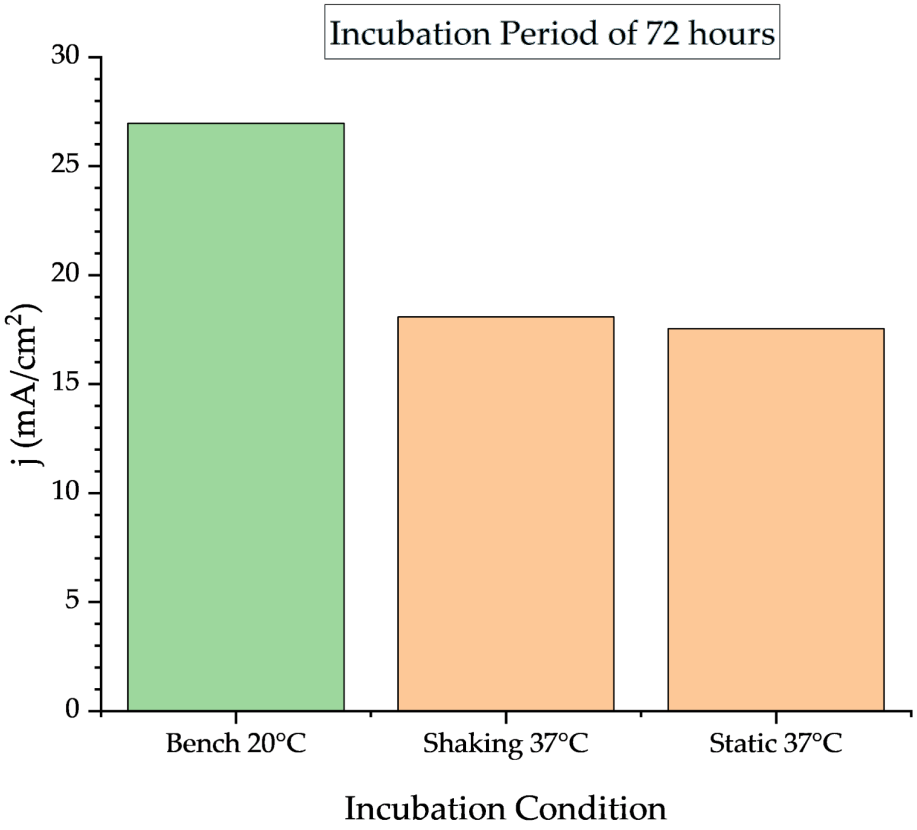

Figure 5.11. AOC after 72 hr of storage time at 20 °C and 30°C. Measurements correspond to samples extracted at the 6th hour of culture and stored under three different conditions.

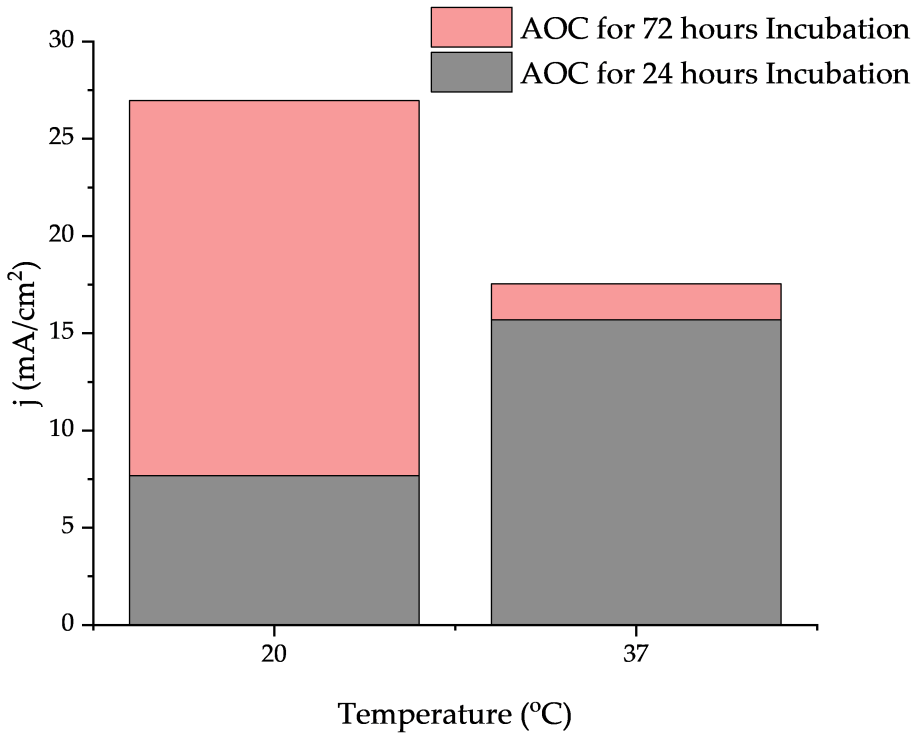

Figure 5.12. AOC after 24h & 72 h of synthetic urine in a *P. vulgaris* bioreactor storage time. Measurements correspond to samples extracted in the 6th culture hour.

5.3.2 Experimental setup: Explore ammonia alkaline cell in a microgravity environment.

The microgravity experiments using the bio-electrochemical reactor system prove that the designed system can decrease the ammonia concentration in a microgravity environment. To contrast against the samples taken in a microgravity environment, samples were taken while the plane was flying at 1 G (ground-based gravity).

As expected, the ammonia conversion did decrease for the microgravity environment. The system was at first tested operation with both electrolytes, SHU and BSHU. Hence, the first BSHU sample from the first two loops showed the lowest ammonia conversion of all samples. This was caused by cross-contamination due to residues of SHU spiking the ammonia concentration in the pipeline

providing a low yield of 5 % ammonia conversion for the first samples. Looking at the second BSHU sample at 6 V had a more reasonable conversion of 15%, which is still lower than the ground base ammonia conversion of 25% for the BSHU sample, see Figure 5.13.

For the SHU samples, it was also observed 19% of ammonia conversion from the SHU sample, see Figure 5.13. It is safe to assume this because of the behavior from the ammonia oxidation current for BSHU and SHU from Figure 5.13 that the current signal for BSHU at 6 V is lower than SHU, which is proportional to the initial ammonia concentration, 6,000 ppm of NH3 for BSHU, and 10,000 ppm NH_3 for SHU. However, observing the rest of the potentials explored, 8 V and 10 V, do not have a significant ammonia conversion, 3% and 5% respectively for BSHU. This could be because the ammonia concentration was competing with the bubble formation from water hydrolysis occurring it the system. It also is observed in Figure 5.13 that at 8 V, the ammonia conversion increased to 28%, comparable to ground conversion at 6V. But then decreased to 26% conversion when increased the potential to 10 V.

As for the rest of the attempts shown in chronological order in Figure 5.14, we observe that by increasing the potential from 6 V to 8 V, then 10 V, and the respective current response, there is a higher drop in current with each cycle. This can come from the fact that there is bubble formation proportional to the potential increase, which in turn difficult the charge transfer and ammonia conversion in the solution.

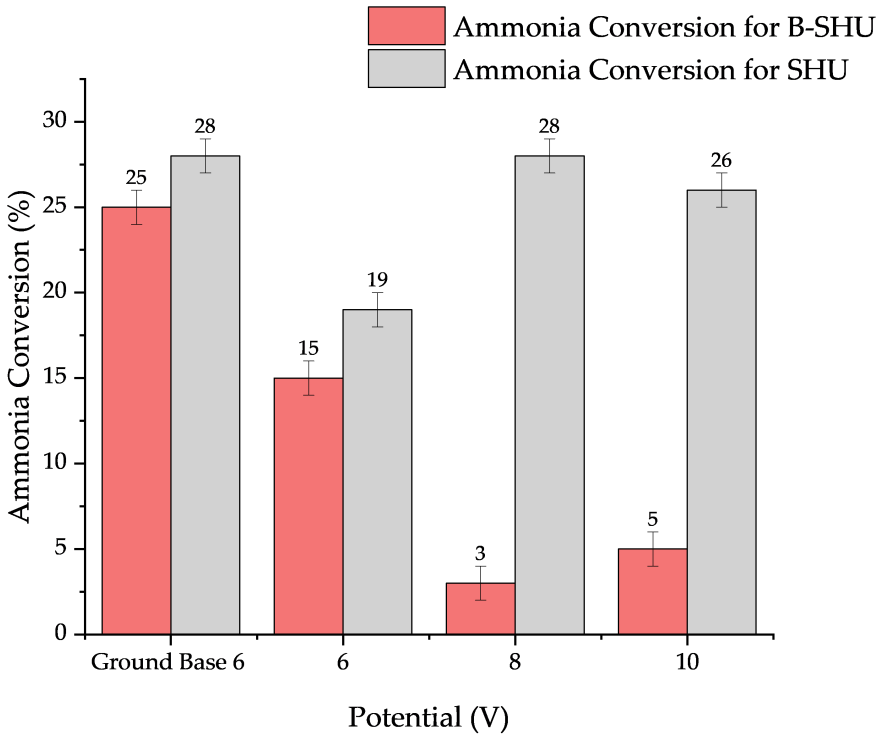

Figure 5.13. Ammonia conversion from the ammonia oxidation reactor in a microgravity environment from the parabolic flight.

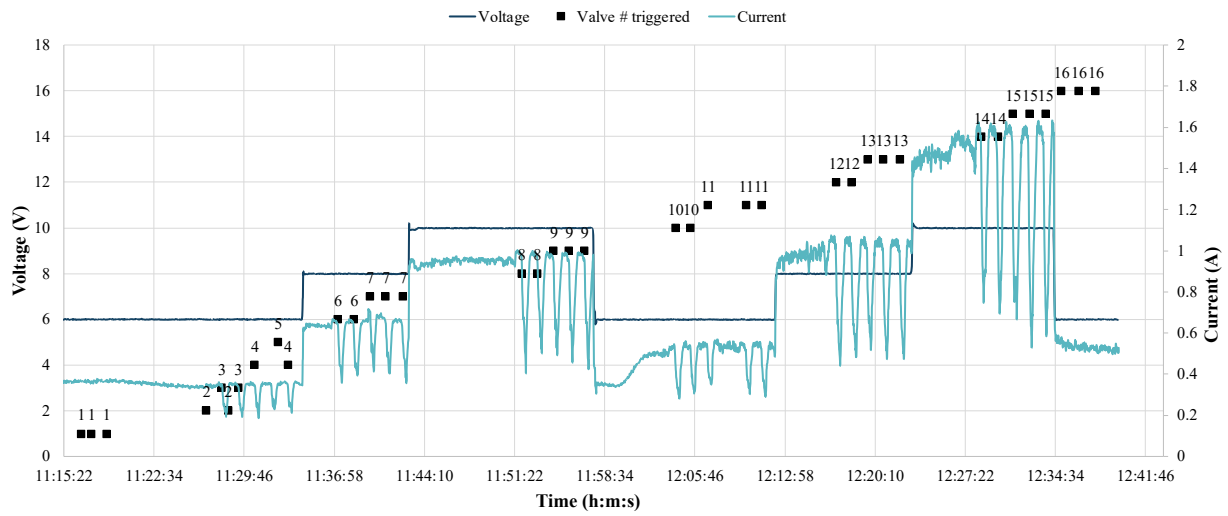

Figure 5.14. *Graph of Parameters (Voltage and Current) vs. time.* The squares in the graph accompanied with numbers represent the times a specific valve was open to collect samples. The samples for BSHU were collected with valves 1 through 9 at different potentials. Then valves 10 through 16 represent the valves that collected samples from SHU at the potentials presented in the graph.

5.3.3 Experimental setup: Evaluate the automated shake-flask bioreactor with real human urine in tandem with ammonia alkaline cell.

This section describes the experiment in two sub-sections. First, the findings of *P. vulgaris* bioreactor in real human urine (RHU) contrasted to BSHU. Second, the ammonia oxidation reactor to treat the effluent using RHU.

5.3.3.2 P. vulgaris Growth Rate

First, was compared the *P. vulgaris* growth rate while using 3M HCl to control the pH, as was done in section 5.3.1, to contrast the use of RHU. We observed that there was a significant change between the colony-forming units per mL (CFU/mL) in BSHU and RHU at the 24th hour of the

experiment. The difference in concentration at the 24th hour (Log CFU/mL =8.8) and 0-hour (Log CFU/mL =7.8) for RHU, Figure 5.15, is equivalent to 5.67x10^{8} CFU/mL. This is significantly higher than 7.60 x10^{7} CFU for BSHU in Figure 5.6. We attribute the observed increase in the CFU/mL at the 24th hour to the fact that RHU contains many metabolites which support bacterial growth, and BHSU does not.

When we substituted the HCl solution with phosphate buffer solution (PBS), during the first 12 hours, there was a similar behavior in *P. vulgaris* growth rate as it was with HCl, see Figure 5.16. However, at 24 hours, the bacteria concentration was not as abundant as it was with HCl. The growth rate difference is the result of the bioreactor not requiring high volumes of HCl solution as it did with the PBS while controlling the pH to 6.5. The bioreactor with PBS at pH 6.5 requires frequent flushing due to the large amount of PBS added by the system. This caused a decrease in bacterial concentration, hence the difference in the observed growth rates. We avoided frequent overflow of the bioreactor by increasing the pH adjustment to pH 7.4, near the PBS buffer region, of pH 7.2.[74]

The shake flask bioreactor system showed an improvement in PBS volume consumption. Furthermore, the precipitate formed in the effluent while using PBS is perceived to have decreased, but the precipitation difference has not been measured. Also, the effluent of RHU controlled with PBS had a pH lower than 8.11. However, while using an HCl solution to control the pH, the incubated effluent at 24 hours had a pH that ranged from 8.9 to 9.2. Although we are using a less hazardous material than HCl, the system with PBS struggled to increase the pH. This gives us a shift in the chemical equilibrium towards ammonium ion, see reaction 4, allowing us to centrifuge the effluent without removing ammonia into a gas phase. However, the ammonia oxidation

reaction is more favorable at higher pH. Thus, it would require incorporating a base such as NaOH during electrochemical ammonia oxidation.

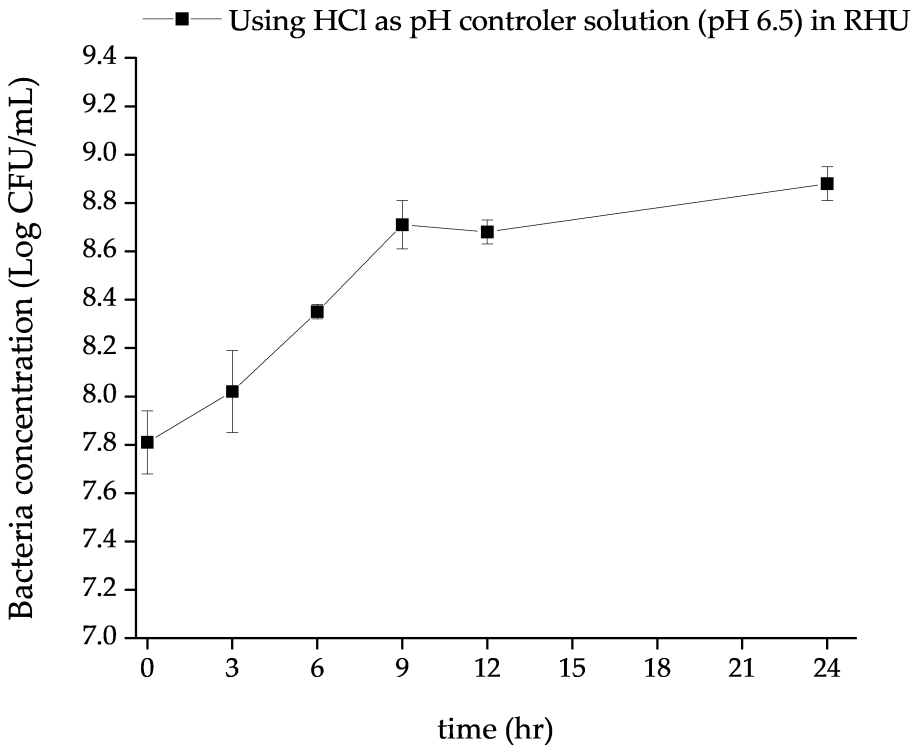

Figure 5.15. *P. vulgaris* growth rate in shake flask bioreactor. pH controlled with HCl in Real Human Urine.

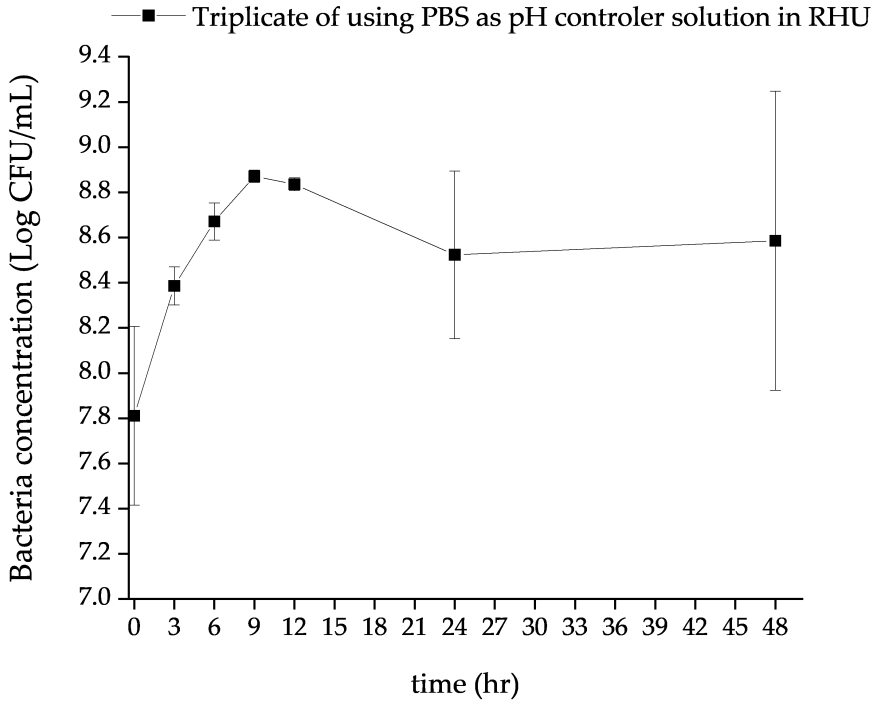

Figure 5.16. *P. vulgaris* growth rate in shake flask bioreactor. pH controlled with PB in Real Human Urine

5.3.3.3 Electrochemical Analysis

The ammonia oxidation reactor (AOR) experiments intend to explore the performance of the joint system of the incubated bioreactor effluent and the ammonia oxidation reactor. The initial average ammonia concentration in RHU is reported in Table 5.1. These were measured for different batches of RHU before use. The high standard deviation for the first batch is due to opening the bottle at other times. Since the bacteria were removed before use, the bottle with RHU was open under an air atmosphere. After taking samples, the bottle was stored in the incubator. Thus, the bacteria would produce more ammonia from the effluent. As for the fourth batch, it did have enough solutions just to run a single trial. Consequently, we only have a single ammonia concentration measurement from batch #4.

Table 5.2. Average of Ammonia concentration for incubated Real Human Urine.

Initial ammonia concentration (ppm)

Batch #	*Average*	*St. Dev*
1	*9170*	*2447*
2	*9140*	*715*
3	*8614*	*431*
4	*8990*	---

Figure 5.17. summarizes that if we circulate the RHU at 4 V for 12 hours, the ammonia concentration decreases by 30%. To decrease the ammonia concentration by approximately 90%, the time required is an exposure time of 12 hours in a cycling system at 6 V. The ammonia concentration measurements for the samples exposed to 8 V for 12 hours show that higher voltage decreases the initial ammonia concentration by 96%. As such, we reduced the cycling time to 6 hours at 8 V, causing a reduction in the ammonia concentration by 85%. The samples that were reported with a conversion higher than 85% changed color from yellow to clear (Figure 5.18.) Thus, other reactions had been happening simultaneously at the electrode since ammonia and urea are colorless in an aqueous solution.

Simultaneously to the ammonia conversion study, we performed a chronoamperometry study to better understand the AOR. As mentioned before, we used different voltages, 4 V, 6 V, and 8 V. The study at 4 V was observed in Figure 5.19, that the current measured was lower than 10 mA. The chronoamperometric data shows that the current is slightly increasing with time, which means something is happening at the electrode's interface and enhancing the charge transfer. It seems that at 4 V, the overpotential does induce the ammonia oxidation reaction, but the rate is too slow. As

for the chronoamperometric data obtained at 6 V, Figure 5.19, we observe that it behaves during the first two hours as it did for 4 V, but with a higher current output.

Moreover, after two hours, the current plateaus, indicating something in the electrochemical circuit has changed. After the plateau region, there is a peak, meaning that the interface could be changing, and the electrochemically active materials could be decreasing. As for 8 V, Figure 5.19, it is observed the same behavior for the chronoamperometry at 6 V, but with less definition on the peaks and curves. Thus, at 8 V, the system goes through the same electrochemical process as it did for 6 V but faster.

When chronoamperometry at 10 V was attempted, we reached the system threshold of 1 A, in turn, obtained a potentiometric study (Figure 5.20). After approximately 3.5 hours for the first attempt at 10 V, the potential stopped decreasing and slowly increasing while holding the 1 A of current, implying that the surface developed an impediment for charge transfer at the surface. After this attempt, the cathode looked as shown in Figure 5.21, it seems as if carbon had deposited on platinum. However, this statement requires further research. The electrode surface was polished with alumina, but the dark stain was strong and could not be removed entirely before the second trial. The second 10 V trial, Figure 5.22, had an odd behavior; it started to increase the potential from 7 V instead of decreasing from 10 V as it did during the first attempt. Afterward, it increases the potential, which sustains the previous statement that the surface requires to increase in the potential to overcome the barrier. Even though the potentiostat is set to 10 V, the starting potential is lower. This could imply that the deposited layer in the Pt foil could promote the redox reaction at lower potentials for urine purification. Furthermore, this accelerated process shows what a platinum foil electrode would face after long usage periods indicating the need for better electrocatalysis design and system tailoring to eliminate catalyst fouling.

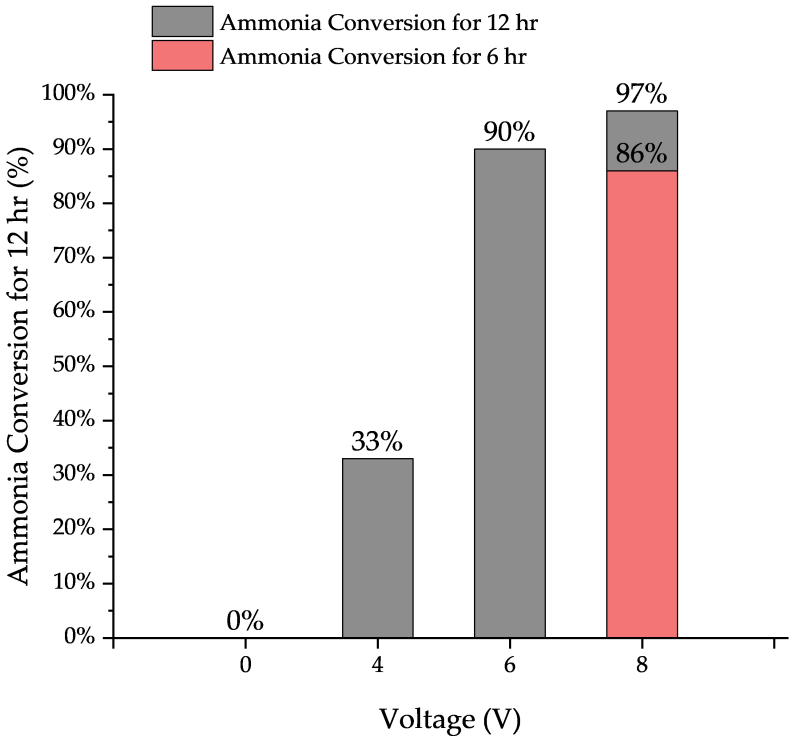

Figure 5.17. Ammonia conversion from AOR using 50 mL RHU aliquots. Different working potentials in the AOR for 6 hr at 8V, and 12 hours at 4 V, 6V, and 8 V,

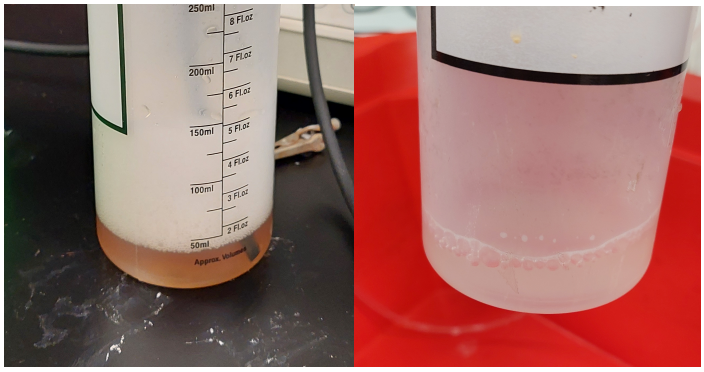

Figure 5.18. Color change in a sample of RHU after exposure through AOR. (left) Real human Urine before processed; (right) Real human Urine after Processing at 6 V for 12 hours

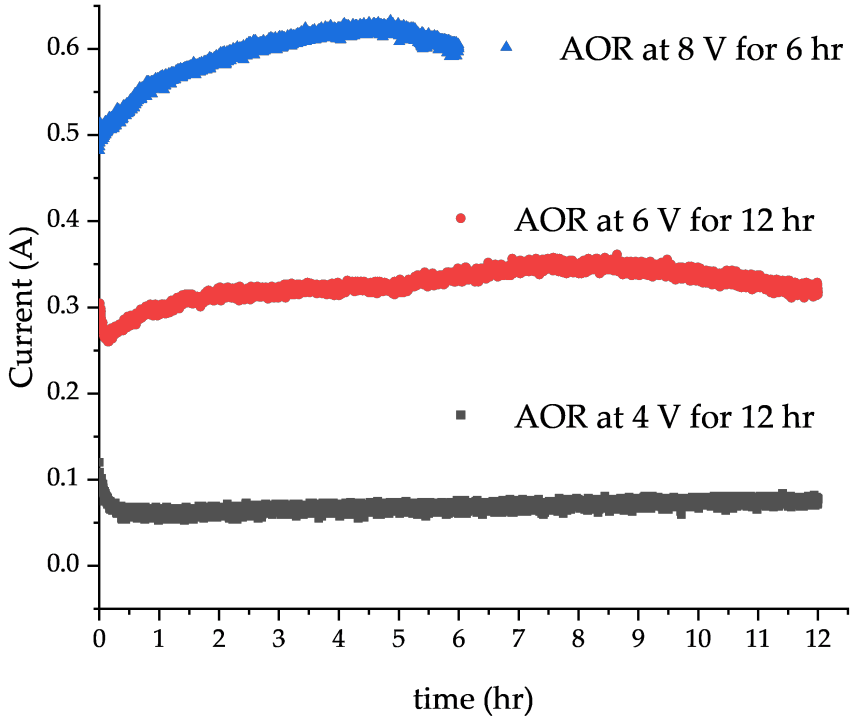

Figure 5.19. Chronoamperometric data from AOR with RHU as electrolyte. (**black**) RHU exposed to 4 V for 12 hr, (**red**) RHU exposed to 6 V for 12 hr, and (**blue**) RHU exposed to 8 V for 6 hr.

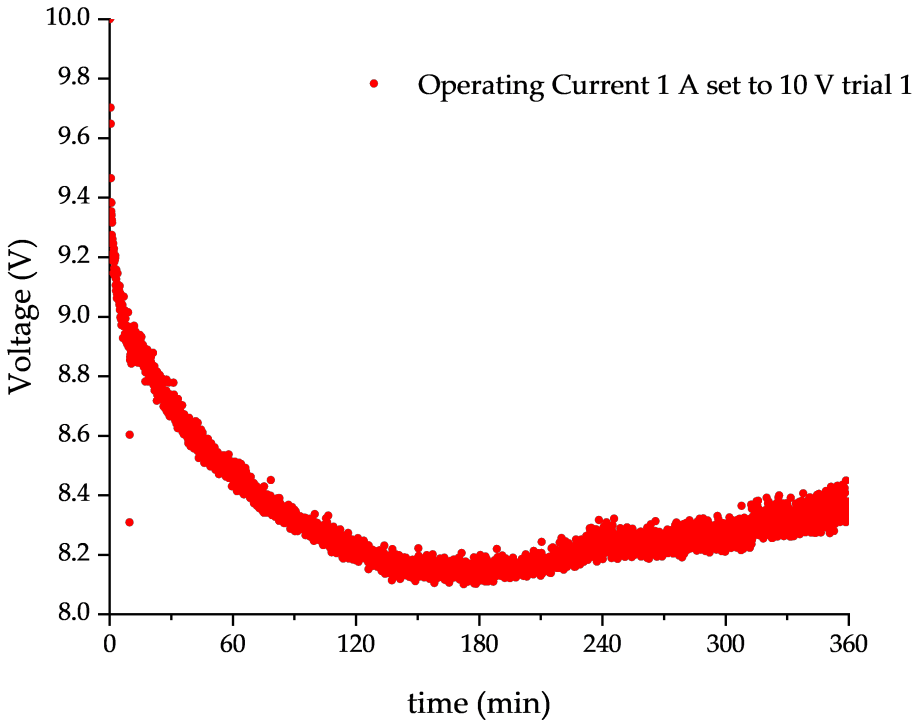

Figure 5.20. Potentiometric data of the AOR with RHU at 1 A, starting at 10 V for 7 hours using clean Pt foils.

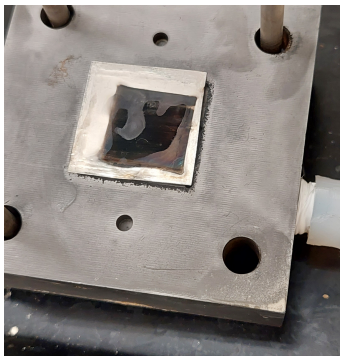

Figure 5.21. Platinum Foil after processing RHU for 6 hours at 10 V and 1 A.

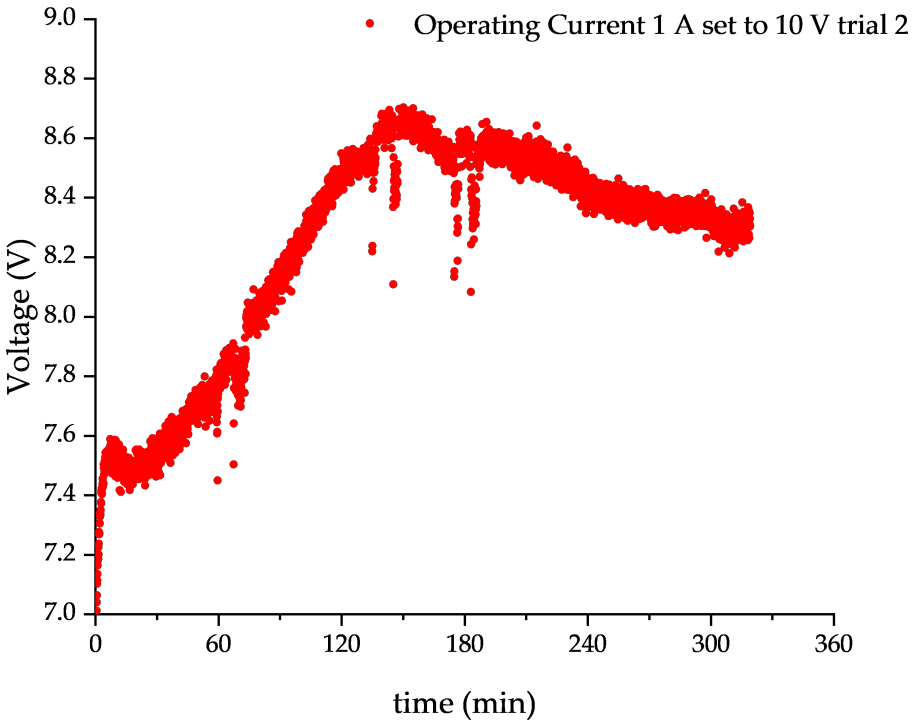

Figure 5.22. Second attempt of potentiometric data of the AOR with RHU at 1 A, starting at 10 V for 6 hours using stained Pt foils.

5.4 Chapter Five: Conclusions

The reported results at the start of the chapter show that the basic guide used operational parameters for a continuous bioreactor was useful to optimize the working parameters of the shake-flask reactor better. The shake-flask design simulated a continuous bioreactor prototype with controlled pH, aeration rate, and flow rate. The bacteria, *P. vulgaris,* showed that it could provide sustained urea consumption and the urea-to-ammonia conversion process could work for long periods.

Also, this the work in this chapter presents an alternative to enhance the water recovery from closed-loop wastewater systems by designing an add-in process to remove urea and ammonia from urine. The shake-flask bioreactor model also works as a continuous bioreactor to treat real human urine by using *P. vulgaris* as the source of microbial urease. *P. vulgaris* was shown to remove urea from human urine while sustaining a high bacterial concentration in RHU. When using the bioreactor in combination with an ammonia oxidation reactor, the ammonia concentration remaining in the urine stream is less than 5%. Furthermore, it is demonstrated that a pH 1.8 buffer, such as phosphate buffer, can be used to control the pH of the bioreactor. The use of phosphate buffer will also reduce the formation of precipitates. Furthermore, this work presents the feasibility of using the described system in environments with zero to low gravitational force, such as onboard the ISS.

The bio-electrochemical reactor system is still under development. It could certainly be improved through further optimizations such as electrocatalysis design to improve electrolysis efficiency and nanostructure electrode designs to improve bubble detachment when exposed to microgravity scenarios. Furthermore, the bio-electrochemical system needs to be aligned with other water treatment systems to enable potable water recovery and reuse. Similarly, the findings reported here allow the study of chemical species in the urine taking part in the electrochemical process. To

understand this system better, future work for this project may include: (a) the analysis of effluent at the in-between process and until the end of the process and (b) analyze the black material which is electro-deposited at the surface of the cathode electrode.

Chapter Six

6. Design and build

In this chapter, we designed and built a carbon brush electrode with Ni nanoparticles and Pt nano-cubes for electrode surface modification. First, we synthesized Ni nanoparticles and Pt nano cubes to deposit on the carbon fiber brush. Then we created the ink to adhere both nanoparticles to the carbon fiber surface. The resulting modified carbon fiber brush was tested on bioreactor-processed synthetic human urine. Results showed that using the designed carbon fiber brush in a cell for two hours oxidized ammonia present in the BSHU at a slower rate than the ammonia volatilization rate at alkaline conditions.

6.1 Introduction

Platinum is a precious metal with excellent catalytic properties due to its high activity in fuel cell reaction in oxidation and reduction processes.[41] Hence, Pt can be used for ammonia oxidation fuel cell, and the treatment of wastewaters.[75,76] The ammonia oxidation catalysed by Pt occurs at a potential of – 0.77 V vs. SHE.[63] Additionally, the use of some Pt morphology enhances the ammonia oxidation.[73,77,78] Pt nanoparticle morphology has been studied for AOR, and has been observed that the presence of the facet (100) in the crystal structure of platinum favour ammonia oxidation peak current.[78,79] In addition, the use of Pt nano cubes (PtNCs) has proven to be very effective in this type of reaction under similar conditions.[16] The presence of cubic structures can be determined through the use of cyclic voltammetry.[78,80] Where the peak/shoulder located between the potential of 0.27 V and ~ 0.37 V vs. RHE, is attributed to the presence of the facet 100.[80] The use of Pt NCs-modified anodes ensures highly efficient removal of ammonia as the one needed for the bioreactor efflux. Since Pt is a good catalytic it can also be used to catalyze urea,

another component present in the wastewater.[81] Urea electrochemical oxidation using Pt occurs at 1.7 V vs. RHE, producing CO_2 and N_2, below said potential the products remain in solution. [81] Another metal that it is know that Ni can be used treat wastewaters, since Ni catalyzes the oxidation of urea.[55,82] Ni catalysed the urea oxidation reaction at a potential range from above 1.27 V and below 1.44 V vs. RHE, which happens at a lower potential that it does with Pt.[54] Thus, a combination between the Pt that enhances ammonia oxidation and Ni would enhance urea oxidation and would create a better electrode to treat the urea and ammonia from wastewaters.

Also, it is desirable to increase the surface while reducing the amount of metal required for the electrode. To achieve this, in this chapter we explain how we integrated the use of a carbon fiber brush. A carbon fiber brush has been used in many areas of research because of it is a cheap material, has good electrical conductivity, and the large surface area is suitable for modification with nanoparticles or bacteria.[58,83,84]

In this work we develop Pt and Ni inks to modify carbon fiber brush electrodes (CFBE). The modified CFBE were first subjected to different electrochemical analytical methods to characterize the electrochemical behavior and was evaluated the performance of carrying out the ammonia oxidation reaction in processed BSHU. The electrochemical technique used to characterize the electrode is cyclic voltammetry, which allows us to evaluate the current as a function of potential to understand what is happening on the surface of each electrode with modification employed in the CFBEs. Also, we employed chronoamperometric technique to evaluate through time the performance of removing ammonia from bacteria-processed BSHU using the modified CFBE.

6.2 Experimental setup

6.2.1 *Nanoparticle Synthesis and Electrochemical Characterization*

This section will discuss the process of synthesizing and electrochemical characterization of the platinum nano cubes and nickel nanoparticles.

6.2.1.1 Platinum Nano cubes (Pt NCs)

The Pt NCs synthesis is based on the synthesis reported by Martinez-Rodríguez et al.[80] In summary, the reduction of platinum from potassium tetrachloroplatinate (K_2PtCl_4) as a precursor in the presence of sodium borohydride ($NaBH_4$) as a reducing agent. This takes place in a water-in-oil microemulsion solution that contains 81 % (vol) n-heptane (C_4H_{16}), 16 % (vol) surfactant (BRIJ 30), and 3 % (vol) of a 100 mM K_2PtCl_4, 15 % HCl (vol) aqueous solution.[80] After the reaction is completed, the Pt NCs phase of the solution is transferred to vials for a series of medium washes. The washes were performed progressively with an increasing polarity gradient, consisting of acetone, methanol, and water. The medium washes were done 1-3 times per day, depending on each solution's deposition rate.

Once the water suspension solutions are obtained, an electrochemical characterization of the Pt NCs is performed to ensure the cubic shape. The Pt NCs were characterized by using Scanning Electron Microscopy and Energy Dispersive Spectroscopy (SEM-EDS), Transmission Electron Mciroscopy (TEM), and through electrochemical characterization. For the electrochemical characterization, the Pt NCs should be immobilized on a surface. As such, we selected to modify a glassy carbon electrode (GCE) with an aliquot of the suspension. Cyclic voltammetry (CV) on the Pt NC-modified GCE in an N_2-purged 0.5 M H_2SO_4 solution a was carried out at a rate of 50mV/s using a reversible hydrogen electrode (RHE) as a reference to determine nanoparticle structure. Additionally, the electrochemical characterization of Pt was performed in an N_2-purged

0.1 KOH solution at a rate of 50mV/s using an RHE. The CV profiles provide a series of peaks that help confirm the nanoparticle morphology. After confirming the nanoparticle cubic structure, the Pt NCs are dried and weighted to prepare a Pt NCs-based ink.

The ink preparation consists of first preparing a suspension of 1mg of nanoparticles in 150µL of deionized water. Then the suspension is mixed into a solution composed of deionized water (24.6% vol), ethanol (46.2% vol), isopropanol (% vol), and 3.36 mg of Nafion ® resin per mL of solution.

6.2.1.2 Nickel Nanoparticles (Ni NPs)

To synthesize the Ni NPs we followed a procedure reported by Cossar.[85] Briefly, we used $NiCl_2 \bullet 6 H_2O$ precursor dissolved in ethanol (99% purity) to obtain a concentration of 0.14 mM. We prepared a solution of $NaBH_4$ 0.28mM dissolved in ethanol (99% purity), which is added to the solution with the Ni precursor, in a stoichiometric proportion of two to one, $NaBH_4$: $NiCl_2$. The reaction takes place in a beaker using a magnetic stirring plate at ambient temperature for 45 minutes, this product was then separated by centrifugation (10 min at 6,000 rpm). Finally, to extract the Nickel nanoparticles, we decanted the liquid part of the resultant mixture and cleansed with ethyl alcohol. This was repeated at least three times. The Ni NPs were dried at 60℃ overnight to prepare the ink following the procedure described earlier.

The Ni NPs were characterized by using SEM-EDS, TEM, and through electrochemical characterization. The Ni NPs were set in carbon tape for the SEM-EDS and dried in a dehumidification chamber overnight.

For the electrochemical characterization, the Ni NPs were deposited on a surface of a GCE. Cyclic voltammetry (CV) on the Ni NPs-modified GCE in a 0.1 KOH solution at a rate of 50mV/s using an RHE. The ink preparation procedure is the same as the one described earlier in this chapter.

6.2.2 Carbon fiber brush electrode (CFBE) Preparation, Modification, Electrochemical Characterization, and Performance Assessment.

To create the Carbon fiber brush electrode (CFBE) we used carbon fiber (bought at eBay) and stainless-steel wire with a 0.81mm diameter. In making the CFBE, small 1.5 cm long strands of carbon fiber were cut. The strands were held at the center of the wires, then the wires were twisted and twirled the fibers into a brush form. Then the CFBE was electrochemically characterized in a 0.1 KOH solution at a rate of 50mV/s using an RHE.

Afterward, the CFBE was submerged in ink containing the Pt NCs and Ni NPs for 2 minutes while shaking and mixing, followed by drying at 60 °C for 10 min. The ink was prepared by adding 1mg of catalyst into 150μL of deionized water. The catalyst composition was as follows: 100% Pt NCs, 80% Pt NCs: 20% Ni NP, 60% Pt NCs: 40% Ni NPs, and 40% Pt NCs: 60% Ni NPs. The measurements had up to ± 2.5% of the composition value.

The modified electrodes were then electrochemically characterized in a 0.1 KOH solution at a rate of 50mV/s using an RHE. The solution was purged with N_2 for 10 min before performing the characterization. Soon after, the solution was saturated with carbon monoxide (CO) while sustaining the working electrode's potential at 0.1V vs. RHE for 2 min. Then, sustaining the potential at 0.1V vs. RHE, the system was purged for 10 min with N_2, subsequently performed an electrochemical stripping of carbon monoxide (CO), in a 0.1 KOH solution at a rate of 10 mV/s vs. RHE. Then a second characterization of the CFBE in a 0.1 KOH solution was performed at a rate of 50mV/s using an RHE. Followed by drying the modified CFBE for at least 10 mins at 60 °C.

To assess the CFBE utility we performed chronoamperometry. The electrolyte solution used to evaluate the CFBE performance was a batch bioreactor processed BSHU solution. The

chronoamperometric study was executed in 4 mL of BSHU solution, for 2 hr, at a potential of 0.78 V vs. RHE.

To measure the efficacy of the electrode removing ammonia, an NH_3-ISE was used to record the ammonia concentration in ppm. The electrode was calibrated using different NH_3 solution with different concentrations that ranged from 10,000 to 10 ppm NH_3. To measure the ammonia concentration, we followed the procedure of the NH_3 ISE manual. Since ammonia is a highly volatile compound at the alkaline conditions at which the chronoamperometry was studied, the ammonia concentration was measured 3 times. (1) to the bulk BSHU solution before the chronoamperometric experiment, (2) to the solution after the chronoamperometric experiment, and (3) to a control BHSU solution exposed to the same conditions of the chronoamperometry experiment.

6.3 Results and Discussion

6.3.1 Results and Discussion: Nanoparticle Synthesis

The following section will discuss the observations made from synthesizing and characterizing the nanoparticles and creating the catalytic ink for the CFBE modification.

6.3.1.1 Pt Nano-cubes (Pt NCs)

After synthetizing the Pt NCs precipitates, the excess solvent was decanted. Given the most abundant solvent in the solution is polar the rinsing process started with acetone, followed by methanol, and finished with water. A premature rinsing with the subsequent solvent, would cause the nanoparticles to suspend permanently or agglomerate. This is believed to be caused by remaining traces of heptane in the PT NCs surface.

To ensure we had Pt NCs, a droplet of Pt NCs suspension was set in carbon tape for the SEM-EDS analysis. The sample was dried in a dehumidification chamber overnight. In the SEM image, (Figure 6.1 a), we observed a cluster of small edgy particles, the cluster with an estimated size between 300-500 nm. However, in Figure 6.1 b, has higher resolution of the Pt NCs, possible to obtain with TEM, where the nanoparticle size is between 10-20 nm. The EDS analysis (Figure 6.2) allowed us to corroborate that our sample was in fact Pt, and the carbon peak was attributed to the carbon tape used to place the sample.

We performed a CV to characterize the surface of the Pt NCs. The CV from the Pt NCs in Glassy Carbon Electrode (GCE) in 0.5M H_2SO_4 vs. RHE at a 50 mV/s scan rate in the range of 0.05 V and 0.8 V (Figure 6.3). We can observe the peaks in the range of ~ 0.27 V and ~ 0.37 V, are the corresponding signal from a facet (100) in a cubic nanoparticle structure.[41,86] Also, it was performed a CV for 4 Pt NCs in Glassy carbon in 0.1M KOH vs. RHE at a 50 mV/s scan rate, Figure 6.4. Where can be also observed the peak/shoulder located at ~ 0.27 V and ~ 0.37 V correspond to the facet (100) characteristic from a Pt cubic nanoparticle structure.[41,86]

Once Pt NCs was characterized, we proceeded to prepare a Pt Ink. We observed that the amount of Nafion-H ® resin used in the ink influenced the platinum electrochemical signal and depended on the electrochemical surface area to be evaluated. An ink prepared for a GCE BASI ® required smaller amounts of Nafion-H ® (0.34 mg per mL of ink) than it did for CFBEs (3.36 mg per mL of ink). Small amounts of Nafion-H ® used for GCE would not help in the adhesion of the nanoparticles to the surface of the CFBE and there were losses between rinses. We also observed that too much Nafion-H ® (6 mg/mL) obstructed the electrochemical activity of the nanoparticle, Figure 6.5. While the amounts of Nafion-H ® reported in the procedure used for ink making would not provide a small distortion in electrochemical response of the Pt NCs, Figure 6.6, which is not

as defined as signals observed in Figure 6.3 and Figure 6.4. To optimize the electrochemical signal was performed the CO-stripping, which will be described later in this chapter.

a) b)

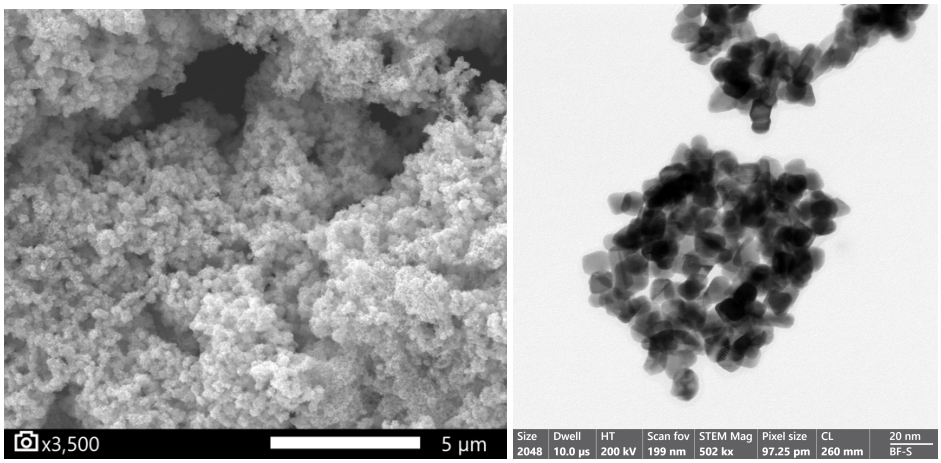

Figure 6.1. Platinum Nanocubes Cluster, **a)** SEM image of Platinum Nanocubes Cluster, at x3,500 magnification. **b)** TEM image of Platinum Nanocubes.

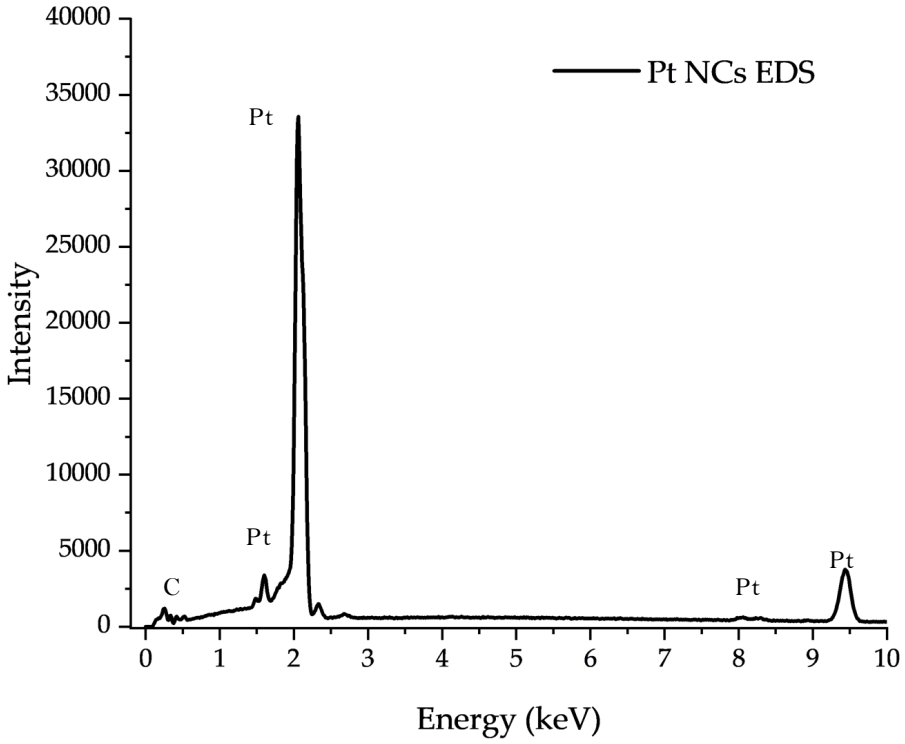

Figure 6.2. Spectrum from Platinum Nanocubes X-ray Fluorescence-Energy Dispersive Spectroscopy (EDS).

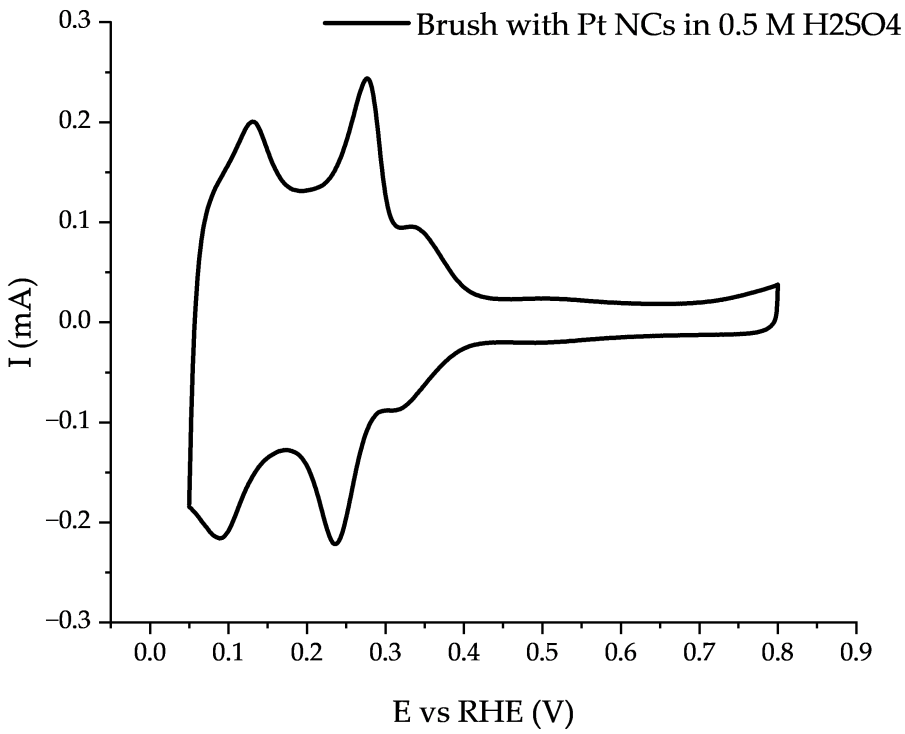

Figure 6.3. Pt-NCs in Carbon Fiber Brush Electrode in 0.5M H_2SO_4 vs RHE at a 50 mV/s scan rate, peak/shoulder located at ~ 0.27 V and ~ 0.37 V, which corresponds to a cubic nanoparticle structure

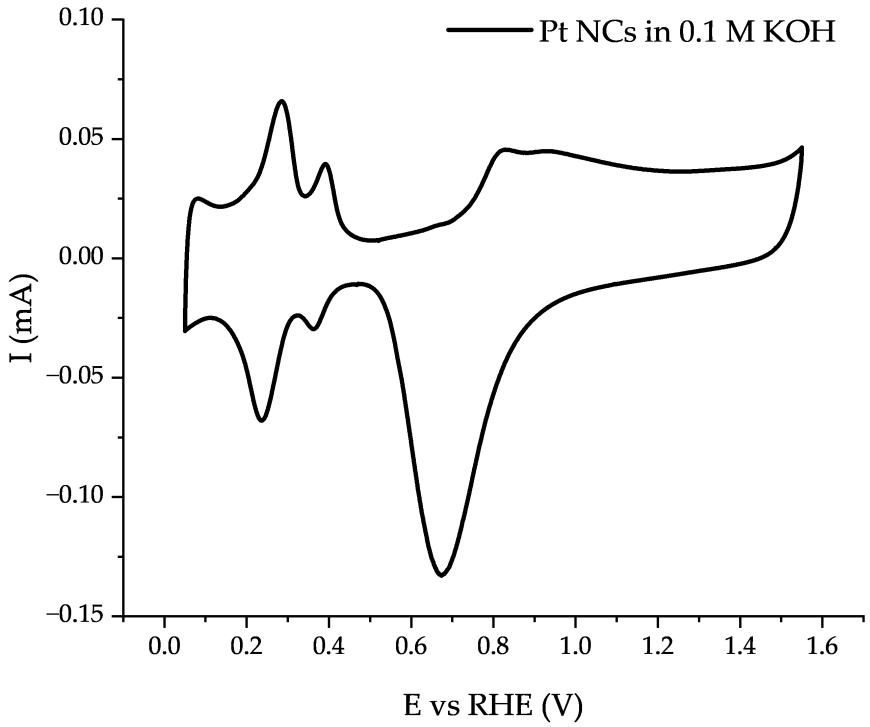

Figure 6.4. Pt-NCs in Glassy Carbon in 0.1M KOH vs. RHE at a 50 mV/s scan rate, peak/shoulder located at ~ 0.27 V and ~ 0.37 V, which corresponds to a facet 100.

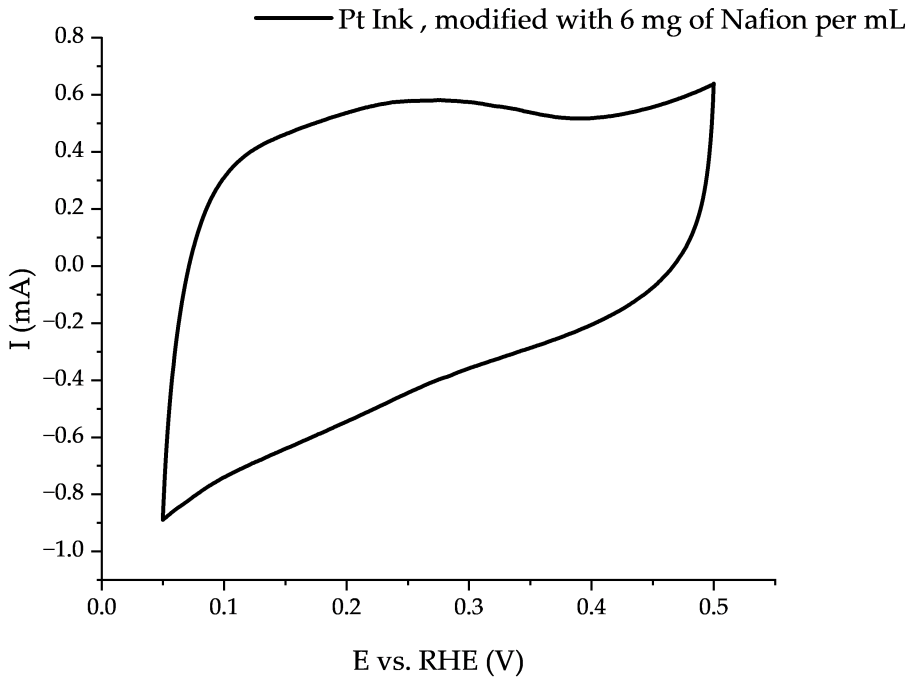

Figure 6.5. Cyclic Voltammetry of a Pt-ink with 6mg of Nafion-H ® per mL of ink, in 0.1M KOH vs. RHE at a scan rate of 50 mV/s.

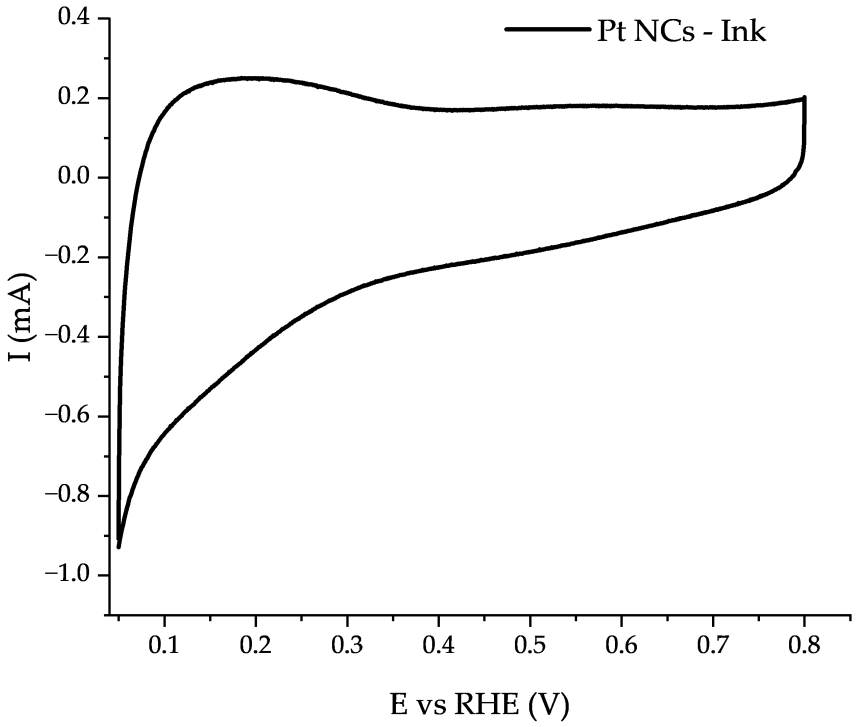

Figure 6.6. Cyclic Voltammetry of Pt NCs Ink modified GCE in in 0.5M H_2SO_4 vs. RHE at a 50 mV/s scan rate.

6.3.1.2 Nickle Nanoparticles (Ni NPs)

The Ni NPs synthesis and rinsing process were simpler than for Pt NCs. To ensure Ni NPs would not oxidize in the presence of water, the nanoparticles were rinsed and stored an ethanol. The characterization of Ni NPs was done by SEM-EDS. The image obtained from the SEM (Figure 6.7 a) was not clear and neither the shape nor the size of the nanoparticles could be determined. However, for when was performed a TEM (see in Figure 6.7 b), it does resemble the spherical shape reported by Cossar.[85] Sonication used to try to break the cluster of Ni NPs did not seem effective. The EDS spectra showed that aside from Ni NPs (Figure 6.8) there were also traces of NaCl that had not been removed by the ethanol rinses. This is explained by the fact NaCl is a

byproduct of the synthesis and NaCl has low solubility in ethanol (0.055% weight percent in ethanol).[85,87] Hence, through the rinsing and centrifugation process it remained as a crystal.

Additionally, the nanoparticles were characterized using CV profiles. This provides electrochemical responses that can be contrasted and confirm the presence of nickel deposited on the GCE. Figure 6.8 shows the characteristic oxidation peak of Ni^{2+} to Ni^{3+} at the potential window between 1.35 V and 1.55 V vs. RHE. That demonstrated that we had Ni NPs adhered to the GCE. As for the electrochemical behavior of Ni NPs in the Ink, we observed similar electrochemical behavior as it did without ink (Figure 6.9). Hence, the presence of the ink did not seem to further affect the electrochemical behavior of Ni NPs, as it did with Pt NC's.

a) b)

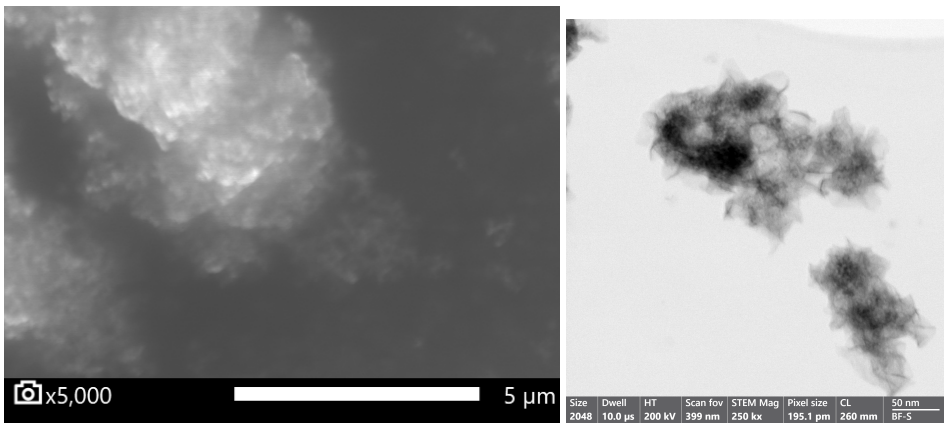

Figure 6.7. Image of Nickel Nanoparticles. a) SEM image of Nickel Nanoparticles Cluster, at x5,000 magnification. b) TEM image of Nickel Nanoparticles.

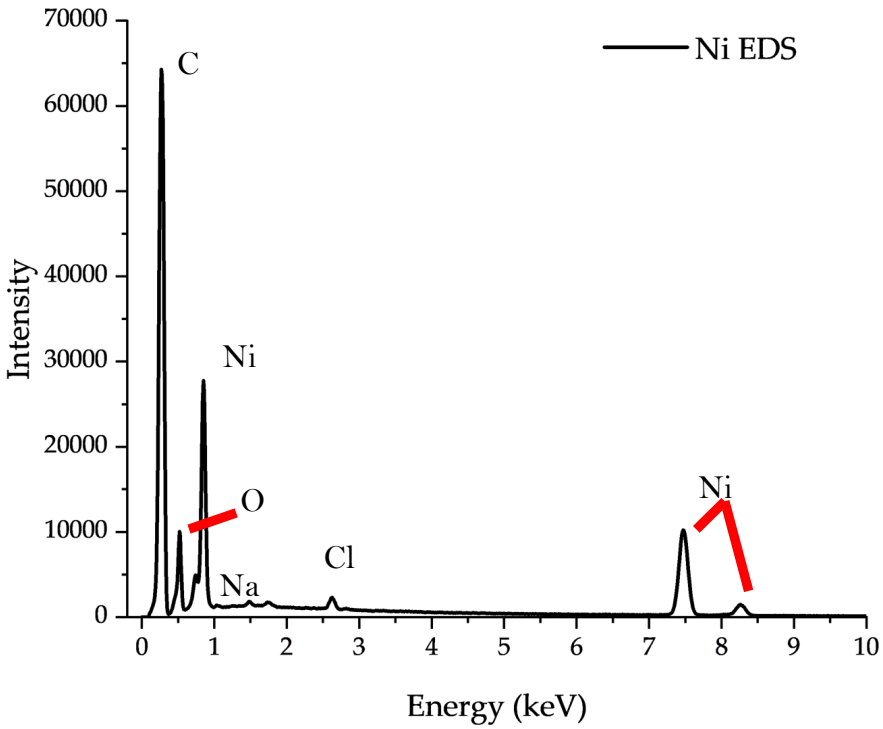

Figure 6.8. EDS spectra of a sample of Ni Nanoparticles.

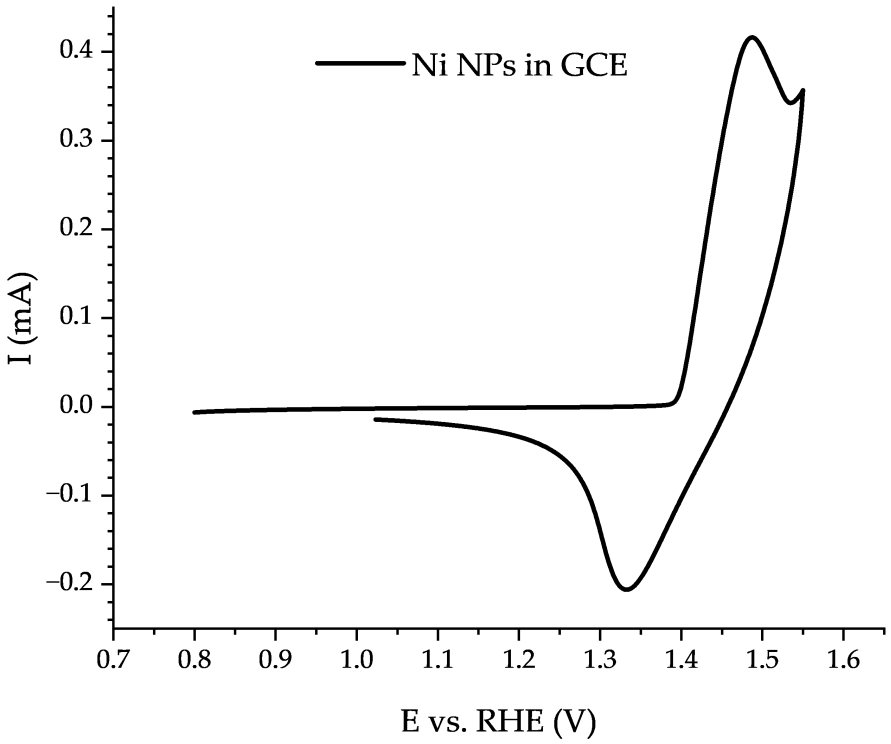

Figure 6.9. Ni-NPs deposited in Glassy carbon in 0.1M KOH vs. RHE at a 20 mV/s scan rate.

6.3.2 Results and Discussion: Carbon fiber brush electrode (CFBE) electrochemical characterization, and performance assessment.

This section discusses the results obtained from the electrode modification and electrochemical characterization, as well as the performance of the electrode in removing ammonia from processed BSHU.

6.3.2.1 Electrochemical Characterization

There were many CFBEs crafted, with similar sizes, to ensure the surface area was similar. All of them were tested with an electrochemical characterization, and voltammogram behavior was contrasted against a glassy carbon BASI ® electrode. The CFBE behavior can be observed in Figure 6.10. The difference between the largest and smallest electrodes was about 30% of

response. The maximum current achieved by the largest CFBE was 0.175 mA, while the smallest CFBE reached 0.121 mA, with an average difference of 30% in active surface area between the two. This allowed us to create a baseline of what electronic signal is coming from the CFBE.

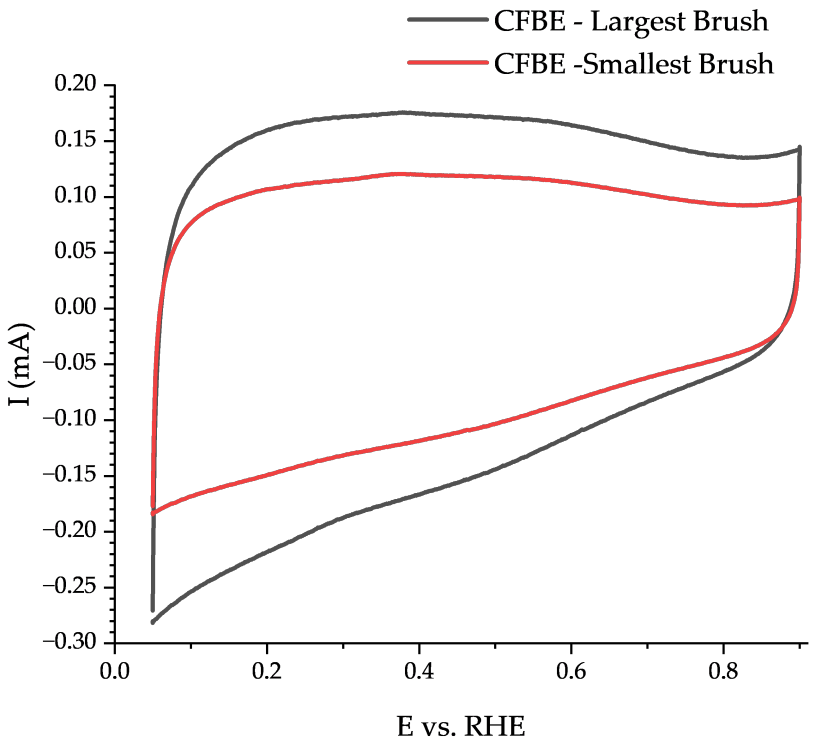

Figure 6.10. Cyclic Voltammetry CFBE in 0.1 M KOH vs. RHE at a scan rate of 50mV/s. The samples represent the largest (black) and smallest (red) CFBE.

The modification process required several iterations to obtain the current ink composition. Since the large surface area obtained from the CFBE required more Nafion-H ® to adhere the nanoparticles, in contrast to the attempts performed with a GCE.

After modification, the CV of the CFBEs with different platinum inks, it was observed that all the ink composition directly correlated with the presence of Pt in the ink (Figure 6.11). It was observed that the ink with 80% Pt NCs and 20% Ni NCs, did not give the expected result, as to be significantly higher than 60 % Pt NCs and 40% Ni NC, but lower than 100% Pt NCs. It is believed that several things could have happened: first possible explanation of the discrepancy in the result is due to the random chance of the nanoparticles. However, the subsequent trials at the same result as the first, which led us to the following explanation, that the Pt NCs did not evenly suspend, and some were agglomerated at the bottom of the microcentrifuge tube. Hence, the Pt NCs did not adhere evenly to the surface of the CFBE regardless of sonication and mechanical mixing.

As mentioned before, the Pt's current signal obtained after modifying the CFBE with ink did not provide clean peaks in the CV associated to the hydrogen desorption. Hence, we opted to electrochemically clean the nanoparticle surface using CO-Stripping. Figure 6.12 shows the linear sweep voltammetry to oxidize the CO into CO_2 expected to occur between the potential window of 0.6 V and 0.9 V. In addition, we can see in the potential window between ~0.27 V and ~ 0.37 V a peak that can be attributed to the presence of nickel in this system.[88] The CO-stripping also allowed us to measure the ECSA after the modification and it provided an enhancement of the current signal obtained from the Pt surface (Figure 6.13) where the desorption peaks of hydrogen, are more pronounced than before the CO-stripping (Figure 6.11).

To accurately determine the ECSA we integrated the current signal divided by the obtained ESCA after the CO-Stripping obtaining the voltammogram defined by the current density *j* (Figure 6.14).

Using the current density permits to accurately correlate the electrochemical activity of the CFBE independent of the Pt content in the different inks. It was observed that the CFBE that had the most electrochemically active surface was the brush that contained 60% Pt NCs and 40% Ni NC. Also,

we observed that after the CO-stripping, there was a heighten peak in the potential window (between ~0.27 V and ~ 0.37 V) associated to the Pt facet (100). At higher nickel composition, this peak was not observed, which means that Pt NCs electrochemical activity benefit from the presence of the ink at a composition of 60% Pt NCs and 40% Ni NC, due to the contribution from Ni.

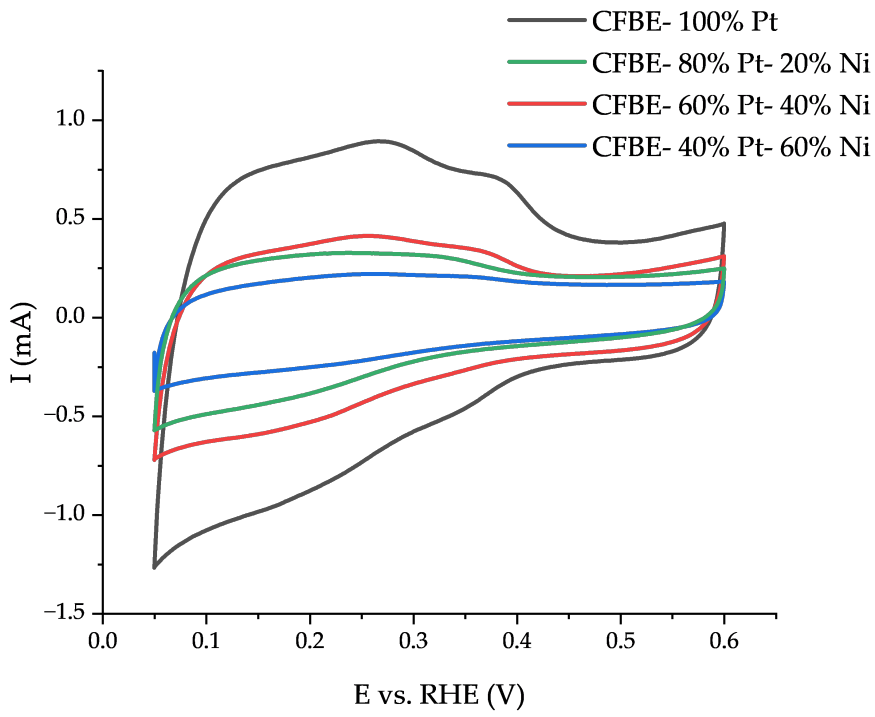

Figure 6.11- Cyclic voltammogram of CFBE with different Pt loading in 0.1 M KOH vs. RHE (V) at a scan rate of 50mV/s. The Pt: Ni mass loading ratio is presented in percentages represented by: (black) 100% Pt, (red) 80% Pt: 20% Ni, (blue) 60% Pt: 40% Ni, and (green) 40% Pt: 80% Ni.

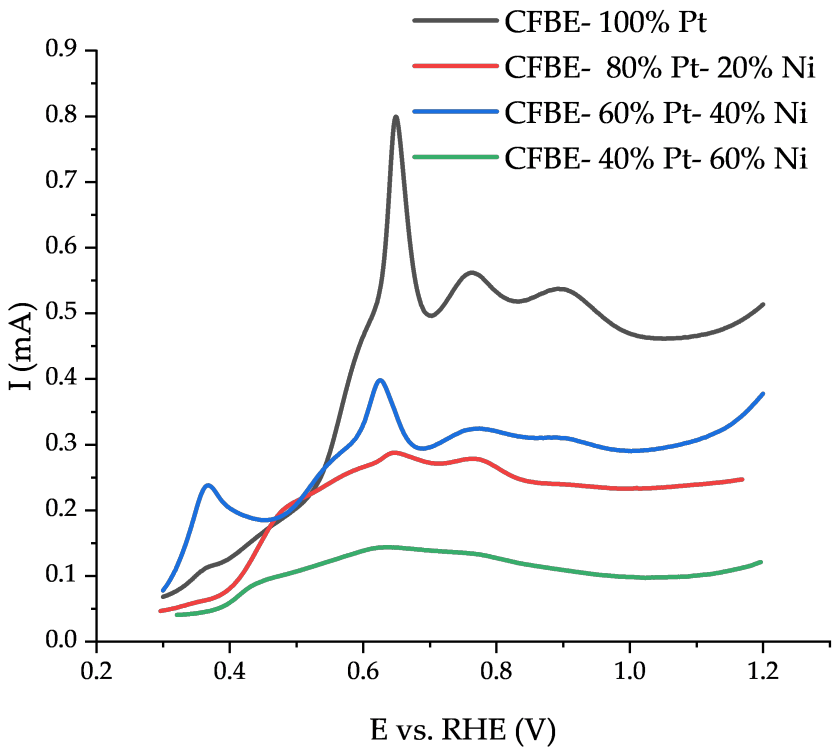

Figure 6.12. Linear Sweep voltammogram for CO-stripping of CFBE with different Pt loading, in 0.1 M KOH vs. RHE (V) at a scan rate of 10mV/s. The Pt: Ni mass loading ratio is presented in percentages represented by: (black) 100% Pt, (red) 80% Pt: 20% Ni, (blue) 60% Pt: 40% Ni, and (green) 40% Pt: 80% Ni.

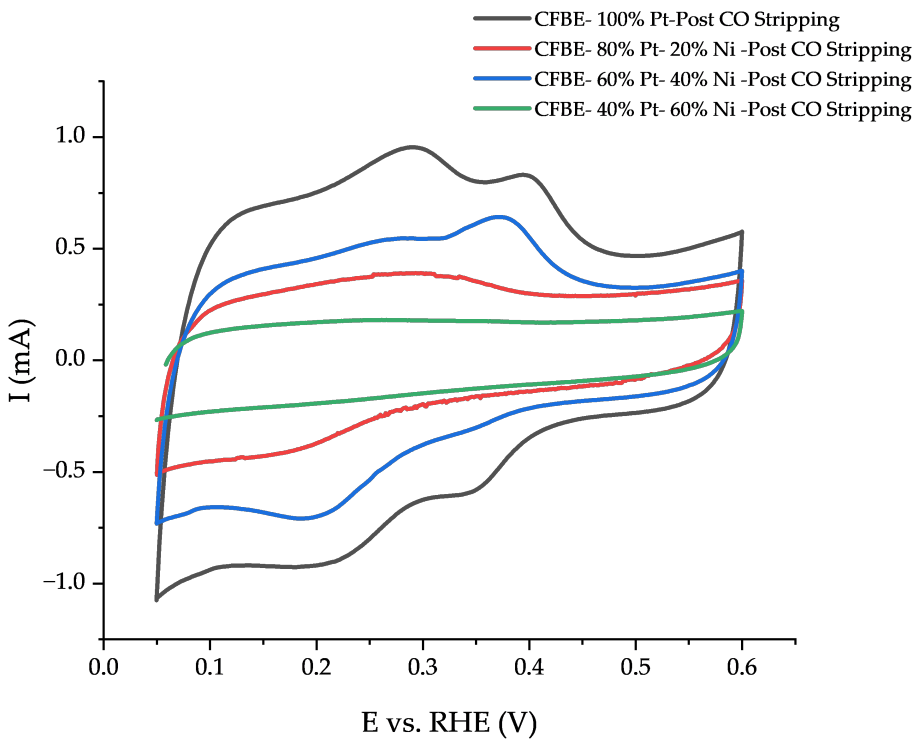

Figure 6.13. Cyclic voltammogram after CO-Stripping of CFBE with different Pt loading in 0.1 M KOH vs. RHE (V) at a scan rate of 50mV/s. The Pt: Ni mass loading ratio is presented in percentages represented by: (black) 100% Pt, (red) 80% Pt: 20% Ni, (blue) 60% Pt: 40% Ni, and (green) 40% Pt: 80% Ni.

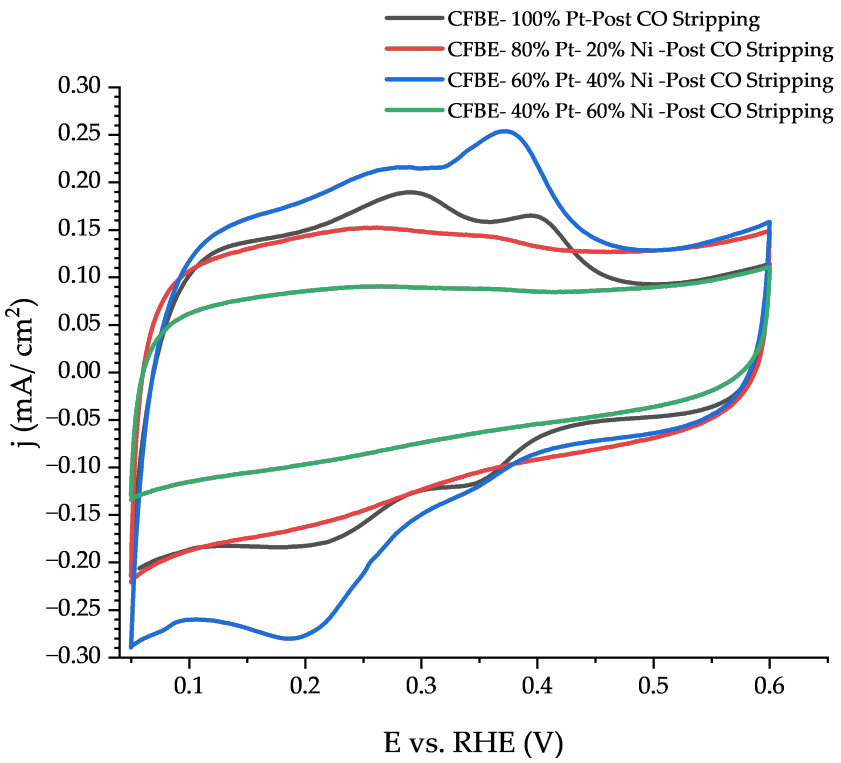

Figure 6.14. Cyclic voltammogram After CO-Stripping of CFBE with different Pt loading in 0.1 M KOH vs. RHE (V) at a scan rate of 50mV/s. The current density (y-axis) diagram is obtained by normalizing with the ECSA, obtained from integrating the activated surface area from the CO-Stripping. The Pt: Ni mass loading ratio is presented in percentages represented by: (black) 100% Pt, (red) 80% Pt: 20% Ni, (blue) 60% Pt: 40% Ni, and (green) 40% Pt: 80% Ni.

6.3.2.2 Performance Assessment

After the successfully modifying the CFBE, their performance was tested by removing ammonia from 4 mL of processed BSHU for 2 hr. This volume and time window was selected like the previous study where 50mL of real human urine required 12 hours for the ammonia concentration to be reduced by 90%.[89] The initial ammonia concentration of the samples was 14,000 ppm. For the chronoamperometry, the samples were not purged with N_2 to remove the O_2 because it would

also remove the ammonia present in the samples. The chronoamperometry was studied at a fixed potential of 0.78V which provided an over potential for the ammonia oxidation potential yet was not high enough to oxidize the Pt NCs which would change its cubic morphology. The first 20 min of the chronoamperometry current went from positive to negative because this is a complex mixture that does not have only ammonia in the system, and many other species (i.e., glucose, urea, creatinine) are likely present. Since all the CFBE had different mass loadings, they were normalized using the ECSA of each CFBE. In the last hour of the chronoamperometric study, after all the current signals were stabilized Figure 6.15 shows the electrochemical activity comes from 100% Pt, which has high catalytic activity. As explained before, several chemical species are present in the process BSHU, hence the high current density from the CFBE with 100% Pt.

As for the ammonia removal, the ammonia concentration was measured using a calibration curve which was calibrated daily, and the calibration curved varied per day. The calibration curves for the measurements were prepared from standard solutions reported and the measured ISE electrode response potential Table 6.1. Then the measured values converted from measured potential to [NH3] in ppm by using the equation (6.1) and equation 6.2, which has an of R^2=0.9998, for a given calibration.

$$y = -0.0266x + 3.8106. \quad \text{Eq 6.1}$$

$$[\text{NH3 ppm}] = 10^{y} \quad \text{Eq 6.2}$$

The remaining ammonia from the electrolyte of the chronoamperometry readings were compared to a blank electrolyte prepared at the same time as the electrolyte for the chronoamperometric study. When we compared the processed electrolyte and the blank electrolyte (Figure 6.16) we

observed the composition that had the best ammonia removal by 30% ±10%, was 80% Pt: 20% Ni, while the CFBE with 60% Pt: 40% Ni, had the best electrochemical response, with an ammonia removal of -4%±1%. However, utilizing an NH_3-ISE at such high concentrations has a 5% error in the measurements. It means that virtually the best [Pt: Ni] composition used in the CFBE for ammonia removal was 80% Pt: 20% Ni, followed by 100% Pt, regardless of their low electrochemical activity shown by the chronoamperometry. This can be because there was enough Ni in the mixture to attract molecules that were competing in the oxidation of NH_3. Higher Ni composition (60% Pt: 40% Ni, and 40% Pt: 80% Ni), could imply that there was not enough Pt to perform a noticeable removal of NH_3. Since, their ammonia removal is about 5%, which is within the instrumental error. This means that the volatilization rate of the ammonia present in the BSHU at alkaline conditions is relatively faster than the ammonia oxidation through chronoamperometric study utilizing the CFBE with most of the modifications, but 80% Pt: 20% Ni.

Table 6.1. Concentration of Standard solution of NH_3 in ppm, and potential signal from the NH_3-ISE electrode.

[NH_3] (ppm)	mV
10	105.2
100	69
1000	30.5
10000	-7.4

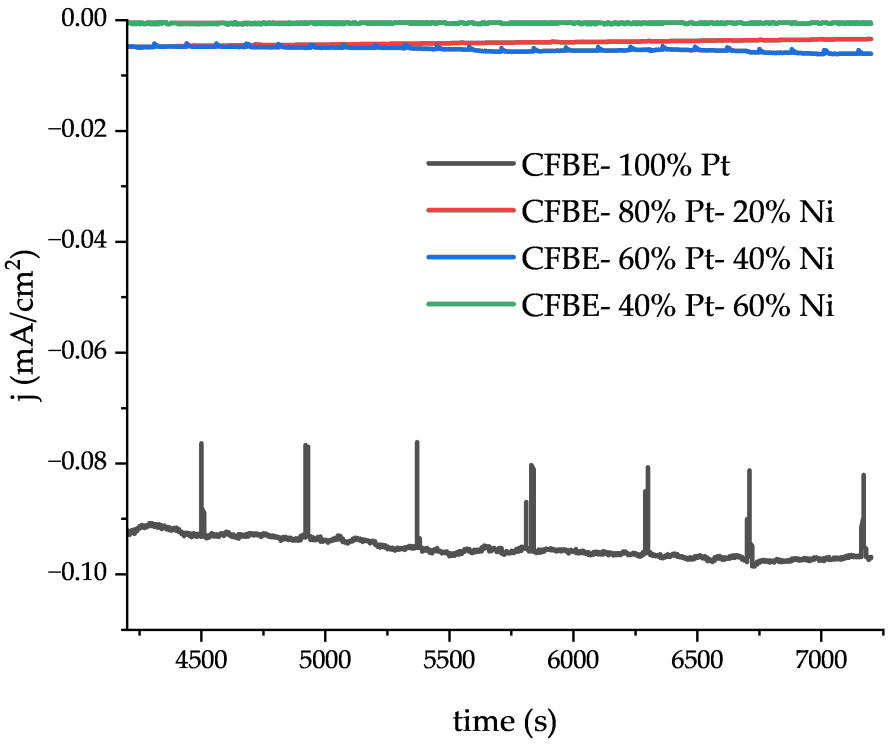

Figure 6.15. Chronoamperometry of modified CFBE with different Pt loading in BSHU. Showing the last exposure hour of the CFBE in BSHU. For a better comparison between the CFBE performance, the graph has been modified with the current density (y-axis), obtained by normalizing with the ECSA. The Pt: Ni mass loading ratio is presented in percentages represented by: (black) 100% Pt, (red) 80% Pt: 20% Ni, (blue) 60% Pt: 40% Ni, and (green) 40% Pt: 80% Ni.

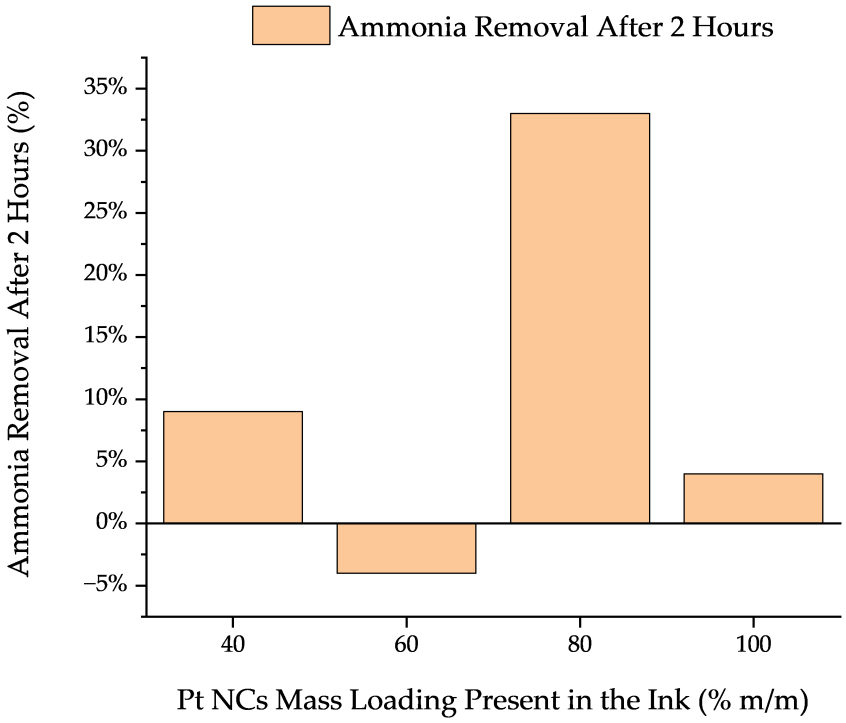

Figure 6.16. Ammonia Removal vs. Pt NC's mass loading. The reported values have an error of ± 5%, associated to instrumentation.

6.4 Chapter Six: Conclusions

Data presented in this chapter showed that carbon fiber electrode can be used as an alternative for ammonia oxidation from synthetic human urine. The combination of nanoparticles of two metallic catalyst, Pt NCs, and Ni NPs, may be used to modify a CFBE. We observed that the Pt: Ni combination that showed a significant electrochemically active surface was 60% Pt: 40% Ni. Among the tested modifications of Pt: Ni combination to CFBE, 80% Pt: 20% Ni, showed to be more effective in removing ammonia from basal synthetic human urine that had been processed from a bioreactor with *P. vulgaris*.

Some alternative approaches that can be implemented in enhancing the results of this research include using dynamic light scattering (DLS) analysis, to analyze the particle size and size distribution of the nanoparticles. We can also implement the use of maceration while preparing the metallic catalyst nanoparticles. Some of the future work to be conducted is to explore higher catalytic concentrations when preparing the inks along with variations of other supporting membranes. Additionally, the chronoamperometric study can be enhanced by setting a closed system in which the ammonia volatilized from the electrolyte can be contained to more efficiently quantify the amount of ammonia being removed from the samples at a given time.

Chapter Seven

7. General Conclusions

This thesis focused on designing and building a bioreactor to treat wastewaters for close-loop environment systems. To achieve this, we confirmed the feasibility to design a continuous bioreactor prototype that follows the chemostat designing principles to keep *Proteus vulgaris* alive in basal synthetic human urine, BSHU. This was possible by evaluating *P. vulgaris* growth rates at different BSHU flow rates of feed and extraction and we determined the influence of pH control in this system. We obtained the optimal flow rates and hence, we decided to proceed using a flow rate equal to the 10% volume of the bioreactor total volume that did not exceed 250 mL. Alongside flow rate and pH control studies for bacterial growth, we simultaneously evaluated the effects of these two factors on ammonia production. Additionally, we designed a pH controller for the culture pH without constant monitoring. pH control benefits the growth rate of *P. vulgaris* and contains the ammonia. We determined that the maximum ammonia oxidation current which is higher than 17 $\mu A/cm^2$ for 24 hours coming from batch incubation processes.

Furthermore, this thesis demonstrated that bio-electrochemical systems effluent reduces ammonia and urea concentrations from synthetic urine feed streams using basal synthetic human urine (BSHU). All this resulted in a basic guide that can be used to explore operational parameters for the design of a continuous bioreactor with a shake-flask reactor assembly. We showed that *P. vulgaris,* could provide sustained urea consumption and the urea-to-ammonia conversion process can potentially work for long periods of time. Providing alternatives to optimize water recovery from closed-loop wastewater systems by designing an integrated process to remove urea and ammonia from urine is extremely important. Additionally, using *P. vulgari*s as the source of

microbial urease in a continuous shake-flask bioreactor model, as reported, works well to treat real human urine.

Moreover, the bio-electrochemical system was shown to have the potential to be used in a system in environments with zero to low gravitational force, such as aboard the ISS, or the possible future Lunar/Martian base. As it has been proven to work in a zero-gravity parabolic loop flight test with bioreactor-treated synthetic urine. In addition, the bio-electrochemical system was evaluated with real human urine proven to be successful for the removal of urea and ammonia.

Another part of the scope of this thesis, was the design and build of high surface area electrodes. The high surface electrodes consisted of crafted carbon fiber brush with a combination of synthesized Ni nanoparticles and Pt nano-cubes which would serve to modify the surface of the CFBE. This could be used in the removal of ammonia and urea from a wastewater system as basal synthetic human urine. We observed that 60% Pt and 40% Ni showed the most significant electrochemically active surface; however, among the modifications the combination of 80% Pt: 20% Ni, showed to be more effective in removing ammonia from basal synthetic human urine than had been processed in a bioreactor with *P. vulgaris*.

7.1 Recommendation for Future Work

The bio-electrochemical reactor system is still under development. It can be upgraded and optimized further, using new cell structures with a design that has smaller flow channels between the electrodes in the cell. This could improve electrolytic efficiency and could improve bubble detachment produced under microgravity scenarios. Furthermore, we could explore the alternative to study with longer microgravity exposure times.

The bio-electrochemical system needs to be aligned with other water treatment systems to enable water recovery and reuse for potable purposes. Similarly, the results reported provide the

opportunity to study chemical species in the urine taking part in the electrochemical process. To understand this type of system better future work for this project should include the analysis of effluents at the in-between process and until the end of the processes and the in-situ analysis at the cell surface using the processed human urine.

Regarding the design and construction of the high-surface Pt-Ni electrode study, we need to evaluate the influence of higher catalytic concentration in the inks along with the variation of other supporting membranes and test them in processed BSHU or similar set ups. Furthermore, we can improve the chronoamperometric study by setting a closed system to prevent ammonia vapors from escaping from the system.

References

(1) UN Water. *World Water Development Report 2018: Nature-Based for Water*. https://www.unwater.org/publications/world-water-development-report-2018 (accessed 2022-10-23).

(2) UN. *International Decade for Action "Water For Life" 2005-2015*. https://www.un.org/waterforlifedecade/scarcity.shtml (accessed 2019-10-16).

(3) The United Nations Educational. *Managing Water under Uncertainty and Risk*; 2012; Vol. 54.

(4) Motho, M.; Kolawole, O. D.; Motsholapheko, M. R.; Mogomotsi, P. K. Influence of Household Demographic and Socio-Economic Factors on Water Demand in Ngamiland District, Botswana. *Water Science* **2022**, *36* (1), 48–59. https://doi.org/10.1080/23570008.2022.2048581.

(5) Boretti, A.; Rosa, L. Reassessing the Projections of the World Water Development Report. *npj Clean Water* **2019**, *2, 15*. https://doi.org/10.1038/s41545-019-0039-9.

(6) Amoatey, P.; Bani, R. Wastewater Management. In *Waste Water - Evaluation and Management*; 2011. https://doi.org/10.5772/16158.

(7) Venzke, C. D.; Giacobbo, A.; Ferreira, J. Z.; Bernardes, A. M.; Rodrigues, M. A. S. Increasing Water Recovery Rate of Membrane Hybrid Process on the Petrochemical Wastewater Treatment. *Process Safety and Environmental Protection* **2018**, *117*, 152–158. https://doi.org/10.1016/j.psep.2018.04.023.

(8) WHO; UNICEF. *25 Years Progress on Sanitation and Drinking Water*; 2015. https://apps.who.int/iris/bitstream/handle/10665/177752/9789241509145_eng.pdf?sequence=1&isAllowed=y.

(9) Crini, G.; Lichtfouse, E. Advantages and Disadvantages of Techniques Used for Wastewater Treatment. *Environ Chem Lett* **2019**, *17* (1), 145–155. https://doi.org/10.1007/s10311-018-0785-9.

(10) NOVA. *Life support systems in space flight.* http://members.nova.org/~sol/station/life-sup.htm (accessed 2019-05-21).

(11) *Water on the Space Station | Science Mission Directorate*. NASA Science. https://science.nasa.gov/science-news/science-at-nasa/2000/ast02nov_1 (accessed 2022-08-11).

(12) Lindeboom, R. E. F.; Paepe, J. De; Vanoppen, M.; Alonso-fariñas, B.; Coessens, W. A Five-Stage Treatment Train for Water Recovery from Urine and Shower Water for Long-Term Human Space Missions. *Desalination* **2020**, *495*, 114634. https://doi.org/10.1016/j.desal.2020.114634.

(13) NASA. *Environmental control and life support system evolution analysis*. https://www.nasa.gov/sites/default/files/atoms/files/g-281237_eclss_0.pdf (accessed 2021-01-25).

(14) Nicolau, E.; Fonseca, J. J.; Rodríguez-Martínez, J. A.; Richardson, T. M. J.; Flynn, M.; Griebenow, K.; Cabrera, C. R. Evaluation of a Urea Bioelectrochemical System for

Wastewater Treatment Processes. *ACS Sustainable Chem Eng* **2014**, *2* (4), 749–754. https://doi.org/10.1021/sc400342x.
(15) Bouatra, S.; Aziat, F.; Mandal, R.; Guo, A. C.; Wilson, M. R.; Knox, C.; Bjorndahl, T. C.; Krishnamurthy, R.; Saleem, F.; Liu, P.; Dame, Z. T.; Poelzer, J.; Huynh, J.; Yallou, F. S.; Psychogios, N.; Dong, E.; Bogumil, R.; Roehring, C.; Wishart, D. S. The Human Urine Metabolome. *PLoS One* **2013**, *8,* e73076. https://doi.org/10.1371/journal.pone.0073076.
(16) Morales-Cruz, M.; López-Nieves, M.; Morales-Hernández, R.; Rivera-Crespo, G. C.; Toranzos, G. A.; González-González, I.; Cabrera, C. R. Proteus Vulgaris - Pt Electrode System for Urea to Nitrogen Conversion in Synthetic Urine. *Bioelectrochemistry* **2018**, *122*, 206–212. https://doi.org/10.1016/j.bioelechem.2018.03.017.
(17) Schönning, C. Evaluation of Microbial Health Risks Associated with the Reuse of Source Separated Human Urine, Swedish Institute for Infectious Disease Control (SMI), 2001. https://www.semanticscholar.org/paper/Urine-diversion-—-hygienic-risks-and-microbial-for-Schönning/d7ee4b250838eaacd739464114fdae1483c64c6c.
(18) Wang, J.; Wei, Y. Recovery of Monovalent Mineral Salts from Urine in Controlled Ecological Life Support System by Nanofiltration: Feasibility Study. *Desalination* **2020**, *479* (April 2020), 114344. https://doi.org/10.1016/j.desal.2020.114344.
(19) Putnam, D. F. *Composition and Concentrative Properties of Human Urine*; by NASA: Washington, DC. 1971.
(20) STEIN, W. H.; Carey, G. C. A Chromatographic Investigation of the Amino Acid Constituents of Normal Urine. *J Biol Chem* **1953**, *201* (1), 45–58. https://doi.org/10.1016/s0021-9258(18)71347-1.
(21) Press, C. S. H. L. Amino Acid Dropout Mixture for Y2H. *Cold Spring Harb Protoc* **2015**, *2015* (5), pdb.rec086736. https://doi.org/10.1101/pdb.rec086736.
(22) Messen, J. H. Urea. *Ullmann's Encyclopedia of Industrial Chemistry*; 2010. https://doi.org/https://doi.org/10.1002/14356007.a27_333.pub2.
(23) Urbańczyk, E.; Sowa, M.; Simka, W. Urea Removal from Aqueous Solutions—a Review. *J Appl Electrochem* **2016**, *46* (10), 1011–1029. https://doi.org/10.1007/s10800-016-0993-6.
(24) Konieczna, I.; Zarnowiec, P.; Kwinkowski, M.; Kolesinska, B.; Fraczyk, J.; Kaminski, Z.; Kaca, W. Bacterial Urease and Its Role in Long-Lasting Human Diseases. *Curr Protein Pept Sci* **2013**, *13* (8), 789–806. https://doi.org/10.2174/138920312804871094.
(25) Mobley, H. L. T.; Hausinger, R. P. Microbial Ureases : Significance , Regulation , and Molecular Characterizationt. *Microbiological Review* **1989**, *53* (1), 85–108. https://doi.org/10.1128/mr.53.1.85-108.1989.
(26) Chen, Y. J.; Nuevo, M.; Hsieh, J. M.; Yih, T. S.; Sun, W. H.; Ip, W. H.; Fung, H. S.; Chiang, S. Y.; Lee, Y. Y.; Chen, J. M.; Wu, C. Y. R. Carbamic Acid Produced by the UV/EUV Irradiation of Interstellar Ice Analogs. *Astron Astrophys* **2007**, *464* (1), 253–257. https://doi.org/10.1051/0004-6361:20066631.
(27) Ferreira, M. P.; de Castro, C. B.; Marques Netto, C. G. C. Explaining Urease Specificity towards Nickel: A Re-Analysis of Its Proposed Mechanism. *ChemRxiv* **2020**. https://doi.org/10.26434/chemrxiv.13161389.v1.

(28) Kistiankowsky, G. B.; Rosexherc, A. J. The Kinetics of Urea Hydrolysis by Urease. *Journal of American Chemical Society* **1952**, *74* (20), 5020–5025. https://doi.org/10.1021/ja01140a009.
(29) Mobley, H. L.; Island, M. D.; Hausinger, R. P. Molecular Biology of Microbial Ureases. *Microbiol Rev* **1995**, *59* (3), 451–480. https://doi.org/10.1128/mr.59.3.451-480.1995.
(30) Balasubramanian, A.; Ponnuraj, K. *3LA4: Crystal structure of the first plant urease from Jack Bean (Canavalia ensiformis)*. https://www.ebi.ac.uk/pdbe/entry/pdb/3la4 (accessed 2022-10-24).
(31) Nicolau, E.; González-González, I.; Flynn, M.; Griebenow, K.; Cabrera, C. R. Bioelectrochemical Degradation of Urea at Platinized Boron Doped Diamond Electrodes for Bioregenerative Systems. *Advances in Space Research* **2009**, *44* (8), 965–970. https://doi.org/10.1016/j.asr.2009.04.003.
(32) Bengtson, I. A. The Proteus Group of Organisms with Special Reference to Agglutination and Fermentation Reactions and to Classification Author (s): Ida A . Bengtson Published by : Oxford University Press Stable URL : Https://Www.Jstor.Org/Stable/30082067. *J Infect Dis* **1919**, *24* (5), 428–481.
(33) Michael L. Shuler; Fikret Kargi. *Bioprocess Engineering Basic Concepts*, Second.; Prentince-Hall, Upper Saddle River, 2002.
(34) Gaur, R.; Singh, A.; Tripathi, A.; Singh, R. Chapter-7: Bioreactors. In *Principles and Applications of Environmental Biotechnology for a Sustainable Future*; Springer: Singapore, 2017. https://doi.org/10.1007/978-981-10-1866-4_7.
(35) Collignon, M.-L.; Williams, A. *What Are the Different Bioreactor Processes?*. Pall. https://www.pall.com/en/biotech/blog/bioreactor-processes.html (accessed 2022-10-25).
(36) Gresham, D.; Hong, J. The Functional Basis of Adaptive Evolution in Chemostats. *FEMS Microbiol Rev* **2015**, *39* (1), 2–16. https://doi.org/10.1111/1574-6976.12082.
(37) Yan, X.; Bergstrom, D. J.; Chen, X. B. Modeling of Cell Cultures in Perfusion Bioreactors. *IEEE Trans Biomed Eng* **2012**, *59* (9), 2568–2575. https://doi.org/10.1109/TBME.2012.2206077.
(38) Coban, H. B.; Demirci, A.; Patterson, P. H.; Elias, R. J. Enhanced Phenylpyruvic Acid Production with Proteus Vulgaris in Fed-Batch and Continuous Fermentation. *Prep Biochem Biotechnol* **2016**, *46* (2), 157–160. https://doi.org/10.1080/10826068.2014.995813.
(39) Thierie, J. Continuous Culture: The Chemostat. In *Introduction to Polyphasic Dispersed Systems Theory*; Springer International Publishing: Switzerland, 2016; pp 47–175. https://doi.org/10.1007/978-3-319-27853-7_4.
(40) Ding, Y.; Sartaj, M. Optimization of Ammonia Removal by Ion-Exchange Resin Using Response Surface Methodology. *International J. Environ. Sci. Technol.* **2016**, *13* (4), 985–994. https://doi.org/10.1007/s13762-016-0939-x.
(41) Vidal-Iglesias, F. J.; Solla-Gullón, J.; Rodríguez, P.; Herrero, E.; Montiel, V.; Feliu, J. M.; Aldaz, A. Shape-Dependent Electrocatalysis: Ammonia Oxidation on Platinum Nanoparticles with Preferential (100) Surfaces. *Electrochem. Commun.* **2004**, *6* (10), 1080–1084. https://doi.org/10.1016/j.elecom.2004.08.010.

(42) Climent, V.; Feliu, J. M. Thirty Years of Platinum Single Crystal Electrochemistry. *Journal of Solid State Electrochemistry* **2011**, *15* (7–8), 1297–1315. https://doi.org/10.1007/s10008-011-1372-1.
(43) Pillai, H. S.; Xin, H. New Insights into Electrochemical Ammonia Oxidation on Pt(100) from First Principles. *Ind Eng Chem Res* **2019**, *58*, 10819–10828. https://doi.org/10.1021/acs.iecr.9b01471.
(44) Afif, A.; Radenahmad, N.; Cheok, Q.; Shams, S.; Kim, J. H.; Azad, A. K. Ammonia-Fed Fuel Cells: A Comprehensive Review. *Renewable and Sustainable Energy Reviews* **2016**, *60*, 822–835. https://doi.org/10.1016/j.rser.2016.01.120.
(45) Lan, R.; Irvine, J. T. S.; Tao, S. Ammonia and Related Chemicals as Potential Indirect Hydrogen Storage Materials. *Int J Hydrogen Energy* **2012**, *37* (2), 1482–1494. https://doi.org/10.1016/j.ijhydene.2011.10.004.
(46) Bunce, N. J.; Bejan, D. Mechanism of Electrochemical Oxidation of Ammonia. *Electrochim Acta* **2011**, *56* (24), 8085–8093. https://doi.org/10.1016/j.electacta.2011.07.078.
(47) Grdeń, M.; Alsabet, M.; Jerkiewicz, G. Surface Science and Electrochemical Analysis of Nickel Foams. *ACS Appl Mater Interfaces* **2012**, *4* (6), 3012–3021. https://doi.org/10.1021/am300380m.
(48) Machado, S. A. S.; Avaca, L. A. The Hydrogen Evolution Reaction on Nickel Surfaces Stabilized by H-Absorption. *Electrochim Acta* **1994**, *39* (10), 1385–1391. https://doi.org/10.1016/0013-4686(94)E0003-I.
(49) Ho, J. C. K.; Piron, D. L. Active Surface Area in Oxide Electrodes by Overpotential Deposited Oxygen Species for the Oxygen Evolution Reaction. *J Appl Electrochem* **1996**, *26* (5), 515–521. https://doi.org/10.1007/BF01021975.
(50) Hall, D. S.; Bock, C.; MacDougall, B. R. An Oxalate Method for Measuring the Surface Area of Nickel Electrodes. *J Electrochem Soc* **2014**, *161* (12), H787–H795. https://doi.org/10.1149/2.0711412jes.
(51) Cossar, E.; Houache, M. S. E.; Zhang, Z.; Baranova, E. A. Comparison of Electrochemical Active Surface Area Methods for Various Nickel Nanostructures. *Journal of Electroanalytical Chemistry* **2020**, *870*, 114246. https://doi.org/10.1016/j.jelechem.2020.114246.
(52) Gmehling, J.; Tiegs, D.; Knipp, U. A Comparison of the Predictive Capability of Different Group Contribution Methods. *Fluid Phase Equilib* **1990**, *54* (C), 147–165. https://doi.org/10.1016/0378-3812(90)85077-N.
(53) Lyons, M. E. G.; Brandon, M. P. A Comparative Study of the Oxygen Evolution Reaction on Oxidised Nickel, Cobalt and Iron Electrodes in Base. *Journal of Electroanalytical Chemistry* **2010**, *641* (1–2), 119–130. https://doi.org/10.1016/j.jelechem.2009.11.024.
(54) Vedharathinam, V.; Botte, G. G. Understanding the Electro-Catalytic Oxidation Mechanism of Urea on Nickel Electrodes in Alkaline Medium. *Electrochim Acta* **2012**, *81*, 292–300. https://doi.org/10.1016/j.electacta.2012.07.007.
(55) Boggs, B. K.; King, R. L.; Botte, G. G. Urea Electrolysis: Direct Hydrogen Production from Urine. *Chemical Communications* **2009**, 4859–4861. https://doi.org/10.1039/b905974a.
(56) Logan, B.; Cheng, S.; Watson, V.; Estadt, G. Graphite Fiber Brush Anodes for Increased Power Production in Air-Cathode Microbial Fuel Cells. *Environ Sci Technol* **2007**, *41* (9), 3341–3346. https://doi.org/10.1021/es062644y.

(57) Logan, B. Material and Configurations For Scalabe Microbial Fuel Cell. US 8,962,165 B2, 2015.
(58) Feng, Y.; Yang, Q.; Wang, X.; Logan, B. E. Treatment of Carbon Fiber Brush Anodes for Improving Power Generation in Air-Cathode Microbial Fuel Cells. *J Power Sources* **2010**, *195* (7), 1841–1844. https://doi.org/10.1016/j.jpowsour.2009.10.030.
(59) United Nation. *Water |United Nations*. https://www.un.org/en/global-issues/water (accessed 2022-10-02).
(60) United Nations. *Resolution A/RES/64/292*; 2010. https://documents-dds-ny.un.org/doc/UNDOC/GEN/N09/479/35/PDF/N0947935.pdf?OpenElement (accessed 2019-05-16).
(61) Carrasquillo, R. L. ISS ECLSS Technology Evolution for Exploration. In *AIAA Aerospace Sciences Meeting and Exhibit*; Reno, Nevada, 2005. https://doi.org/10.2514/6.2005-337.
(62) Bernard, O. Mass Balance Modelling of Bioprocesses. *Lectures given at The Summer School on Mathematical Control Theory*. Trieste 2001, p https://news.ge/anakliis-porti-aris-qveynis-momava. http://www-sop.inria.fr/comore/ICTP_Modelling_Bernard.pdf (accessed 2022-10-02).
(63) Maurer, M.; Pronk, W.; Larsen, T. A. Treatment Processes for Source-Separated Urine. *Water Res* **2006**, *40* (17), 3151–3166. https://doi.org/10.1016/j.watres.2006.07.012.
(64) Barreto-Vazquez, D. Growth of Proteus Vulgaris in Synthetic Human Urine for an Ureolysis System. M.S. Thesis, University of Puerto Rico- Rio Piedras Campus, 2020. https://www.proquest.com/docview/2427302569/FAC999553F144A56PQ/1?accountid=44825.
(65) Scientific, A. *Arduino pH meter*. https://create.arduino.cc/projecthub/atlasscientific/arduino-ph-meter-e94fb4 (accessed 2020-09-17).
(66) Kenkel, J. *Analytical Chemistry for Technicians*, 3rd ed.; Lewis Publishers: United States of America, 2003. https://doi.org/10.5860/choice.40-5229.
(67) Cardona Velez, W.; Rojas-Perez, A.; Barreto-Vazquez, D.; Pagán-Jimenez, A.; Toranzos, G. A.; Cabrera, C. R.; Vijapur, S. H.; Hall, T. D.; Taylor, E. J. Urea Removal and Ammonia Detection Evaluation through Synthetic Urine Continuous Bio-Electrochemical Reactor for Closed Loop Environments. In *International Conference on Environmental Systems*; Texas Tech University Libraries: Online Conference, 2021; p ICES 2021-402.
(68) Crini, G.; Lichtfouse, E. Advantages and Disadvantages of Techniques Used for Wastewater Treatment. *Environ Chem Lett* **2019**, *17* (1), 145–155. https://doi.org/10.1007/s10311-018-0785-9.
(69) Sun, H. Y.; Xu, G. R.; Li, F. M.; Hong, Q. L.; Jin, P. J.; Chen, P.; Chen, Y. Hydrogen Generation from Ammonia Electrolysis on Bifunctional Platinum Nanocubes Electrocatalysts. *Journal of Energy Chemistry* **2020**, *47*, 234–240. https://doi.org/10.1016/j.jechem.2020.01.035.
(70) Fan, L.; Tu, Z.; Chan, S. H. Recent Development of Hydrogen and Fuel Cell Technologies: A Review. *Energy Reports* **2021**, *7*, 8421–8446. https://doi.org/10.1016/j.egyr.2021.08.003.
(71) Jeerh, G.; Zhang, M.; Tao, S. Recent Progress in Ammonia Fuel Cells and Their Potential Applications. *J Mater Chem A Mater* **2021**, *9* (2), 727–752. https://doi.org/10.1039/d0ta08810b.

(72) Vijapur, S. H.; Liu, D.; Hall, T.; Skinn, B.; Taylor, E. J.; Snyder, S.; Cabrera, C.; Barreto-Vazquez, D.; Cardona-Vélez, W. J.; Rojas Perez, A. Next Generation Water Recovery for a Sustainable Closed Loop Living. In *50th International Conference on Environmental Systems*; 2021; ICES-2021-269.

(73) Acevedo, R.; Poventud-Estrada, C. M.; Morales-Navas, C.; Martínez-Rodríguez, R. A.; Ortiz-Quiles, E.; Vidal-Iglesias, F. J.; Sollá-Gullón, J.; Nicolau, E.; Feliu, J. M.; Echegoyen, L.; Cabrera, C. R. Chronoamperometric Study of Ammonia Oxidation in a Direct Ammonia Alkaline Fuel Cell under the Influence of Microgravity. *Microgravity Sci Technol* **2017**, *29* (4), 253–261. https://doi.org/10.1007/s12217-017-9543-z.

(74) Ganesh, K.; Soumen, R.; Ravichandran, Y.; Janarthanan. Dynamic Approach to Predict pH Profiles of Biologically Relevant Buffers. *Biochem Biophys Rep* **2017**, *9* (2017), 121–127. https://doi.org/10.1016/j.bbrep.2016.11.017.

(75) Adli, N. M.; Zhang, H.; Mukherjee, S.; Wu, G. Review—Ammonia Oxidation Electrocatalysis for Hydrogen Generation and Fuel Cells. *J Electrochem Soc* **2018**, *165* (15), J3130–J3147. https://doi.org/10.1149/2.0191815jes.

(76) Afif, A.; Radenahmad, N.; Cheok, Q.; Shams, S.; Kim, J. H.; Azad, A. K. Ammonia-Fed Fuel Cells: A Comprehensive Review. *Renewable and Sustainable Energy Reviews* **2016**, *60*, 822–835. https://doi.org/10.1016/j.rser.2016.01.120.

(77) Martínez-Rodríguez, R. A.; Vidal-Iglesias, F. J.; Solla-Gullõn, J.; Cabrera, C. R.; Feliu, J. M. Synthesis and Electrocatalytic Properties of H2SO 4-Induced (100) Pt Nanoparticles Prepared in Water-in-Oil Microemulsion. *ChemPhysChem* **2014**, *15* (10), 1997–2001. https://doi.org/10.1002/cphc.201400056.

(78) Pillai, H. S.; Xin, H. New Insights into Electrochemical Ammonia Oxidation on Pt(100) from First Principles. *Ind Eng Chem Res* **2019**, *58*, 10819–10828. https://doi.org/10.1021/acs.iecr.9b01471.

(79) Vidal-Iglesias, F. J.; Solla-Gullón, J.; Rodríguez, P.; Herrero, E.; Montiel, V.; Feliu, J. M.; Aldaz, A. Shape-Dependent Electrocatalysis: Ammonia Oxidation on Platinum Nanoparticles with Preferential (100) Surfaces. *Electrochem Commun* **2004**, *6* (10), 1080–1084. https://doi.org/10.1016/j.elecom.2004.08.010.

(80) Martínez-Rodríguez, R. A.; Vidal-Iglesias, F. J.; Solla-Gullón, J.; Cabrera, C. R.; Feliu, J. M. Synthesis of Pt Nanoparticles in Water-in-Oil Microemulsion: Effect of HCl on Their Surface Structure. *J Am Chem Soc* **2014**, *136* (4), 1280–1283. https://doi.org/10.1021/ja411939d.

(81) Urbańczyk, E.; Sowa, M.; Simka, W. Urea Removal from Aqueous Solutions—a Review. *J Appl Electrochem* **2016**, *46* (10), 1011–1029. https://doi.org/10.1007/s10800-016-0993-6.

(82) Wang, D.; Yan, W.; Botte, G. G. Exfoliated Nickel Hydroxide Nanosheets for Urea Electrolysis. *Electrochem commun* **2011**, *13* (10), 1135–1138. https://doi.org/10.1016/j.elecom.2011.07.016.

(83) Mohammadzadeh Kakhki, R. A Review to Recent Developments in Modification of Carbon Fiber Electrodes. *Arabian Journal of Chemistry* **2019**, *12* (7), 1783–1794. https://doi.org/10.1016/j.arabjc.2014.11.058.

(84) My. Platinum Deposition and P. Vulgaris Growth on Carbon Fiber Brush Electrode for Ammonia Oxidation in Microbial Half-Cell Alkaline System, 2018. https://doi.org/10.7868/s0044467718030061.
(85) Cossar, E.; Barnett, A. O.; Seland, F.; Baranova, E. A. The Performance of Nickel and Nickel-Iron Catalysts Evaluated as Anodes in Anion Exchange Membrane Water Electrolysis. *Catalysts* **2019**, *9* (10) 814. https://doi.org/10.3390/catal9100814.
(86) van der Vliet, D. F.; Koper, M. T. M. Electrochemistry of Pt (100) in Alkaline Media: A Voltammetric Study. *Surf. Sci.* **2010**, *604* (21–22), 1912–1918. https://doi.org/10.1016/j.susc.2010.07.027.
(87) Pinho, S., P.; Macedo, E., A. Representation of Salt Solubility in Mixed Solvents: A Comparison of Thermodynamic Models. *Fluid Phase Equilib* **1996**, *116*, 209–216. https://doi.org/10.1016/0378-3812(95)02889-7.
(88) Chatenet, M.; Soldo-Olivier, Y.; Chaînet, E.; Faure, R. Understanding CO-Stripping Mechanism from NiUPD/Pt(1 1 0) in View of the Measured Nickel Formal Partial Charge Number upon Underpotential Deposition on Platinum Surfaces in Sulphate Media. *Electrochim Acta* **2007**, *53* (2), 369–376. https://doi.org/10.1016/j.electacta.2007.01.029.
(89) Cardona-Vélez, W. J.; Gary A. Toranzos; Cabrera, C. R.; Vijapur, S. H.; Hall, T. D.; Taylor, E. J.. Removal of Urea and Ammonia from Real Human Urine Using a Bio-Electrochemical Reactor System for Closed-Loop Environments. In *51st International Conference on Environmental System (ICES)*; Texas Tech University Libraries: Minnesota, 2022; p ICES 2022-245.